8-2016

An Innovative Approach to Johnson Noise Thermometry by Means of Spectral Estimation

Nora Dianne Bull
University of Tennessee, Knoxville, nbull@utk.edu

To the Graduate Council:

I am submitting herewith a dissertation written by Nora Dianne Bull entitled "An Innovative Approach to Johnson Noise Thermometry by Means of Spectral Estimation." I have examined the final electronic copy of this dissertation for form and content and recommend that it be accepted in partial fulfillment of the requirements for the degree of Doctor of Philosophy, with a major in Electrical Engineering.

Seddik Djouadi, Major Professor

We have read this dissertation and recommend its acceptance:

Jamie Coble, Benjamin Blalock, Charles Britton, Milton Ericson

Accepted for the Council:

Carolyn R. Hodges

Vice Provost and Dean of the Graduate School

(Original signatures are on file with official student records.)

An Innovative Approach to Johnson Noise Thermometry by Means of Spectral Estimation

A Dissertation Presented for the

Doctor of Philosophy

Degree

The University of Tennessee, Knoxville

Nora Dianne Bull

August 2016

I would like to dedicate this to my husband, Matthew Ezell. Without his encouragement and patience, I would have never completed my research. Thank you, Matthew, for listening to my hypotheses and talking me through obstacles. I appreciate your patience as I worked through the frustration of taking on a new project and trying to expand my knowledge. You have been my sounding board, my biggest cheerleader, and my best friend. You inspire me to be a better engineer and motivate me to be innovative.

I would also like to dedicate this to my parents, who always encouraged me to push myself to be better and go further than I thought was possible.

Finally, I would like to dedicate this dissertation to my friends who went running, planned craft nights, and sent me funny messages to help me de-stress.

Acknowledgements

I would like to acknowledge Dr. Michael Roberts who has helped me to learn signal processing and grow my knowledge of signals and systems. You have been a great inspiration and motivation to complete a 40+ year project. I was honored to be mentored by one of the original members of the research team. I appreciate you spending your retirement teaching me and playing GO whenever we needed a mental break. Thank you for being patient as I continued to struggle with the new material and always having encouraging words to keep me motivated.

I would also like to acknowledge Dr. Seddik Djouadi who encouraged and mentored me in control systems. I have enjoyed getting to know you better as a friend. My respect for you and your research grows everyday that I work with you. Thank you for your kind words and always exciting stories. I look forward to continuing our joint research in the future.

Also, I would like to acknowledge Oak Ridge National Laboratory which allowed me to take a sabbatical from work to complete my research. Through ORNL, I was mentored by Dr. Chuck Britton and Dr. Nance Ericson. Both of you have been more than colleagues, you are like my work fathers but also my friends. Chuck, you have been a inspiration to be a better engineer through an understanding of engineering fundamentals. Nance, you have always challenged me to think outside of the box and be creative. I hope to continue to work with you throughout my career.

Finally, I would like to acknowledge Department of Energy for providing three years of funding for this project.

'"If we knew what it was we were doing, it would not be called research, would it?"
–Albert Einstein

Abstract

Instrumentation in a nuclear power plant is critical in monitoring the stability and safety levels of a reactor. Temperature is a key measurement performed on the core of a reactor to control the power output and sustain a safe thermal margin. If there is a dramatic change in temperature, failure is likely to follow if action is not taken to cool the system. Traditionally, to measure the temperature of a reactor several resistance temperature detectors (RTD)s were placed in predefined locations on the system. RTDs are typically coiled platinum wire wrapped around a ceramic cylinder and encased in a metal sheath. Due to the harsh environment of nuclear reactors, RTDs degrade and their resistance measurements drift over time. This drift in resistance can be misunderstood as a drift in reactor temperature. In the past, RTDs would be serviced every few years either through calibration or replacement. To service RTDs the reactor is shut down, and a person is sent into a dangerous environment. Using Johnson noise thermometry (JNT) will reduce the need for servicing and provide a high-accuracy temperature measurement. JNT is a fundamental expression of temperature that is invulnerable to drift in the RTD's physical condition. The signal processing behind JNT is presented in this document. Spectral estimation methods are used to remove electromagnetic interference (EMI) from the JNT measurement. These methods are unique to this dissertation. The EMI estimation method is modeled and simulation results are presented. The modeling of the EMI estimation involves locating EMI, analyzing EMI effects, and removing EMI without bias. Finally, results from numerical and experimental verification are

presented. The research presented here is important to the future of the nuclear industry for several reasons. With this technology applied to existing systems, reactor shut down time can be decreased, technician exposure to dangerous radiation zones is decreased, and the cost associated with lengthy shut downs can be reduced. The instrumentation community will benefit through the innovation of signal processing for very small signal versus noise interference.

Table of Contents

List of Tables

List of Figures

Nomenclature

$\mathbf{E}$	Function: Expected value
$\mathbf{H}$	H-Function
$\mathbf{M}$	Mellin Tranform
$\mathbf{M}^{-1}$	Inverse Mellin Tranform
μ	Mean
σ	Variance
C_{a1}	Amplifier/Filter Ch1 Capacitance
C_{a2}	Amplifier/Filter Ch2 Capacitance
C_c	Cable Capacitance
C_c	Pilot Tone Capacitance
$G_{1-E}(f)$	PSD of Ch1 output voltage with EMI subtracted and with PT OFF
$G_{12-E}(f)$	CPSD between Ch1 and Ch2 output voltages with EMI subtracted and with PT OFF
$G_{12-p}(f)$	CPSD between Ch1 and Ch2 output voltage with PT ON but removed

$G_{12p-E-p}(f)$	CPSD between Ch1 and Ch2 output voltages with EMI subtracted and with PT ON but removed
$G_{12p-E}(f)$	CPSD between Ch1 and Ch2 output voltages with EMI subtracted and with PT ON
$G_{12p}(f)$	CPSD between Ch1 and Ch2 output voltage with PT ON
$G_{12}(f)$	CPSD between Ch1 and Ch2 output voltage with the PT OFF
$G_{1}(f)$	PSD of Channel One (Ch1) electronics signal output voltage with the PT OFF
$G_{2-E}(f)$	PSD of Ch2 output voltage with EMI subtracted and with PT OFF
$G_{2}(f)$	PSD of Channel Two (Ch2) electronics signal output voltage with the PT OFF
$G_{A1p}(f)$	CPSD between Antenna and Ch1 output voltage with PT ON
$G_{A1}(f)$	CPSD between Antenna and Ch1 output voltage with PT OFF
$G_{A2p}(f)$	CPSD between Antenna and Ch2 output voltage with PT ON
$G_{A2}(f)$	CPSD between Antenna and Ch2 output voltage with PT OFF
$G_{aA}(f)$	PSD of Antenna Channel electronics signal output voltage
$G_{AE}(f)$	CPSD between Antenna and EMI Source
$G_{p1-E}(f)$	PSD of Ch1 output voltage with EMI subtracted and with PT ON
$G_{p1}(f)$	CPSD between PT and Ch1 output voltage
$G_{p2-E}(f)$	PSD of Ch2 output voltage with EMI subtracted and with PT ON
$G_{p2}(f)$	CPSD between PT and Ch2 output voltage

$G_p(f)$	PSD of Pilot Tone (PT) signal output voltage at the generator output
$G_{Rb}(f)$	Bandlimited Resistor PSD of the sensor (RTD)
$G_{Rc}(f)$	Resistor PSD of the cable
$G_{Rs}(f)$	Resistor PSD of the sensor (RTD)
$G_X(f)$	PSD of the unknown EMI phenomenon
$H_{12}(f)$	Cross Power Frequency Response from sensor to the outputs of Ch1 and Ch2
$H_1(f)$	Amplifier/Filter combination frequency response of Ch1
$H_2(f)$	Amplifier/Filter combination frequency response of Ch2
$H_{A1p}(f)$	Frequency response from output voltage of Antenna electronics to Ch1 output voltage with PT ON
$H_{A1}(f)$	Frequency response from output voltage of antenna electronics to Ch1 output voltage with PT OFF
$H_{A2p}(f)$	Frequency response from output voltage of Antenna electronics to Ch2 output voltage with PT ON
$H_{A2}(f)$	Frequency response from output voltage of antenna electronics to Ch2 output voltage with PT OFF
$H_A(f)$	Amplifier/Filter combination frequency response of Antenna electronics
$H_{EA}(f)$	Frequency response from EMI source to Antenna electronics output voltage
$H_{ES}(f)$	Frequency response from EMI source to sensor

$H_{p1}(f)$	Frequency response from PT voltage to output voltage of Ch1
$H_{p2}(f)$	Frequency response from PT voltage to output voltage of Ch2
$H_p(f)$	Frequency response from PT voltage generated to the current injected into sensor by the PT voltage = transconductance gin
$H_s(f)$	Frequency response from sensor (Rs = resistor noise of sensor) to the amplifier inputs ($\sim$1 in our BW)
R_c	Cable resistance
R_p	Pilot Tone resistance
R_s	Sensor (RTD) resistance
T_s	JNT Sensor Temperature)
$V_{1-E}(f)$	Output voltage of Ch1 with EMI subtracted in the frequency domain
$v_{1-E}(t)$	Output voltage of Ch1 with EMI subtracted in the time domain
$V_{1E}(f)$	Output voltage of Ch1 due to EMI alone in the frequency domain
$v_{1E}(t)$	Output voltage of Ch1 due to EMI alone in the time domain
$V_{1p-E-p}(f)$	Output voltage of Ch1 with EMI subtracted and PT subtracted in the frequency domain
$v_{1p-E-p}(t)$	Output voltage of Ch1 with EMI subtracted and PT subtracted in the time domain
$V_{1p-E}(f)$	Output voltage of Ch1 due to PT with EMI subtracted in the frequency domain

$v_{1p-E}(t)$	Output voltage of Ch1 due to PT with EMI subtracted in the time domain
$V_{1p}(f)$	Output voltage of Ch1 due to PT in the frequency domain
$v_{1p}(t)$	Output voltage of Ch1 due to PT in the time domain
$V_1(f)$	Output voltage of Ch1 in the frequency domain
$V_{2-E}(f)$	Output voltage of Ch2 with EMI subtracted in the frequency domain
$v_{2-E}(t)$	Output voltage of Ch2 with EMI subtracted in the time domain
$V_{2E}(f)$	Output voltage of Ch2 due to EMI alone in the frequency domain
$v_{2E}(t)$	Output voltage of Ch2 due to EMI alone in the time domain
$V_{2p-E}(f)$	Output voltage of Ch2 due to PT with EMI subtracted in the frequency domain
$v_{2p-E}(t)$	Output voltage of Ch2 due to PT with EMI subtracted in the time domain
$V_{2p}(f)$	Output voltage of Ch2 due to PT in the frequency domain
$v_{2p}(t)$	Output voltage of Ch2 due to PT in the time domain
$V_2(f)$	Output voltage of Ch2 in the frequency domain
$v_2(t)$	Output voltage of Channel 2 (Ch2) in the time domain
$V_{a1}(f)$	Equivalent input noise voltage of Ch1 amplifier/filter in the frequency domain
$v_{a1}(t)$	Equivalent input noise voltage of Ch1 amplifier/filter in the time domain

$V_{a2}(f)$	Equivalent input noise voltage of Ch2 amplifier/filter in the frequency domain
$v_{a2}(t)$	Equivalent input noise voltage of Ch2 amplifier/filter in the time domain
$V_{aA}(f)$	Equivalent input noise voltage of antenna amplifier channel in the frequency domain
$v_{aA}(t)$	Equivalent input noise voltage of antenna amplifier channel in the time domain
$V_A(f)$	Antenna electronics output voltage in the frequency domain
$v_A(t)$	Antenna electronics output voltage in the time domain
$V_E(f)$	EMI voltage induced into the sensor in the frequency domain
$v_E(t)$	EMI voltage induced into the sensor in the time domain
$V_p(f)$	Output voltage of PT generator in the frequency domain
$v_p(t)$	Output voltage of PT generator in the time domain
$V_{Rc}(f)$	Noise voltage of cable in the frequency domain
$v_{Rc}(t)$	Noise voltage of cable in the time domain
$V_{Rs}(f)$	Noise voltage of sensor in the frequency domain
$v_{Rs}(t)$	Noise voltage of sensor in the time domain
CPSD	Cross Power Spectral Density
DFT	Discrete Fourier Transform
EMI	Electromagnetic Interference

FT	Fourier Transform
INRIM	National Institute of Metrological Research, Italy
NIM	National Institute of Metrology, People's Republic of China
NIST	National Institute of Standards and Technology, USA
NMIJ	National Metrology Institute of Japan
NPT JNT Temp	Nonpilot Tone Johnson Noise Thermometry Temperature
NPTRPSD	Nonpilot Tone Resistor Power Spectral Density
ORNL	Oak Ridge National Laboratory, USA
PSD	Power Spectral Density
PT	Pilot Tone
PT JNT Temp	Pilot Tone Johnson Noise Thermometry Temperature
PTRPSD	Pilot Tone Resistor Power Spectral Density
RPSD	Resistor Power Spectral Density
RTD	Resistance Thermometer Device
$v_1(t)$	Output voltage of Channel 1 (Ch1) in the time domain

Chapter 1

Introduction

Johnson noise thermometry (JNT) was demonstrated for in-core reactor temperature measurement 45 years ago [3] but was applied for general temperature measurements more than 87 years ago [4]. Even with a lifetime of research, JNT was never commercialized due to the small signal to noise ratio. Johnson noise is the desired noise signal, and electromagnetic interference (EMI) is the unwanted signal. Measuring Johnson noise inside an environment with significant EMI, like a nuclear reactor, has proven difficult. Mechanical vibrations, pumps, and other equipment around the nuclear reactor contribute transient and periodic EMI to the measurement. This measurement is heavily dependent upon the characteristic shape of the Johnson noise power spectrum, advanced digital signal processing, and innovative electronic measurement design. In recent years, the greatest impact on JNT research has been the improvement in digital signal processing and the software algorithm presented here. The principal expense in a Johnson noise measurement system is the cost of developing the signal processing system that handles the JNT signal and removes the other noise sources from the signal. Neither the electronics to implement JNT nor the well-shielded transducer and cabling are especially expensive components. Well-implemented JNT has the potential to compete economically with other low-uncertainty thermometry techniques at high temperatures throughout

nuclear power plants. Further, JNT has the potential to become the preferred thermometry technique throughout the process control industry due to its robustness and low measurement uncertainty at a reasonable price. Once commercialized, other industries outside nuclear instrumentation interested in reliable high-temperature monitoring, such as large data and high-performance computing and automotive electronics, are likely to adopt this technology.

1.1 Johnson Noise: A Brief History

Temperature is simply the measurement of kinetic energy at an atomic level. In Einstein's study of Brownian motion [5], the existence of spontaneous thermal fluctuations in electrical circuits was discovered to be Johnson noise [6] and is a first-principle representation of temperature that is invulnerable to chemical and mechanical changes in a material's properties [7]. This invulnerability is due to the type of measurement JNT makes. Basically JNT is a continuous, first-principle recalibration method of measuring temperature. John "Bert" Johnson published a paper while working at Bell Telephone Laboratories (formally known as AT&T's Department of Development and Research) in 1928 discussing the measured effect and problems of thermal noise within electronics [6], [8], [9]. Then in 1929, Harry Nyquist (also at Bell Telephone Laboratories) published a paper deriving the thermal noise effect by means of thermodynamics and statistical mechanics [10], [11]. While Johnson was credited with the discovery, Nyquist made it relevant by developing the following theorem about the power spectral density (PSD) of the noise voltage of a resistor [6]:

$$d\overline{V_T^2} = 4hfRe(Z)\left[\frac{1}{2} + \frac{1}{exp(hf/k_Bt) - 1}\right]df, \tag{1.1}$$

where h is Planck's constant, k_B is Boltzmann's constant, f is the frequency, and Z

is the zero-state energy of the system. When operating in frequencies below a few gigahertz, the equation is simplified to:

$$\overline{V_T^2} = 4k_B T R \Delta f, \tag{1.2}$$

where Δf is the frequency bandwidth in hertz of measurement, R is the resistance of the sensor in Ohms, T is the absolute temperature in Kelvins of the resistor, and $\overline{V_T^2}$ is the measured mean-squared noise voltage [12], [13]. In 1946, A. W. Lawson and Earl A. Long published the possibilities of using Johnson noise to measure extreme temperatures [14],[15],[16]. Then in 1949 J. B. Garrison and Lawson published the idea of using a resistor as the sensor in the Johnson noise thermometer [4]. This is the method still used today for Johnson noise thermometers. This method is ideal because the resistance and temperature are the only properties of the material that the noise voltage depends upon [6]. However, the noise signal is very small and is highly dependent upon the environment the noise thermometer is placed into. Figure 1.1 displays the electrical representation of a resistor and the noise voltage associated with it. Figure 1.2 demonstrates an example of time domain JNT noise voltage and the frequency domain JNT noise voltage Fourier transformed from the time domain noise voltage. Johnson noise distribution is Gaussian in three dimensions and can be illustrated by a random walk process.

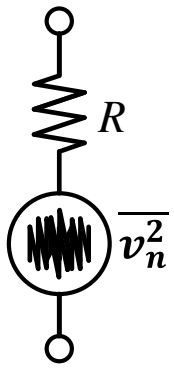

Figure 1.1: Circuit representation of noise voltage of a resistor

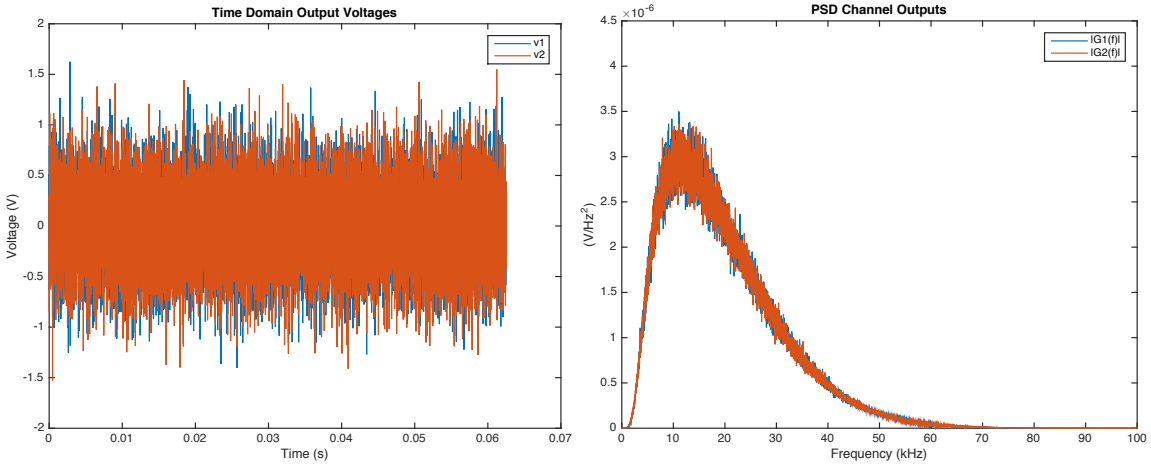

(a) Time Domain JNT Voltage **(b)** Frequency Domain JNT PSD

Figure 1.2: Output JNT voltages and power spectral density from channel 1 and channel 2

1.2 Brownian Motion vs. Johnson Noise

Brownian motion was originally observed by Jan Ingenhausz in 1785 while working with powdered charcoal on an alcohol surface. However, the discovery is credited to Robert Brown in 1827 while studying the random movement of pollen grains suspended in water. Brown thought he was observing "evidence of life". Brownian motion is a macroscopic view of the random movement of fine particles in any dimensional space [17]. Albert Einstein explained Brownian motion in 1905 in terms of random thermal motions [18]. The theory of random thermal motion states that any particle suspended in a liquid has equal probability to move in any direction [11]. The noise produced by this is called Brownian noise, brown noise, red noise, or random walk noise. Einstein's theory on Brownian motion is based on the kinetic theory of gases and states the mean kinetic energy per degree of freedom of a particle's energy is given by Equation 1.3 [11]:

$$\frac{1}{2}M\overline{v_x^2} = \frac{1}{2}k_B T, \tag{1.3}$$

where M is the mass of the particle, v_x is the instantaneous velocity component in the x-direction, $\overline{v_x^2}$ is the mean-squared value that equals the variance for a zero mean process, k_B is Boltzmann's constant, and T is the absolute temperature in Kelvins. From this equation, it becomes obvious that the thermal noise in any conductive material is simply the Brownian motion of electronics due to ambient temperature. This is what Bert Johnson was observing. It turns out that most random noise is shaped by the mean and covariance of the random processes. This is explained in more detail in the random variable section of this dissertation (section 1.6).

1.3 Johnson Noise Thermometry Outside of Oak Ridge National Laboratory

Several countries and research facilities are interested in JNT today. The basic principle in Nyquist's equation of noise voltage of a resistor is the foundation of the research, but the method and application vary from institute to institute. Several institutions have collaborated over the years. Research collaborations, as recently as 2014, have pursued parallel but slightly different JNT research paths.

The National Institute of Metrology (NIM, People's Republic of China) published an article in 2014 discussing the improved electronics developed recently at the institute, along with the National Institute of Standards and Technology (NIST, USA) [19]. NIST published in an article 2010 about its desire to reduce the nonlinearities in its system. To reduce the nonlinearities, NIST developed a Josephson Junction array probe and driver called a "quantum voltage noise source" (QVNS) [20]. The idea is to use the QVNS circuit output voltage as a reference to compare to the JNT sensor output voltage. NIM focused its efforts on researching the statistical uncertainty due to the switching between the QVNS array and the sensor resistance temperature detector (RTD). Through the addition of appropriate shielding and grounding, they were able to remove uncertainty from the switching network and EMI [19]. NIST

focuses on absolute temperature dependance due to the ratio of the PSD of the Johnson noise voltage to the PSD of the QVNS array. NIST only addresses EMI rejection through a band-pass and low-pass filter/integrator [20].

The National Metrology Institute of Japan (NMIJ) has also collaborated with NIST, as recently as 2012. NMIJ is very interested in the cancellation of time-dependent drift in the measurement due to switching at the input of its electronics [21]. NMIJ does not address EMI concerns in any of its publications. The National Institute of Metrological Research (INRIM, Italy) had unique research of all the institutions mentioned and used a completely different electronics system [22]. INRIM injects a calibration signal into their electronics, which could be misconstrued as the same pilot tone (PT) used by Oak Ridge National Laboratory (ORNL) [23]. To fully model the system electronics ORNL injects a current in parallel (which ORNL call "pilot tone"). INRIM injects a voltage into step-down transformers in series.

All of these institutions address different faults within JNT research and application. However, none of them addresses the signal processing and software EMI removal techniques addressed in this dissertation. Also, the test environments for their JNT systems are clean laboratory environments with minimal EMI sources corrupting the final overall temperature measurements. ORNL's system is designed to endure very harsh environments with large amounts of EMI and still compute the correct temperature. The system and signal processing designed for this research project are described in more detail in Chapters 2 and 3. The differences between the research performed at these organizations and the research performed at ORNL are presented in Table 1.1.

Table 1.1: Comparison of JNT Methods

	NMIJ[i]	NIST[ii]	INRIM[iii]	NIM[iv]	ORNL[v]
	Japan [21]	*USA [20]*	*Italy [22]*	*People's Republic of China [19]*	*USA [23]*
Sensors	Josephson junction array probe and driver designed specifically for NMIJ testing along side RTD (they are calling QVNS)	Josephson junction array probe and driver designed specifically for NMIJ testing along side RTD (collaborated with NMIJ)	Unknown	Statistical uncertainty due to switching between QVNS array and RTD	Standard off-the-shelf RTDs readily available and already utilized in industry
Time Domain Drift Corrections	Cancellation of time dependent drift of amplifiers due to switching at input of amplifier	Not Reported	Not Reported	Not Reported	No switching at amplifier's inputs, therefore no time drift concerns
Signal Processing Development	No further development on signal processing methodology	Not Reported	Not Reported	Not Reported	Major focus on signal processing for improved EMI rejection and JNT measurement
EMI Rejection	Not Reported	EMI rejection through band-pass and low-pass filter/integrator	No documented EMI removal	EMI rejection through shielding and grounding and researching appropriate shielding	EMI rejection through hardware filtering and signal processing
Harmonics	Not Reported	Concerned with 2nd-order harmonics only	Not Reported	Not Reported	Interested in removing all harmonics
Temperature Calculations	Not Reported	Absolute Temperature dependent on the ratio of the PSD of Johnson noise voltage to the PSD of QVNS array	Not Reported	Absolute Temperature dependent on the ratio of the PSD of Johnson noise voltage to the PSD of QVNS array (cited methods used by NMIJ)	Absolute temperature dependent only on PSD of output noise voltage due to Johnson noise by Nyquist approximation
Electronic Monitoring and Calibration	Not Reported	Not Reported	Injecting calibration signal with step-down transformers in series	Not Reported	Injecting a current in parallel to monitor transfer function of electronics
Electronic Design	Not Reported	Not Reported	Amplifiers are open loop	Not Reported	Closed Loop amplifier design
Laboratory Environment	Low-noise Laboratory environment	Low-noise Laboratory environment	Low-noise Laboratory environment	Low-noise Laboratory environment	Very noisy, real-world, application; industrial environment

[i] National Metrology Institute of Japan
[ii] National Institute of Standards and Technology
[iii] National Institute of Metrological Research
[iv] National Institute of Metrology
[v] Oak Ridge National Laboratory

1.4 Johnson Noise Thermometry at ORNL

In the late 1960s and early 1970s ORNL [3] developed an interest in using thermometry in the High Flux Isotope Reactor (HFIR) to measure the fuel centerline temperatures of the center rod in the core. The Instrumentation and Controls division provided tungsten-rhenium thermocouples to measure temperatures of 1500°C [24]. Within days of the initial measurements, temperature drifts were noticed in the system, so Vaughn Blalock (University of Tennessee) and Cas Borkowski developed the first JNT implementation at ORNL [25]. From the background research previously mentioned (section 1.3), they knew the resistance and noise voltage measurements were critical for JNT to be successful. The amplifier and filter electronics, still used in the system today, were initially designed in the mid-1970s. While working on this system, ORNL researchers determined that EMI contributions to the noise measurement were obstacles that needed to be overcome [23]. In 1977, ORNL won an R&D 100 award for its work on JNT. In the mid-1980s, Dr. M. J. Roberts (University of Tennessee) joined the team to develop much-needed signal processing for spectral analysis of time-domain quality checks [23]. Several methods were developed for long-term high-reliability nuclear power applications, including placing the sensor in parallel with a capacitor to eliminate the system's dependance on sensor resistance. The shortcomings of this method are that the measurement requires a large bandwidth and there is no EMI compensation. Another method developed was placing the sensor in parallel with an inductor-capacitor-tuned circuit that narrows the spectral range and reduces the bandwidth. The drawback to this method is the inductor's core loss is a noise source just like Johnson noise [26]. Neither of these methods is still used in the system today. In the early 1990s correlation techniques and spectral analysis were integrated into the signal processing, eliminating amplifier/filter noise and detecting and rejecting periodic EMI. In 2002, ORNL joined with the United States and Korean Nuclear Energy Research Initiative program to perform correlation measurements. The temperature measurement system had a 1%

measurement uncertainty requirement at 1375 K, an 8-second response time limit, and a requirement for 7 years of unattended operation. No conventional thermometer could meet these goals [23]. However, the Johnson noise thermometers that had been developed by ORNL, originally for fuel centerline measurement, were believed to be able to meet these stringent requirements [27]. In April of 2012, ORNL led the US Department of Energy Advanced Small Modular Reactor (SMR) Research and Development program. The purpose of JNT in this and other projects was to develop and demonstrate a drift-free Johnson noise–based thermometer suitable for deployment near the core in advanced SMR plants. Figure 1.3 shows the system developed. While it became apparent in the mid-1980s that signal processing is critical in the measurement, it took a long time for the final version of the software to be completed. The new software algorithm is the main subject of this dissertation. While the early research at ORNL is critical to the current system, only the research performed in the 1980s, 1990s, and 2000s is relevant to the research presented in this document. This is the research period during which the signal processing aspects were developed.

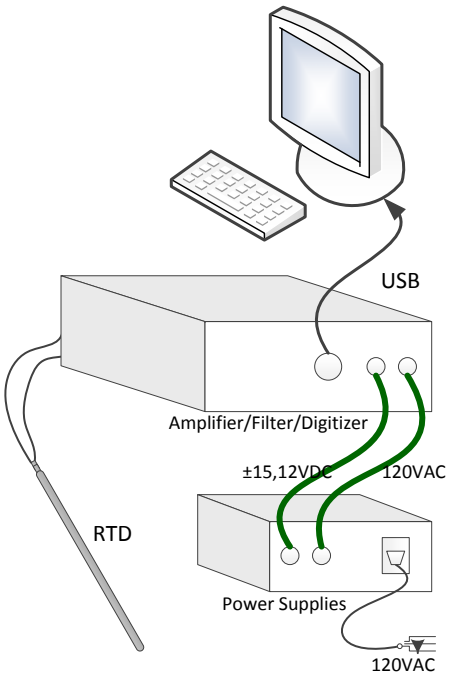

Figure 1.3: Depiction of JNT system hardware

1.5 ORNL Signal Processing

Directly measuring temperature using Johnson noise is very challenging because so many variables must be known or measurable and stable. The resistance of the RTD sensor needs to be independently and accurately measured, as well as the amplifier gain, passband, and filtering effects of the connection cabling. Early Johnson noise thermometers measured a ratio of two noise voltages to avoid these difficulties. One noise voltage is at the measurement temperator and the other voltage at a known temperature. The two noise voltages are then switched onto a single amplifier/filter channel, similar to the work presented by NMIJ, NIM, and NIST. Also similar to NMIJ, NIM, and NIST, changing the connector of the sensor to the high-gain measurement circuit introduced noise and decreased reliability [28].

The frequency band in which the measurement is performed is also very important. The capacitive effect of the cable between the sensor and the first stage amplifier will greatly impact the bandwidth of the measurement. If the cable has significant

capacitance, it will block the high frequency portion of the sensor noise before it reaches the measurement system. The cable capacitance is susceptible, over time, to the temperature and radiation environment inside the containment structure of a reactor. Because the electronics are housed outside of the containment, a 25 meter cable is required, which adds a great deal of capacitance (many nanofarads). ORNL currently corrects for this effect using a pilot tone (PT) sweeping technique (discussed in Chapter 3) that measures channel gain and frequency variations. The measurement is band limited across 15–40 kHz. Bandlimiting data is discussed further in later sections of this document.

Two signal-processing concepts were investigated before the present method was implemented [29], [8]. In the first of the two methods, an RTD is connected in parallel into the input of two high input-impedance amplifier/filter electronics channels. Because each amplifier/filter channel consists of the sum of a correlated noise voltage and the uncorrelated amplifier noise voltage, the outputs of the amplifiers/filters are partially correlated. The two output signals from the amplifiers/filters are combined and time averaged causing the correlated part of the noise to persist and the uncorrelated noise to approach zero. Figure 1.4 illustrates the concept of cross correlation; the measured voltage from one amplifier/filter channel is Fourier transformed (FTed) and correlated with the second Fourier-transformed channel voltage to form a cross power spectral density (CPSD) measurement, effectively eliminating the noise contribution from the amplifier/filter electronics.

The Johnson noise signal consists only of a flat-white spectral energy distribution. As displayed in Figure 1.4 and Figure 1.5, the shape of the Johnson noise PSD function is a result of the combined effects of filtering out both low and high frequencies (outside of the bandwidth of the measurement) from the noise and the frequency-dependent gain of the amplifier/filter channel. The low frequency filtering eliminates the nonthermal noise generated by mechanical vibrations. These low frequency microphonic signals are typically less than a few tens of a kilohertz. The highband-frequency filtering minimizes the impact of sensor-to-amplifier cable capacitance,

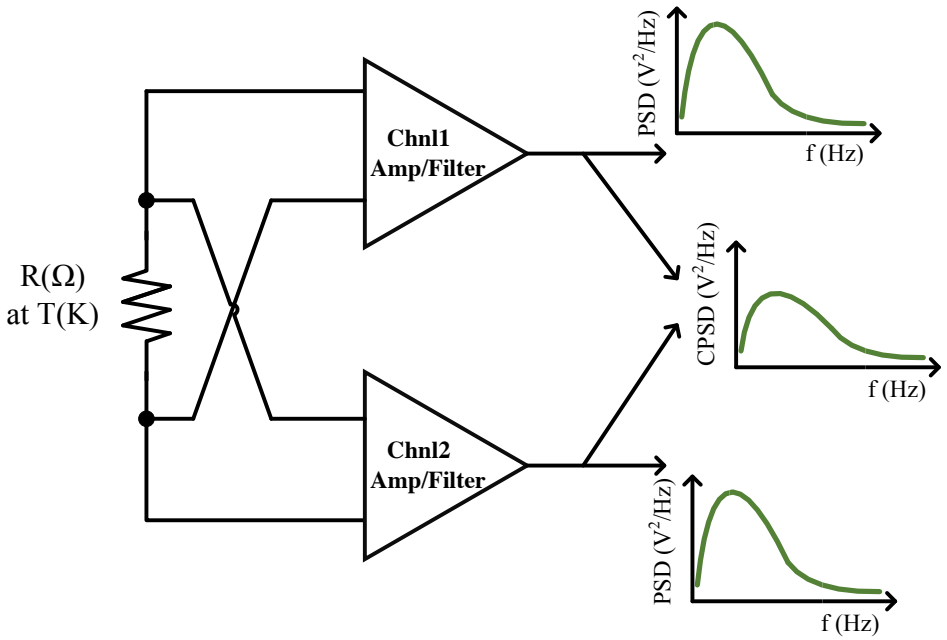

Figure 1.4: Power spectral density (PSD) function of each amplifier/filter channel path containing correlated and uncorrelated noise. Also shown, the cross power spectral density (CPSD) function from both amplifiers/filters with only correlated noise.

restricting the high frequency signal transmission. From there, CPSD is calculated and has the units of volts squared per hertz, (V^2/Hz). CPSD conveys the power content per unit frequency of the measured noise signal. It is derived from the individual channel voltages (Figure 1.4).

The second method focuses on removing not only microphonics again but also EMI "spikes" as the biggest problems for practical implementation. Depending on the environment, these effects can completely dominate the noise measurement by saturating the amplifier/filter channels. Grounding, filtering, and shielding become critical to preventing these noise sources from corrupting the Johnson noise measurement. However, the method cannot completely prevent EMI from corrupting the measurement. To reduce these effects one must use both knowledge of the spectral energy content of Johnson noise and digital signal processing to recognize and eliminate interferences. Narrowband EMI always appears as spikes in the long-term

average CPSD. They can be recognized and removed with only a small reduction in measurement bandwidth as illustrated in Figure 1.5. The present method of signal processing used on the ORNL JNT system is depicted in Figures 1.6 and 1.7. The final calculations solve for the nonpilot tone resistor power spectral density (NPTRPSD), the despiked NPTRPSD, the pilot tone resistor power spectral density (PTRPSD), the despiked PTRPSD, the sensor resistance (Rs), the sensor temperature, the nonpilot tone Johnson noise thermometry temperature (NPT JNT temperature), the pilot tone Johnson noise thermometry temperature (PT JNT temperature), and the characterization of the pilot tone attenuator ($|H_p(f)|^2$).

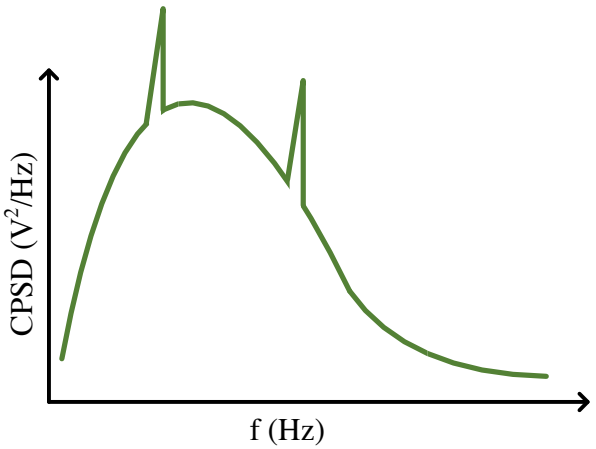

Figure 1.5: Cross power spectral density output of two amplifier/filter channels $[G_{12}(f)]$ with narrowband EMI spikes. $G_{12}(f)$ = JNT noise + transfer function of electronics + EMI spikes

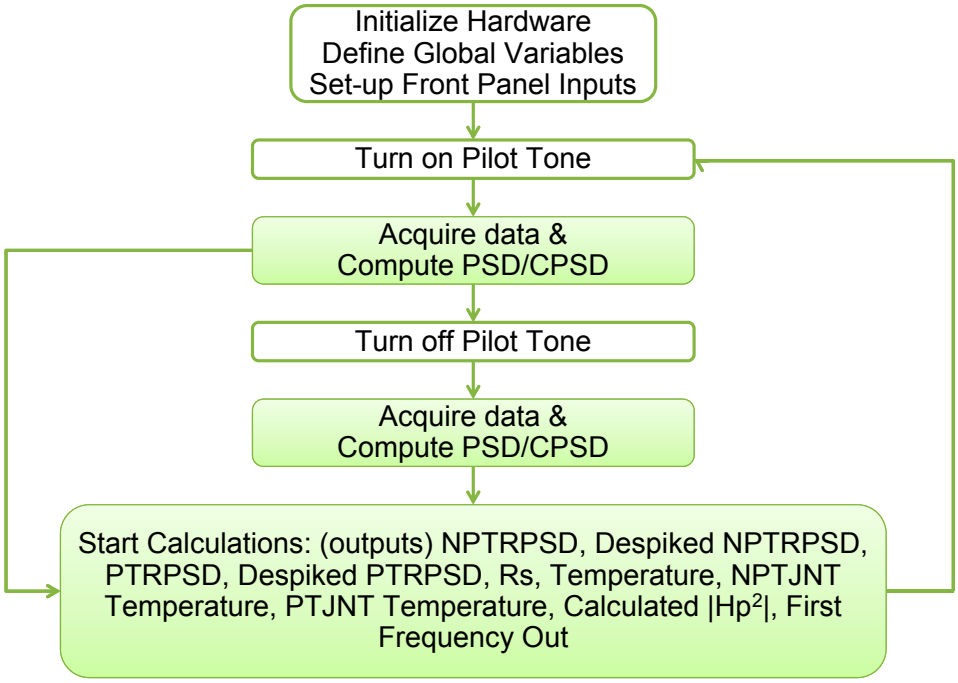

Figure 1.6: Flow chart of steps taken in the JNT signal processing

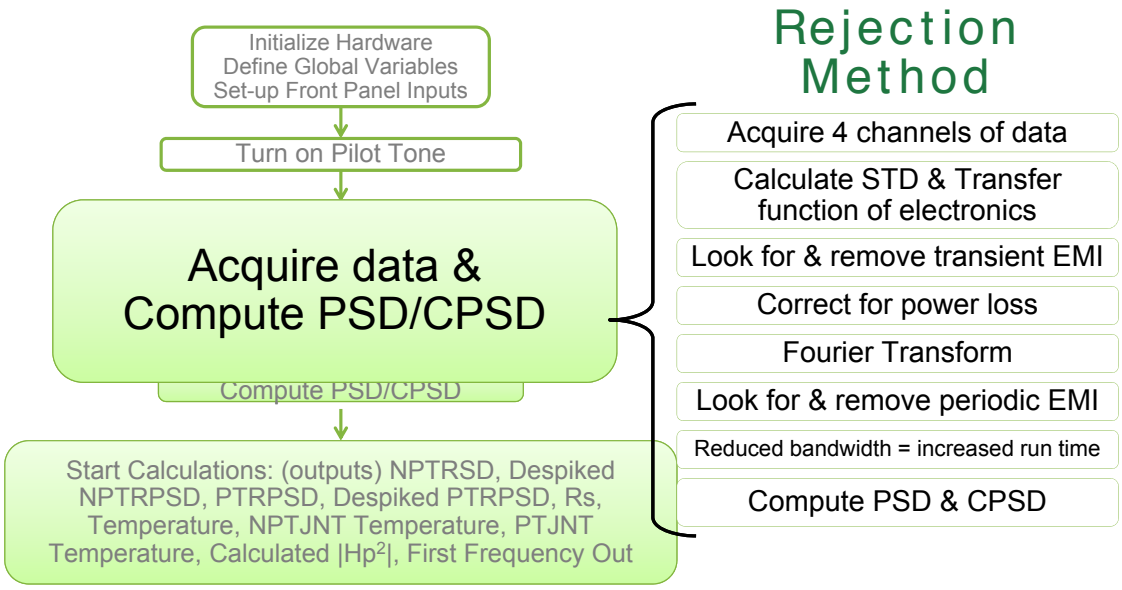

Figure 1.7: Descriptive diagram of the "Acquire Data and compute power spectral density and cross power spectral density" block

Voltages are sampled in blocks made of 16 sub blocks (Figure 1.8). Each sub block is evaluated for noise spikes. A sub block of data is considered to have an EMI spike if the standard deviation of that sub block of data is twice the standard deviation of the overall block data. Figure 1.9 is a flow chart of the EMI removal technique. If a spike is detected, the sub block is rejected, as well as the sub block before and after (total of 3 of the 16 sub blocks). The entire block of data is only rejected when all 16 sub blocks are rejected. The power of the signal is reduced due to the loss of sub blocks and therefore needs to be corrected. The power is directly proportional to the number of sub blocks accepted. To correct the loss of power, divide the signal by the ratio of the number of accepted sub blocks to the 16 sub blocks (Equation 1.4). All of the rejection performed before Fourier transforming the signal into the frequency domain is time-domain windowed. A rectangular window is used for time-domain EMI rejection. After the power is corrected, the signal is then FTed, and the signal processing begins in the frequency domain. If more data points were acquired inside a block, it would allow for more sub blocks, reducing the overall number of sub blocks rejected versus accepted in a block. Currently in the software presented here, 2^{14} or 16,384 data points build the total data block. Taking more data points is preferred but is limited by the hardware of the computer.

$$\text{Corrected Signal} = \text{Signal}\left(\frac{16 \text{ sub blocks}}{\text{Number of accepted sub blocks}}\right) \tag{1.4}$$

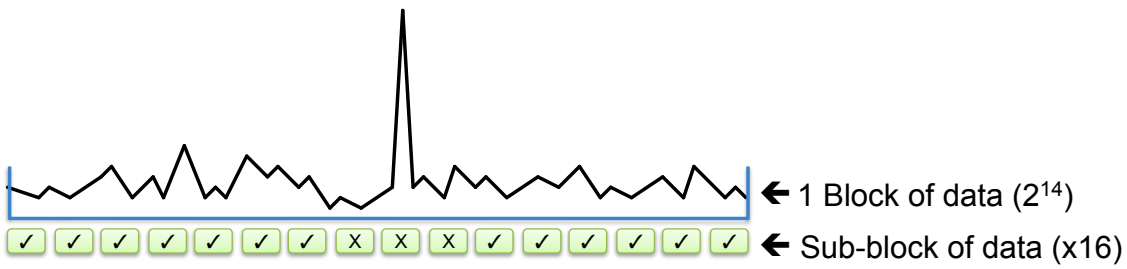

Figure 1.8: Sample block of data with 16 sub blocks; total data points = 2^{14}

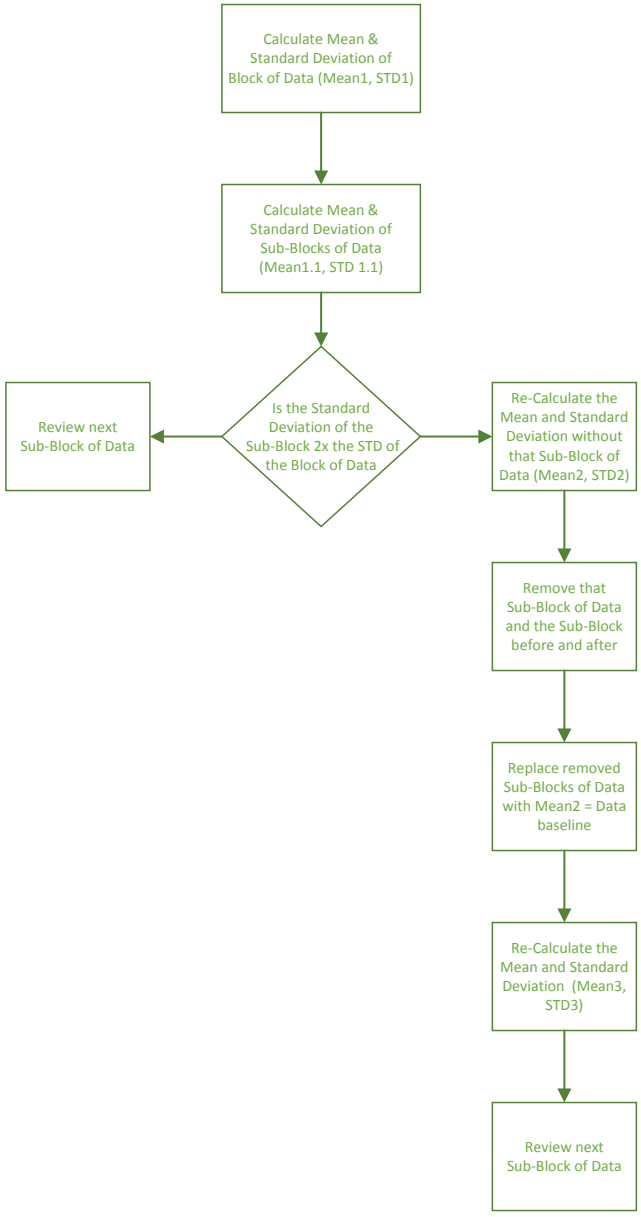

Figure 1.9: Spike removal flow chart

Since rectangle windowing is used in the time domain, the Fourier Transform (FT) of a rectangle over infinite time corresponds to a sinc function in the frequency domain (Figure 1.10) [30]. This EMI removal technique is referred to as "despiking". The despiking algorithm is discussed further in Chapter 2. Equations 1.5–1.7 display the rectangle, sinc function and FT [30].

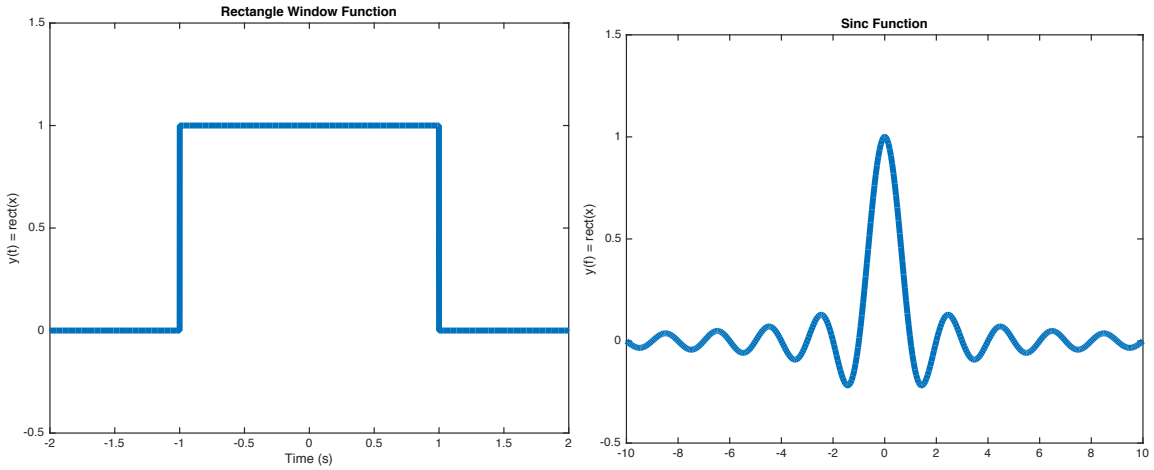

(a) Time domain rect window **(b)** Frequency domain sinc filter

Figure 1.10: Windowing function

$$rect(t) = \begin{cases} 0 & \text{if} \quad |t| > \frac{1}{2} \\ \frac{1}{2} & \text{if} \quad |t| = \frac{1}{2} \\ 1 & \text{if} \quad |t| < \frac{1}{2} \end{cases} \tag{1.5}$$

$$sinc(f) = \frac{sin(\pi f)}{\pi f} \tag{1.6}$$

$$\int_{-\infty}^{\infty} rect(t) e^{-j2\pi ftdt} = \frac{sin(\pi f)}{\pi f} = sinc(\pi f) \tag{1.7}$$

Because the rectangle function (rect) samples over the entire time block, the sinc function repeats at 0, Δf, 2Δf, 3Δf, etc. (where Δ is the sampling rate divided by the number of points in a block of data) infinitely over the bandwidth of the measurement, as displayed in Figure 1.11. The gain of the Johnson noise and all EMI

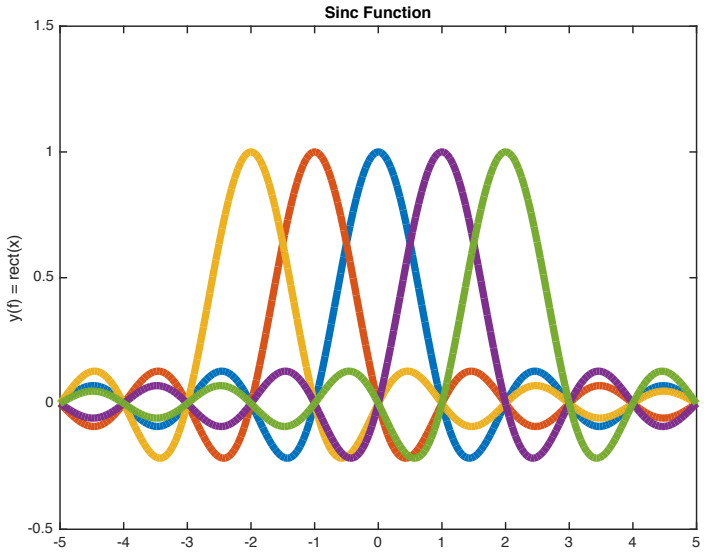

Figure 1.11: Graphical representation of frequency domain sampling

detected under a single sinc function are added together to equal the total noise value of that sinc. This works perfectly if all noise falls at f, Δf, 2Δf, 3Δf, etc., but the problem with this signal processing technique is that noise is random and can fall anywhere in the frequency band. If the noise falls somewhere between f and any Δf, the noise is detected by multiple sinc functions and the magnitude is added to the noise value for all sinc functions. What if the JNT signal does not fall where a single sinc function will capture it? Furthermore, depending on where the signal spike falls, the multiple sinc functions detect different gains for the same noise signal. The EMI noise sources need to be differentiated and subtracted out appropriately. To do this, spectral estimation is used. Signals detected with a magnitude less than the standard deviation are captured. Signals with magnitudes greater than twice the standard deviation are removed and replaced with the baseline (or signal floor). Determining this signal floor is critical and can be incorrect if there is too much unwanted noise.

Once the data have gone through this process, the computations can begin. The PSD and CPSD for the channel outputs are calculated. Also, cross-frequency responses are needed. With this information and the Callendar-Van Dusen equation, the temperature is computed. The Callendar-Van Dusen equation is a mathematical

representation of the relationship between resistance and temperature of a platinum RTD; refer to Equation 1.8 [31].

$$R(t) = R(0)[1 + A \times t + B \times t^2 + (t - 100)C \times t^3]; \tag{1.8}$$

where $R(0)$ is the resistance measured at $0°C$ and A, B, and C are constants derived from resistance measurements across a range of temperatures. As a function of temperature, RTD exhibits a nonlinear parabolic resistance. A table of values for $R(0)$, A, B, and C for each RTD and cable combination is built for testing. These computations depend highly on clean data from each of the channel outputs and the coherence between them. Coherence refers to how similar the output arrays are across the given time or frequency domain. Then the signal processing starts all over with a new block of data.

Ultimately, the goal of this research is to measure temperature reliably, repeatably, and independently of electronics and EMI. The temperature is dependent on many variables that are influenced by EMI corruption. The cross power spectral density $G_{12}(f)$ (explained in Chapter 2) is greatly influenced by EMI corruption. Correctly calculating $G_{12}(f)$ depends on good EMI removal techniques as well as a full understanding of what this variable represents. $G_{12}(f)$'s distribution is derived in the next section. If $G_{12}(f)$'s distribution does not follow these derivations, the temperature computation will be incorrect.

1.6 Random Processes and Probability Density Functions

Random processes are discussed in this chapter to fully explain the complexity of measuring the sensor noise voltage, the EMI noise voltage, and other noise voltage sources. The study of random variables is an approach to mapping outcomes from random processes to numbers. The mapping of these random processes to quantifiable

values is important because then mathematical notation can be applied to these outcomes. There are two types of random variables: discrete and continuous. Discrete random variables take values in a finite or countable set, while continuous random variables take on values in an interval or collection of intervals. The most common mathematical notation applied to random variables is the probability density function.

The probability density function represents the probability that a random variable falls between two limits. The probability density function is given by the following equation:

$$f_X(x) = \frac{d}{dx} F_X(x), \tag{1.9}$$

where $f_X(x)$ is the probability per unit x and $F_X(x)$ is the probability [1]. The probability density function has four properties:

1. $f_X(x)$ is non-negative, $f_X(x) \geqslant 0$, - $\infty < x < \infty$
2. $f_X(x)$ has unit area, $\int_{-\infty}^{\infty} f_X(x)dx = 1$
3. $F_X(x)$ is the cumulative integral of $f_X(x)$, $\int_{-\infty}^{x} f_X(\lambda)d\lambda$
4. The probability that X falls between two limits is the integral of the probability density function between those two limits: $\mathrm{P}[x_1 < x \leqslant x_2] = \int_{x_1}^{x_2} f_X(x)dx$

The probability density function is important in this research because the noise voltage associated with JNT is a random process. The output voltages of each channel chnl1 ($V_1(f)$) and chnl2 ($V_2(f)$) are complex-value random processes with a Gaussian distribution for the real and imaginary parts and a mean equal to zero.

$V_1(f)$ is the FT of $v_1(t)$ with both its real and imaginary parts having a mean of zero [32]. Equations 1.10-1.15 derive the transformation of the moments or the variance and covariance [33].

$$\begin{aligned}
&\mathbf{E}\left[v_1^*(t)v_1(\tau)\right] \\
&= \mathbf{E}\left[\{[(v_{Rs}^*(t)+v_{Rc}^*(t))*h_s^*(t)]*h_1^*(t)\}\{[(v_{Rs}(\tau)+v_{Rc}(\tau))*h_s(\tau)]*h_1(\tau)\}\right]
\end{aligned} \tag{1.10}$$

where

$$\begin{aligned}
v_1^*(t) &= [(v_{Rs}^*(t)+v_{Rc}^*(t))*h_s^*(t)]*h_1^*(t) \\
&= v_{Rs}^*(t)*h_s^*(t)*h_1^*(t)+v_{Rc}^*(t)*h_s^*(t)*h_1^*(t)+v_{a1}^*(t)*h_1^*(t) \\
&= v_{Rs}^*(t)*h^*(t)+v_{Rc}^*(t)*h^*(t)+v_{a1}^*(t)*h_1^*(t) \\
&= \int_0^t [h^*(t-\tau_2)\times v_{Rs}^*(\tau_2)]\,d\tau_2+\int_0^t [h^*(t-\tau_2)\times v_{Rc}^*(\tau_2)]\,d\tau_2 \\
&\quad+\int_0^t [h_1^*(t-\tau_2)\times v_{a1}^*(\tau_2)]\,d\tau_2 \\
&= \int_0^t [h^*(t-\tau_2)\times v_{Rs}^*(\tau_2)+h^*(t-\tau_2)\times v_{Rc}^*(\tau_2) \\
&\qquad+h_1^*(t-\tau_2)\times v_{a1}^*(\tau_2)]d\tau_2,
\end{aligned} \tag{1.11}$$

with $h^*(t)=h_s^*(t)*h_1^*(t)=\int_0^t h_s^*(t-\tau)h_1^*(\tau)d\tau$ [33].

$$
\begin{aligned}
v_1(\tau) &= [(v_{Rs}(\tau) + v_{Rc}(\tau)) * h_s(\tau)] * h_1(\tau) \\
&= v_{Rs}(\tau) * h_s(\tau) * h_1(\tau) + v_{Rc}(\tau) * h_s(\tau) * h_1(\tau) + v_{a1}(t) * h_1(\tau) \\
&= v_{Rs}(\tau) * h(\tau) + v_{Rc}(\tau) * h(\tau) + v_{a1}(\tau) * h_1(\tau) \\
&= \int_0^\tau [h(\tau - \tau_5) \times v_{Rs}(\tau_5)]\, d\tau_5 + \int_0^\tau [h(\tau - \tau_5) \times v_{Rc}(\tau_5)]\, d\tau_5 \\
&\quad + \int_0^\tau [h_1(\tau - \tau_5) \times v_{a1}(\tau_5)]\, d\tau_5 \\
&= \int_0^\tau [h(\tau - \tau_5) \times v_{Rs}(\tau_5) + h(\tau - \tau_5) \times v_{Rc}(\tau_5) \\
&\qquad + h_1(\tau - \tau_5) \times v_{a1}(\tau_5)] d\tau_5,
\end{aligned}
\tag{1.12}
$$

with $h^*(\tau) = h_s^*(\tau) * h_1^*(\tau) = \int_0^\tau h_s^*(\tau - \tau_3) h_1^*(\tau_3) d\tau_3$ [33], $h_s(\tau)$ is the frequency response from the sensor to the amplifier inputs, and $h_1(\tau)$ is the amplifier/filter combination frequency response of chnl1.

$$
\begin{aligned}
&[v_1^*(t)v_1(\tau)] = \\
&\left[\int_0^t (h^*(t-\tau_2)v_{Rs}^*(\tau_2) + h^*(t-\tau_2)v_{Rc}^*(\tau_2) + h_1^*(t-\tau_2)v_{a1}^*(\tau_2))d\tau_2\right] \times \\
&\left[\int_0^\tau (h(\tau-\tau_5)v_{Rs}(\tau_5) + h(\tau-\tau_5)v_{Rc}(\tau_5) + h_1(\tau-\tau_5)v_{a1}(\tau_5))d\tau_5\right] \\
&= \int_0^t \int_0^\tau [(h^*(t-\tau_2)v_{Rs}^*(\tau_2) + h^*(t-\tau_2)v_{Rc}^*(\tau_2) + h_1^*(t-\tau_2)v_{a1}^*(\tau_2))\times \\
&\qquad (h(\tau-\tau_5)v_{Rs}(\tau_5) + h(\tau-\tau_5)v_{Rc}(\tau_5) + h_1(\tau-\tau_5)v_{a1}(\tau_5))]d\tau_5 d\tau_2 \\
&= \int_0^t \int_0^\tau [h^*(t-\tau_2)h(\tau-\tau_5)v_{Rs}^*(\tau_2)v_{Rs}(\tau_5) \\
&\qquad + h^*(t-\tau_2)h(\tau-\tau_5)v_{Rs}^*(\tau_2)v_{Rc}(\tau_5) \\
&\qquad + h^*(t-\tau_2)h_1(\tau-\tau_5)v_{Rs}^*(\tau_2)v_{a1}(\tau_5) \\
&\qquad + h^*(t-\tau_2)h(\tau-\tau_5)v_{Rc}^*(\tau_2)v_{Rs}(\tau_5) \\
&\qquad + h^*(t-\tau_2)h(\tau-\tau_5)v_{Rc}^*(\tau_2)v_{Rc}(\tau_5) \\
&\qquad + h^*(t-\tau_2)h_1(\tau-\tau_5)v_{Rc}^*(\tau_2)v_{a1}(\tau_5) \\
&\qquad + h_1^*(t-\tau_2)h(\tau-\tau_5)v_{a1}^*(\tau_2)v_{Rs}(\tau_5) \\
&\qquad + h_1^*(t-\tau_2)h(\tau-\tau_5)v_{a1}^*(\tau_2)v_{Rc}(\tau_5) \\
&\qquad + h_1^*(t-\tau_2)h(\tau-\tau_5)v_{a1}^*(\tau_2)v_{a1}(\tau_5)] \quad d\tau_5 d\tau_2
\end{aligned}
\tag{1.13}
$$

$$
\begin{aligned}
&\mathbf{E}\left[v_1(t)^* v_1(\tau)\right] \\
&= \mathbf{E}[\int_0^t \int_0^\tau [h^*(t-\tau_2)h(\tau-\tau_5)v_{Rs}^*(\tau_2)v_{Rs}(\tau_5) \\
&\qquad + h^*(t-\tau_2)h(\tau-\tau_5)v_{Rs}^*(\tau_2)v_{Rc}(\tau_5) \\
&\qquad + h^*(t-\tau_2)h_1(\tau-\tau_5)v_{Rs}^*(\tau_2)v_{a1}(\tau_5) \\
&\qquad + h^*(t-\tau_2)h(\tau-\tau_5)v_{Rc}^*(\tau_2)v_{Rs}(\tau_5) \\
&\qquad + h^*(t-\tau_2)h(\tau-\tau_5)v_{Rc}^*(\tau_2)v_{Rc}(\tau_5) \\
&\qquad + h^*(t-\tau_2)h_1(\tau-\tau_5)v_{Rc}^*(\tau_2)v_{a1}(\tau_5) \\
&\qquad + h_1^*(t-\tau_2)h(\tau-\tau_5)v_{a1}^*(\tau_2)v_{Rs}(\tau_5) \\
&\qquad + h_1^*(t-\tau_2)h(\tau-\tau_5)v_{a1}^*(\tau_2)v_{Rc}(\tau_5) \\
&\qquad + h_1^*(t-\tau_2)h(\tau-\tau_5)v_{a1}^*(\tau_2)v_{a1}(\tau_5)] \quad d\tau_5 d\tau_2] \\
&= \int_0^t \int_0^\tau [h^*(t-\tau_2)h(\tau-\tau_5)d\tau_5 d\tau_2]\mathbf{E}[v_{Rs}^*(\tau_2)v_{Rs}(\tau_5) + v_{Rs}^*(\tau_2)v_{Rc}(\tau_5) \\
&\qquad + v_{Rs}^*(\tau_2)v_{a1}(\tau_5) + v_{Rc}^*(\tau_2)v_{Rs}(\tau_5) + v_{Rc}^*(\tau_2)v_{Rc}(\tau_5) + v_{Rc}^*(\tau_2)v_{a1}(\tau_5)] \\
&+ \int_0^t \int_0^\tau [h_1^*(t-\tau_2)h(\tau-\tau_5)]\mathbf{E}[v_{a1}^*(\tau_2)v_{Rs} + v_{a1}^*(\tau_2)v_{Rc} \\
&\qquad + v_{a1}^*(\tau_2)v_{a1}(\tau_5)]d\tau_5 d\tau_2].
\end{aligned}
\tag{1.14}
$$

if $\tau_5 \neq \tau_2$, $\mathbf{E}[v_{Rs}^*(\tau_2)v_{Rs}(\tau_5)] = 0$ because $\mathbf{E}[v_{Rs}^*(\tau_2)] = 0$ and $\mathbf{E}[v_{Rs}(\tau_5)] = 0$. Also, $\mathbf{E}[v_{Rs}^*(\tau_2)v_{Rc}(\tau_5)] = 0$, $\mathbf{E}[v_{Rs}^*(\tau_2)v_{a1}(\tau_5)] = 0$, $\mathbf{E}[v_{Rc}^*(\tau_2)v_{Rs}(\tau_5)] = 0$, $\mathbf{E}[v_{Rc}^*(\tau_2)v_{Rc}(\tau_5)] = 0$, $\mathbf{E}[v_{Rc}^*(\tau_2)v_{a1}(\tau_5)] = 0$, $\mathbf{E}[v_{a1}^*(\tau_2)v_{Rs}(\tau_5)] = 0$, $\mathbf{E}[v_{a1}^*(\tau_2)v_{Rc}(\tau_5)] = 0$, $\mathbf{E}[v_{a1}^*(\tau_2)v_{a1}(\tau_5)] = 0$, $\mathbf{E}[v_{a1}^*(\tau_2)v_{Rs}(\tau_5)] = 0$, $\mathbf{E}[v_{a1}^*(\tau_2)v_{Rc}(\tau_5)] = 0$, $\mathbf{E}[v_{a1}^*(\tau_2)v_{a1}(\tau_5)] = 0$ because $\mathbf{E}[v_{Rc}^*(\tau_2)] = 0$, $\mathbf{E}[v_{a1}^*(\tau_2)] = 0$, $\mathbf{E}[v_{Rc}(\tau_5)] = 0$, $\mathbf{E}[v_{a1}^*(\tau_5)] = 0$. Therefore if $\tau_5 \neq \tau_2$, all of the signals are uncorrelated.

If $\tau_5 = \tau_2$, $\mathbf{E}[v_{Rs}^*(\tau_2)v_{Rs}(\tau_5)]$ is correlated, $\mathbf{E}[v_{Rc}^*(\tau_2)v_{Rc}(\tau_5)]$ is correlated, $\mathbf{E}[v_{a1}^*(\tau_2)v_{a1}(\tau_5)]$ is correlated. All other expected values equal zero since the voltages are uncorrelated even when $\tau_5 = \tau_2$. This simplifies Equation 1.14 to Equation 1.15

[33].

$$
\begin{aligned}
&\mathbf{E}\left[v_1^*(t)v_1(\tau)\right] \\
&= \int_0^t \int_0^\tau [h^*(t-\tau_2)h(\tau-\tau_5)d\tau_5 d\tau_2]\mathbf{E}[v_{Rs}^*(\tau_2)v_{Rs}(\tau_5) + v_{Rc}^*(\tau_2)v_{Rc}(\tau_5)] \\
&\quad + \int_0^t \int_0^\tau [h_1^*(t-\tau_2)h(\tau-\tau_5)d\tau_5 d\tau_2]\mathbf{E}[v_{a1}^*(\tau_2)v_{a1}(\tau_5)] \\
&= \int_0^t \int_0^\tau [h^*(t-\tau_2)h(\tau-\tau_2)d\tau_2 d\tau_2]\mathbf{E}[v_{Rs}^*(\tau_2)v_{Rs}(\tau_2) + v_{Rc}^*(\tau_2)v_{Rc}(\tau_2)] \\
&\quad + \int_0^t \int_0^\tau [h_1^*(t-\tau_2)h(\tau-\tau_2)d\tau_2 d\tau_2]\mathbf{E}[v_{a1}^*(\tau_2)v_{a1}(\tau_2)] \\
&= \int_0^t [h^*(t-\tau_2)h(\tau-\tau_2)d\tau_2]\mathbf{E}[v_{Rs}^*(\tau_2)v_{Rs}(\tau_2) + v_{Rc}^*(\tau_2)v_{Rc}(\tau_2)] \\
&\quad + \int_0^t [h_1^*(t-\tau_2)h(\tau-\tau_2)d\tau_2]\mathbf{E}[v_{a1}^*(\tau_2)v_{a1}(\tau_2)] \\
&= \int_0^t [h^*(t-\tau_2)h(\tau-\tau_2)d\tau_2]\mathbf{E}[|v_{Rs}^*(\tau_2)|^2 + |v_{Rc}^*(\tau_2)|^2] \\
&\quad + \int_0^t [h_1^*(t-\tau_2)h(\tau-\tau_2)d\tau_2]\mathbf{E}[|v_{a1}^*(\tau_2)|^2],
\end{aligned}
\tag{1.15}
$$

Therefore, the assumption can be made that Equation 1.10 simplifies to Equation 1.16.

$$
\mathbf{E}\left[v_1^*(t)v_1(\tau)\right] = \left(\mathbf{E}\left[|v_{Rs}(t)|^2\right] + \mathbf{E}\left[|v_{Rc}(t)|^2\right] + \mathbf{E}\left[|v_{a1}(t)|^2\right]\right) * h_s^2 * h_1^2. \tag{1.16}
$$

The $|v_{Rs}^*(\tau_2)|^2$, $|v_{Rc}^*(\tau_2)|^2$, $|v_{a1}^*(\tau_2)|^2$ have chi-square distribution with a mean equal to zero and a variance equal to the square of the standard deviation. Therefore, $[v_1^*(t)v_1(\tau)]$ has a gaussian distribution when $\tau_5 = \tau_2$ because the product of two

gaussian distributed random variables is another gaussian distribution [34]. Also, the variance of $[v_2^*(t)v_2(\tau)]$ has a gaussian distribution when $\tau_5 = \tau_2$. It can then be concluded that:

$$G_{12}(f) = \mathbf{E}\left[\frac{v_1^*(f)v_2(f)}{\Delta}\right] \tag{1.17}$$

$G_{12}(f)$'s real and imaginary parts have a chi-square distribution when normalized because $G_{12}(f)$ is an estimate of an expected value of the random process. The chi-square distribution is a specific case of the Fox H-function. The Fox H-function or the "H-function law" is a symmetric Fourier kernel to the general Meijer G-function (Figure 1.12) [35], [36]. It is transformed by means of the Mellin integral transform. The H-function distribution was introduced by Charles Fox in 1961 [37]. Cornelis Simon Meijer introduced the G-function in 1936 with which his name is associated. The definition of the H-function is given in Equations 1.18 and 1.19 [35]. There are some slight variations of this definition, but this will be the one used here, where $0 \leq m \leq q$, $0 \leq n \leq p$, $\alpha_j > 0$ for j $= 1, 2, ..., p$, $\beta_j > 0$ for j $= 1, 2, ..., q$. Note, $\alpha_j > 0$ for j $= 1, 2, ..., p$, $\beta_j > 0$ for j $= 1, 2, ..., q$ are complex numbers and therefore no pole of $\Gamma(b_j - \beta_j s)$ for j $= 1, 2, ..., m$ occurs with any pole of $\Gamma(1 - \alpha_j + \alpha_j s)]$ for j $= 1, 2, ..., m$.

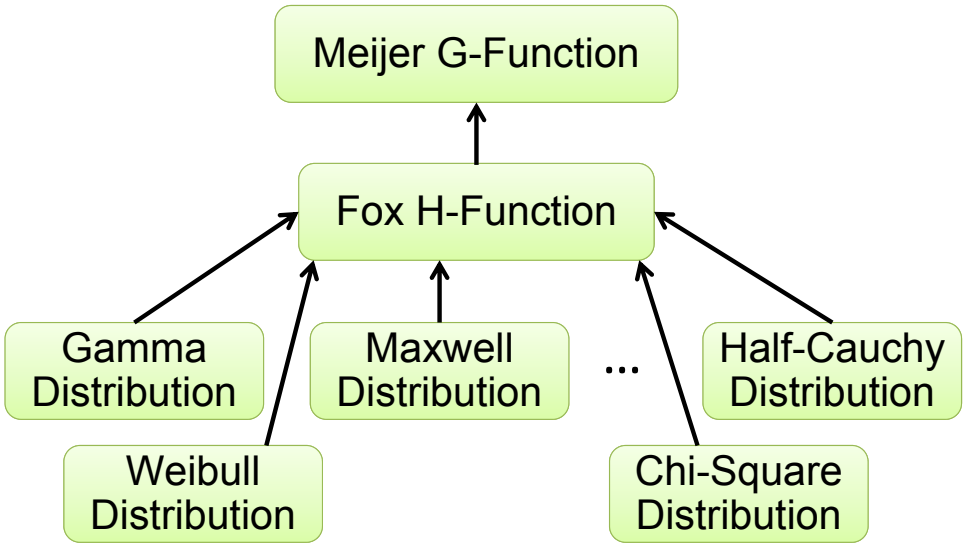

Figure 1.12: Flow chart of distribution functions

$$\mathbf{H}_{p,q}^{m,n}\left[z\left|\begin{matrix}(a_1,\alpha_1), & \ldots & ,(a_p,\alpha_p)\\ (b_1,\beta_1), & \ldots & ,(b_q,\beta_q)\end{matrix}\right.\right] = H(z) \tag{1.18}$$

$$H(z) = \frac{1}{2\pi i}\int_C \frac{\left[\prod_{j=1}^{m}\Gamma(b_j-\beta_j s)\right]\left[\prod_{j=1}^{n}\Gamma(1-a_j+\alpha_j s)\right]}{\left[\prod_{j=m+1}^{q}\Gamma(1-b_j+\beta_j s)\right]\left[\prod_{j=n+1}^{p}\Gamma(a_j-\alpha_j s)\right]} z^s ds \tag{1.19}$$

$$= \mathcal{M}^{-1}\left(\frac{\left[\prod_{j=1}^{m}\Gamma(b_j+\beta_j s)\right]\left[\prod_{j=1}^{n}\Gamma(1-a_j-\alpha_j s)\right]}{\left[\prod_{j=m+1}^{q}\Gamma(1-b_j-\beta_j s)\right]\left[\prod_{j=n+1}^{p}\Gamma(a_j+\alpha_j s)\right]}\right)$$

where $\mathcal{M}^{-1}$ is the inverse Mellin transform [38]. The H-function distribution is specified by its probability density function, and the relevant range is equal to one due to multiplying the H-function by a normalizing constant. It is a transcendental function that does not have a unity integral over a given range. What makes it relevant to this research is that it is a generalized form of many special cases of classical distribution, as shown in Figure 1.12. It allows for simplified handling of algebraic functions of "mixtures" of these special variables [37]. Equation 1.20 defines the special case of the H-function chi-square distribution [35].

$$\text{Let } \theta = \frac{v}{2} \text{ and } \phi = 2 \text{ for the gamma-distribution}$$
$$f(x) = \frac{x^{\theta-1}e^{-x/\phi}}{\phi^{\theta}\Gamma(\theta)}, \text{ for } x > 0;\ \theta, \phi > 0.$$
$$\text{Therefore the chi-square distribution is} \tag{1.20}$$
$$f(x) = \frac{x^{\frac{v}{2}-1}e^{-x/2}}{2^{\frac{v}{2}}\Gamma(\frac{v}{2})}, \text{ for } x > 0;\ v > 0$$
$$f(x) = \frac{1}{2\Gamma(\frac{v}{2})}\mathbf{H}_{0,1}^{1,0}\left[\frac{1}{2}x \,\middle|\, \left(\frac{v}{2} - 1, 1\right)\right].$$

An evaluation of the H-function properties is another way to prove that $G_{12}(f)$'s real and imaginary parts have a chi-square distribution when normalized. It is also important to understand the mixture of chi-square distributions for the computation of H_p. First, determine if the product of two H-function random variables is another H-function random variable. Then, determine whether the ratio of two H-function random variables is another H-function random variable.

Deriving the product of H-function random variables, using Theorem 6.4.1 from [35]:

$$f_j(x_j) = \begin{cases} k_j \mathbf{H}_{p_j,q_j}^{m_j,n_j}\left[c_j x_j \,\middle|\, \begin{matrix}(a_{j1},\alpha_{j1}), & \ldots & ,(a_{jp_j},\alpha_{jp_j}) \\ (b_{j1},\beta_{j1}), & \ldots & ,(b_{jq_j},\beta_{jq_j})\end{matrix}\right] & ,x_j > 0 \\ 0 & ,\text{otherwise.} \end{cases} \tag{1.21}$$

where $j = 1, 2, ..., n$ and then for the random variable $Y = \prod_{j=1}^{n} X_j$ the probability density function is [35]

$$h(y) = \begin{cases} \left(\prod_{j=1}^{n} k_j\right) \mathbf{H}_{\sum_{j=1}^{n} p_j, \sum_{j=1}^{n} q_j}^{\sum_{j=1}^{n} m_j, \sum_{j=1}^{n} n_j} \left[\prod_{j=1}^{n} c_j y \,\middle|\, \begin{matrix} (a_{11}, \alpha_{11}), & \ldots & , (a_{np_j}, \alpha_{np_j}) \\ (b_{11}, \beta_{11}), & \ldots & , (b_{nq_j}, \beta_{nq_j}) \end{matrix} \right] & , y > 0 \\ 0 & , \text{otherwise.} \end{cases} \tag{1.22}$$

where the sequence of parameters (a_{jv}, α_{jv}) is $v = 1, 2, ..., n_j$ for $j = 1, 2, ..., n$, and $v = n_j + 1, n_j + 2, ..., p_j$ for $j = 1, 2, ..., n$. And the sequence of parameters (b_{jv}, β_{jv}) is: $v = 1, 2, ..., m_j$ for $j = 1, 2, ..., n$, and $v = m_j + 1, m_j + 2, ..., q_j$ for $j = 1, 2, ..., n$ [35].

From [35] PROOF: The Mellin transform of $f_j(x_j)$ is:

$$\mathcal{M}_s\{f_j(x_j)\} = \frac{k_j}{c_j^s} \frac{\left[\prod_{v=1}^{m_j} \Gamma(b_{vj} + \beta_{vj} s)\right] \left[\prod_{v=1}^{n_j} \Gamma(1 - a_{vj} - \alpha_{vj} s)\right]}{\left[\prod_{v=m_j+1}^{q_j} \Gamma(1 - b_{vj} - \beta_{vj} s)\right] \left[\prod_{v=n_j+1}^{p_j} \Gamma(a_{vj} + \alpha_{vj} s)\right]}, \tag{1.23}$$

using

$$h_n(y) = \frac{1}{2\pi i} \int_{c-i\infty}^{c+i\infty} y^{-s} \prod_{i=1}^{n} M_s(f_i(x_i)) ds, \qquad c_1 < c < c_2 \tag{1.24}$$

$$\begin{aligned} h^+(y) &= \mathcal{M}^{-1}\left[\prod_{j=1}^{n} \mathcal{M}_s\{f_j(x_j)\}\right], \qquad y > 0 \\ &= \mathcal{M}^{-1}\left[\prod_{j=1}^{n} \left(\frac{k_j}{c_j^s} \frac{\left[\prod_{v=1}^{m_j} \Gamma(b_{vj} + \beta_{vj} s)\right] \left[\prod_{v=1}^{n_j} \Gamma(1 - a_{vj} - \alpha_{vj} s)\right]}{\left[\prod_{v=m_j+1}^{q_j} \Gamma(1 - b_{vj} - \beta_{vj} s)\right] \left[\prod_{v=n_j+1}^{p_j} \Gamma(a_{vj} + \alpha_{vj} s)\right]} \right)\right], \end{aligned}$$

for $y > 0$

(1.25)

Therefore, from the inverse Mellin transform

$$\frac{1}{2\pi i}\lim_{\beta\to\infty}\int_{c-i\infty}^{c+i\infty} x^{-s}\mathcal{M}_s(f(x))ds. \tag{1.26}$$

Equation 1.25 can be derived across the integral $(c-i\infty, c+i\infty)$:

$$\begin{aligned} h^+(y) &= \frac{\prod_{j=1}^{n} k_j}{2\pi i}\int \frac{\left[\prod_{j=1}^{n}\prod_{v=1}^{m_j}\Gamma(b_{vj}+\beta_{vj}s)\right]\left[\prod_{j=1}^{n}\prod_{v=1}^{m_j}\Gamma(1-a_{vj}-\alpha_{vj}s)\right]}{\left[\prod_{j=1}^{n}\prod_{v=m_j+1}^{q_j}\Gamma(1-b_{vj}-\beta_{vj}s)\right]\left[\prod_{j=1}^{n}\prod_{v=n_j+1}^{p_j}\Gamma(a_{vj}+\alpha_{vj}s)\right]} \\ &\qquad \cdot\left(\left[\prod_{j=1}^{n} c_j\right] y\right)^{-s} ds \\ &= \left(\prod_{j=1}^{n} k_j\right)\mathbf{H}_{\sum_{j=1}^{n} p_j,\sum_{j=1}^{n} q_j}^{\sum_{j=1}^{n} m_j,\sum_{j=1}^{n} n_j}\left[\left(\prod_{j=1}^{n} c_j\right) y \,\middle|\, \begin{matrix}(a_{11},\alpha_{11}), & \ldots & ,(a_{np_n},\alpha_{np_n}) \\ (b_{11},\beta_{11}), & \ldots & ,(b_{nq_n},\beta_{nq_n})\end{matrix}\right]. \end{aligned} \tag{1.27}$$

Therefore, the product of two random processes with chi-square distribution is another random process with chi-square distribution. A general derivative of chi-square distribution is given here. "χ_n^2" represents the chi-square variable with n degrees of freedom [39]. The PDF of χ_n^2 is given in Equation 1.28 [40].

$$p(\chi^2) = \left[2^{n/2}\Gamma(n/2)\right]^{-1}(\chi^2)^{((n/2)-1)}e^{\chi^2/2}, \quad \chi^2 \geq 0 \tag{1.28}$$

where $\Gamma(n/2)$ is the gamma function. The mean and variance of χ_n^2 are given in Equation 1.29 and 1.30 [39].

$$\mathbf{E}\left[\chi_n^2\right] = \mu_{\chi^2} \tag{1.29}$$

$$\mathbf{E}\left[\left(\chi_n^2 - \mu_{\chi^2}\right)\right] = \sigma_{\chi^2}^2 \tag{1.30}$$

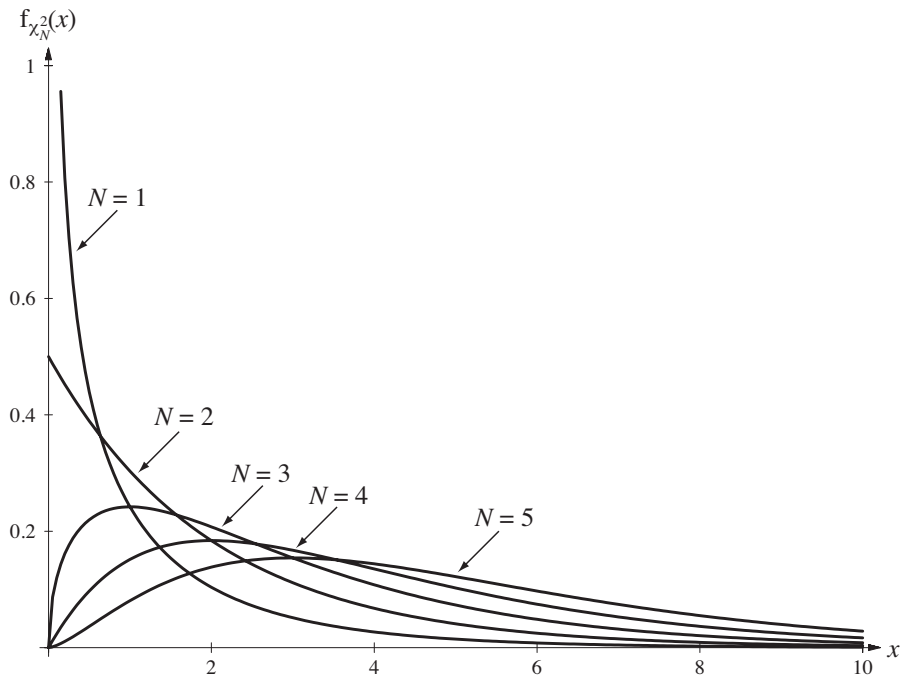

Figure 1.13: PDF of chi-square distribution [1]

Next, the ratio of two random processes with chi-square distribution is evaluated. If y_1 is a chi-square distribution with k_1-degrees of freedom and y_2 is a chi-square with k_2-degrees of freedom; then the density function of $w = y_1 y_2$ is displayed in Equation 1.31 [41]. Where y_2 independent of y_1.

$$h(w) = \frac{w^{\frac{1}{2}k_1+\frac{1}{2}k_2-1} K_{\frac{1}{2}k_1-\frac{1}{2}k_2}(w^{\frac{1}{2}})}{2^{\frac{1}{2}k_1+\frac{1}{2}k_2-1}\Gamma(\frac{1}{2}k_1)\Gamma(\frac{1}{2}k_2)} \tag{1.31}$$

If y_1 and y_2 are independent chi-square distributions with degrees of freedom differing by one (i.e., $k_2 = k_1 + 1$) then the distribution of $h(w)$ is also chi-square with $2k_1$-degrees of freedom [41]. Where $K_{\frac{1}{2}}(w^{\frac{1}{2}}) = \frac{1}{2}[(2\pi)^{\frac{1}{2}} e^{-w^{\frac{1}{2}}} w^{-\frac{1}{2}}]$ and $\Gamma(\frac{1}{2}k_1)\Gamma(\frac{1}{2}k_1 + \frac{1}{2}) = \pi^{\frac{1}{2}} 2^{1-k_1}\Gamma(k_1)$ [41].

The chi-square distribution with n-degrees of freedom converges to gaussian distribution as $n \to \infty$. From this the ratio and product of the distribution is based off of gaussian mixtures. The product of two gaufssian distributions is another gaussian distribution [34]

1.7 Direct Contribution to Research

- Contribution: Develop, optimize, and validate JNT signal processing with EMI removal techniques
- Key Attribute: The ability to remove the EMI without biasing the noise measurement
- Novelty: White noise is the signal of interest. Typically, systems focus on minimizing the effects of white noise, whereas this system relies on it. This makes the measurement uniquely difficult. The application of this signal processing to JNT will limit human exposure to hazardous radiological environments, will allow for shorter nuclear reactor shutdown times, and therefore will save money.

To achieve the goals listed above, the following tasks were completed

1. Review data obtained while performing measurements with JNT system before any EMI spikes have been removed and after EMI spikes are removed. Remove EMI spikes without biasing the overall temperature measurement
2. Analyze effects of the removal of EMI spikes on the resistor PSD (RPSD)
3. Estimate where the EMI spikes are located and how large they are (demonstrate accurate mode)
4. Perform numerical and experimental verification
    - Compute $G_{12}(f)$, $G_{12-E}(f)$, and PDF of RPSD
    - Validate algorithm though MATLAB simulations
        (a) Simple EMI case (single TD sine wave)
        (b) Complex EMI case (multiple TD sine waves)
        (c) a,b with multiple EMI spike to find limits of the model

(d) Simulate testing the limits of the model

(e) EMI environment similar to JNT environment (ambient, broadband, Sandia, and single sine)

Chapter 2

Existing Signal Processing Technique: Rejection Method

2.1 Spectral Estimation

Two techniques of spectral estimation are parametric and nonparametric. Parametric techniques are generally used when there is a known functional model of the system and the only thing lacking is a parameter value or values within the model. Parametric techniques assume that, while using a small number of parameters, a model of a fundamental stationary stochastic process can be fully defined. These parameters must then be found or estimated. Nonparametric techniques do not rely on a known functional model of the system. Instead, they estimate the spectrum of the process without assuming any parameters or fundamental stationary stochastic structures.

2.2 ORNL Techniques for Spectral Estimation

For the signal processing used in the JNT project, a nonparametric technique is applied within the JNT software. In principle, a parametric technique could be used if the amplifiers and filter hardware were modeled accurately. However, it is not

known whether these parameters are reliable over extended periods of testing. One of the goals of the signal processing is to detect if/when the amplifier gain or the filter poles and zero locations change. These parameters could be used with this technique, but that requires a nonlinear least-squares fit approach to the parameter estimation. The nonlinear least-squares approach causes problems with convergence due to the number of estimated parameters and the amount of time required to perform the computation. In addition to these parameters, we have EMI that complicates the parameter estimation of the amplifier gain and filter poles/zero locations. EMI adds further complexity to the signal processing. Using nonparametric techniques for this temperature measurement allows for better PSD and CPSD estimates. The longer the temperature measurement runs, the better the estimate becomes [2]. A discussion of this follows in this chapter.

2.3 Power Spectral Density and Cross Power Spectral Density

PSD is the signal power within a unit bandwidth. Estimation of PSD is commonly done by sampling a stochastic process for a finite time and analyzing the samples with the discrete Fourier transform (DFT) [1]. The PSD of white noise is constant for a given temperature. In other words, the PSD of white noise is constant power per frequency. The double-sided PSD of the open-circuit noise voltage of any resistance is given by Equation 2.1 and is derived from the noise voltage in Equation 1.2. This equation was developed by Harry Nyquist while working at Bell Telephone Laboratory [10].

$$G_v(f) = \left[\frac{2hfR}{exp(hf/kt) - 1}\right], \tag{2.1}$$

where at low frequencies ($f < 100\text{GHz}$), the PSD is approximated by

$$G_v(f) = 2kTR. \tag{2.2}$$

This is true for any resistance at any temperature regardless of its composition or past history [2]. Because the application is to reliably measure absolute temperature over a long period of time regardless of degradation of the sensor, the resistor temperature measurement is possible using only two of the following: (1) the PSD of the open-circuit noise voltage, (2) the PSD of the short-circuit noise current, and (3) the resistance of the sensor. For this application, (1), the open-circuit noise voltage PSD, and (3), sensor resistance, are used for absolute temperature calculation. Even though the sensor resistance drifts over time, it is still possible to use it as one of the variable for resistance-temperature measurements. The real-time DC voltage of the resistor must be monitored as well as the averaged JNT resistance. Corrections can be made along the way to re-calibrate real-time DC voltage measurement. A few important properties of PSD [32] used in this research are listed in Table 2.1. These properties are explained below [1].

Table 2.1: List of Important PSD Properties

1. $G_{x,x}(f) = G_x(f) \geqslant 0$
2. $G_x(-f) = G_x(f)$
3. $G_x(f) = \text{real}$
4. $\int_{-\infty}^{\infty} G_x(f)df = [\mathbf{E}\{G_x(f)\}]$
5. $\int_{-\infty}^{\infty} G_x(f)e^{j2\pi f\tau}df = [R_x(t, t+\tau)]$
   $G_x(f) = \int_{-\infty}^{\infty} [R_x(t, t+\tau)]\, e^{-j2\pi f\tau}d\tau,$
   where $G_x(f)$ = time average of the auto-correlation function, forms a FT pair.

Intuitively, when thinking about EMI detection it seems natural to work in the frequency-domain. However, when analyzing random time-domain processes or signals with frequency-domain techniques, the FT are not as straightforward. The FT of a stochastic process does not exist because $x(t)$ technically exists for all time, and its energy is infinite. Therefore, the process must be truncated and then FTed. Analyzing a continuous time stochastic process, x_Δ, the following steps are taken to approximate the FT. First a new function is defined with a finite energy level.

$$x_\Delta(t) = \left\{ \begin{array}{c} x(t),\ |t| \leq \frac{\Delta}{2} \\ 0,\ |t| > \frac{\Delta}{2} \end{array} \right\} = x(t) rect(t/\Delta) \tag{2.3}$$

The strict sense FT of x_Δ with Δ infinite therefore is

$$x_\Delta(f) = \mathcal{F}(x_\Delta(t)) = \int_{-\infty}^{\infty} x_\Delta(t) e^{-j2\pi ft} dt. \tag{2.4}$$

Using Parseval's theorem:

$$\int_{-\Delta/2}^{\Delta/2} |(x_\Delta(t))|^2 dt = \int_{-\infty}^{\infty} |\mathcal{F}(x_\Delta(t))|^2 df. \tag{2.5}$$

Then dividing through by Δ to get the average signal power over Δ,

$$\frac{1}{\Delta} \int_{-\Delta/2}^{\Delta/2} (x_\Delta(t))^2 dt = \frac{1}{\Delta} \int_{-\infty}^{\infty} |\mathcal{F}(x_\Delta(t))|^2 df. \tag{2.6}$$

As Δ approaches infinity, the left side of the equation becomes the average power over all time, and so is the right side of the equation [1]. Even though the FT does not exist within those limits, the expected value of the FT does exist:

$$\mathbf{E}\left(\frac{1}{\Delta} \int_{-\Delta/2}^{\Delta/2} (x_\Delta(t))^2 dt \right) = \mathbf{E}\left[\frac{1}{\Delta} \int_{-\infty}^{\infty} |\mathcal{F}(x_\Delta(t))|^2 df \right] \tag{2.7}$$

or

$$\frac{1}{\Delta}\int_{-\Delta/2}^{\Delta/2}\mathbf{E}\left(x_\Delta(t))^2\right)dt=\frac{1}{\Delta}\int_{-\infty}^{\infty}\mathbf{E}\left[|\mathcal{F}(x_\Delta(t))|^2\right]df. \tag{2.8}$$

Now, taking the limit as Δ approaches infinity, the expected value of x^2 becomes

$$\lim_{\Delta\to\infty}\frac{1}{\Delta}\int_{-\Delta/2}^{\Delta/2}\mathbf{E}(x^2(t))dt=\lim_{\Delta\to\infty}\frac{1}{\Delta}\int_{-\infty}^{\infty}\mathbf{E}\left[|\mathcal{F}(x_\Delta(t))|^2\right]df \tag{2.9}$$

$$\langle\mathbf{E}(x^2(t))\rangle=\int_{-\infty}^{\infty}\lim_{\Delta\to\infty}\mathbf{E}\left[\frac{|\mathcal{F}(x_\Delta(t))|^2}{\Delta}\right]df=\overline{X^2(f)}, \tag{2.10}$$

where the integral in the right hand side of is the PSD. This is the PSD because it is a measure of the average power per unit frequency of a random process [1].

$$G_X(f)=\lim_{\Delta\to\infty}\mathbf{E}\left[\frac{|\mathcal{F}(x_\Delta(t))|^2}{\Delta}\right] \tag{2.11}$$

and

$$\int_{-\infty}^{\infty}G_X(f)df=\text{signal mean - }x(t)^2=\text{average power of }x(t) \tag{2.12}$$

In the PSD for this research all the power is accounted across all frequency space, also called double-sided [1].

Analyzing a discrete time stochastic process, x_Δ, the following steps are taken to approximate the continuous time FT:

$$\Delta=N\times Ts \tag{2.13}$$

$$G_X(F)=\lim_{N\to\infty}\mathbf{E}\left(\frac{|\mathcal{F}(x_\Delta[n])|^2}{\Delta}\right) \tag{2.14}$$

and

$$\int_0^1 G_X(F)df=\text{signal mean - }x[n]^2 \tag{2.15}$$

where the FT is in discrete-time (DFT) defined by

$$x[n] = \mathcal{F}^{-1}(X(F)) = \int_0^1 X(F)e^{j2\pi Fn}dF \xleftrightarrow{\mathcal{F}} X(F) = \mathcal{F}(x[n]) = \sum_{n=-\infty}^{\infty} x[n]e^{-j2\pi Fn}$$

or (2.16)

$$x[n] = \mathcal{F}^{-1}(X(\Omega)) = \frac{1}{2\pi}\int_0^{2\pi} X(\Omega)e^{j\Omega n}d\Omega \xleftrightarrow{\mathcal{F}} X(\Omega) = \mathcal{F}(x[n]) = \sum_{n=-\infty}^{\infty} x[n]e^{-j\Omega n}.$$

Johnson noise is a continuous time stochastic process that has a constant PSD. It is known that the PSD of a short-circuit white noise current is $G_i(f) = \frac{2\ k\ T}{R}\left(\frac{A^2}{R}\right)$, where A is Amperes and the open-circuit noise voltage PSD is $G_v(f) = 2\ k\ T\ R\left(\frac{V^2}{Hz}\right)$. In the measurements performed for this research the JNT PSD is referred to as the RPSD. The RPSD calculated here is constant over the band-limited frequency range from 15 kHz to 40 kHz and is defined in Equation 2.33 below.

PSD is the FT of autocorrelation, and CPSD is the FT of cross-correlation. The CPSD properties are listed in Table 2.2 [32].

Table 2.2: List of CPSD Properties

1. $R_{XY}(t) \xleftrightarrow{\mathcal{F}} G_{XY}(f)$ or $R_{XY}[n] \xleftrightarrow{\mathcal{F}} G_{XY}(F)$
2. $G_{XY}(t) = G^*_{YX}(f)$ or $G_{XY}[n] = G^*_{YX}(F)$
3. $Re(G_{XY}(f))$ and $Re(G_{YX}(f))$ are both even
4. $Im(G_{XY}(t))$ and $Im(G_{YX}(f))$ are both odd

The next few sections illustrates how the algorithm developed in this research approximates the PSD theory to calculate the absolute temperature of a system being measured by an RTD.

2.4 Sampling Property

An important property to review when discussing PSD is the sampling property of an impulse. The sampling of a stochastic process (for a finite time) is most commonly used for estimation of PSD. The samples are analyzed using a DFT [1]. The definition of the sampling property is, if $g(x)$ is finite and differentiable at $x = x_0$, then

$$\int_{-\infty}^{\infty} g(x)\delta(x - x_0)dt = g(x_0), \tag{2.17}$$

where the product of $g(x)\delta(x - x_0) = g(x_0)\delta(x - x_0)$ because

$$\begin{aligned} g(x)\delta(x - x_0) &= g(x_0)\delta(x - x_0), \quad x = x_0 \\ g(x)\delta(x - x_0) &= g(x_0)\delta(x - x_0) = 0, \quad x \neq x_0 \end{aligned} \tag{2.18}$$

The importance of the sampling property becomes apparent in the section discussing the estimation of a power spectral density. When computing the PSD and CPSD the expected value is found causing the function to no longer be random. However, for this research an estimation of the expected value is computed. This is due to the sample mean property. X_n is a random process with N samples evenly distributed at $n = 1, 2, 3, ..., N$. The estimate of average N samples is found using Equation 2.19 [32].

$$\hat{\bar{X}}_N = \frac{1}{N}\sum_{n=1}^{N} X_n \tag{2.19}$$

where $\hat{\bar{X}}_N$ is a function of the set of samples $\{X_n\}$ and is the estimate of the mean of the random process. Equation 2.19 represents the effect of averaging over the random process and is called the sample mean. This allows for the probability density function of the resistor PSD to be found in chapter 4. In equation 2.20 the expected value is solved for [32].

$$\mathbf{E}\left[\hat{\bar{X}}_N\right] = \mathbf{E}\left[\frac{1}{N}\sum_{n=1}^{N} X_n\right] = \frac{1}{N}\sum_{n=1}^{N}\mathbf{E}\left[X_n\right] \tag{2.20}$$

The variance is solved using Equation 2.21 [32].

$$\begin{aligned}
\sigma^2_{X_N} &= \mathbf{E}\left[\left(\hat{\bar{X}}_N - \bar{X}\right)^2\right] \\
&= \mathbf{E}\left[\hat{\bar{X}}^2_N - 2\bar{X}\hat{\bar{X}}_N + \bar{X}^2\right] \\
&= \mathbf{E}\left[\hat{\bar{X}}^2_N\right] - \bar{X}^2 \\
&= -\bar{X}^2 + \mathbf{E}\left[\frac{1}{N}\sum_{n=1}^{N} X_n \frac{1}{N}\sum_{m=1}^{N} X_m\right] \\
&= 0 + \mathbf{E}\left[\frac{1}{N}\sum_{n=1}^{N} X_n \frac{1}{N}\sum_{m=1}^{N} X_m\right] \\
&= \frac{1}{N^2}\sum_{n=1}^{N}\sum_{m=1}^{N}\mathbf{E}\left[X_n X_m\right]
\end{aligned} \tag{2.21}$$

where $\mathbf{E}\left[X_n X_m\right] = \mathbf{E}\left[X^2\right]$ for $n = m$ [32] and $-\bar{X}^2 = mean = 0$. For Johnson noise the mean is zero and the variance is defined by the limits of the integral.

2.5 Mathematical Derivation for Power Spectral Density and Cross Power Spectral Density

The following information is from an unpublished document, by Dr. M. J. Roberts, discussing the mathematics behind the correlation techniques utilized in this research. After transient EMI is removed from the measured data (or the signal is windowed), the signal is FTed and periodic EMI is removed from the data, the PSD and CPSD are calculated from the output noise voltage of each amplifier/filter channel. This

process is derived in this section. Full derivation of these equations is in Appendix A [2].

$$\begin{aligned} v_1(t) &= \{[v_{Rs}(t) + v_{Rc}(t)] * h_s(t) + v_{a1}(t)\} * h_1(t) \\ v_2(t) &= \{[v_{Rs}(t) + v_{Rc}(t)] * h_s(t) + v_{a2}(t)\} * h_2(t), \end{aligned} \tag{2.22}$$

where $v_1(t)$ is the output voltage measured from amplifier/filter chnl1, $v_2(t)$ is the output voltage from amplifier/filter chnl2, $v_{Rc}(t)$ is the cable noise voltage with resistance of $R_c(t)$, $v_{Rs}(t)$ is the sensor noise voltage of the RTD with sensor resistance of R_s, $v_{a1}(t)$ is the input noise voltages of chnl1, and $h_1(t)$ is the impulse response of chnl1. Function $h_s(t)$ is the impulse response of sensor resistance in series with the cable resistance, and the cable capacitance in parallel with the input capacitances of the amplifier/filters, to sensor or cable resistance noise voltage. Figure 2.1 shows the JNT system with the noise sources. The FT of Equation 2.22 is given in Equation 2.23.

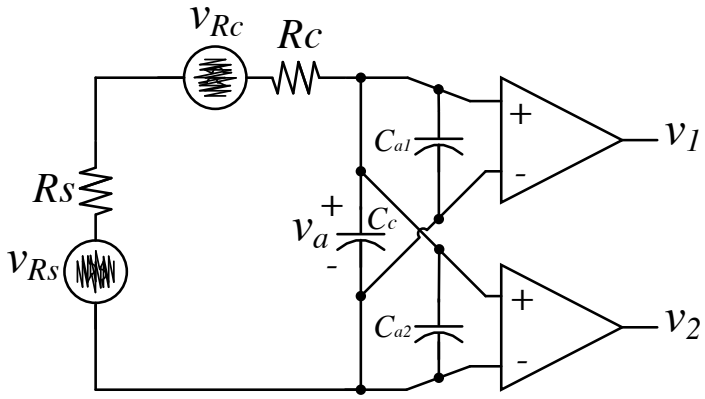

Figure 2.1: Simple electrical representation of JNT system and associated noise sources [2]

$$\begin{aligned} V_1(f) &= \{[V_{Rs}(f) + V_{Rc}(f)]H_s(f) + V_{a1}(f)\}H_1(f) \\ V_2(f) &= \{[V_{Rs}(f) + V_{Rc}(f)]H_s(f) + V_{a2}(f)\}H_2(f) \end{aligned} \tag{2.23}$$

Denoting these output voltages in the frequency domain, $V_{a1}(f)$ is the FT of the input noise voltage of chnl1. $H_1(f)$ is the frequency response of chnl1 to its input terminals where $H_1(f) = V_1(f)/V_a(f)$. And $H_s(f)$ is the frequency response of the sensor resistance in series with the cable resistance, and the cable capacitance in parallel with the input capacitances of the amplifiers/filters, to noise voltage of the sensor resistance or cable resistance, where

$$H_s(f) = \frac{1}{j2\pi f(R_s + R_c)C + 1} \tag{2.24}$$

The capacitance in the denominator is the parallel combination of the cable capacitance and the input capacitances of the amplifier/filter channels: $C = C_c + C_{a1} + C_{a2}$.

All of these calculations assume an ideal environment, which is not the case for the application environment. As discussed previously, there are many sources of EMI that contribute to the measurement and cause errors in the final temperature calculations. Hardware filtering and signal processing remove a large amount of EMI. The two sources of EMI spikes are transient (removed in time-domain signal processing) and periodic (removed in frequency-domain signal processing). Figure 2.2 is an electrical representation of the system with the noise sources and added EMI.

Taking into account the extra noise source for EMI, Equations 2.25 and 2.26 are the updated output voltage from each amplifier/filter channel and the updated frequency domain expression.

$$\begin{aligned} v_1(t) &= \{[v_{Rs}(t) + v_{Rc}(t) + v_E(t)] * h_s(t) + v_{a1}(t)\} * h_1(t) \\ v_2(t) &= \{[v_{Rs}(t) + v_{Rc}(t) + v_E(t)] * h_s(t) + v_{a2}(t)\} * h_2(t) \end{aligned} \tag{2.25}$$

$$
\begin{aligned}
V_1(f) &= \{[V_{Rs}(f) + V_{Rc}(f) + V_E(f)]H_s(f) + V_{a1}(f)\}H_1(f) \\
V_2(f) &= \{[V_{Rs}(f) + V_{Rc}(f) + V_E(f)]H_s(f) + V_{a2}(f)\}H_2(f)
\end{aligned}
\tag{2.26}
$$

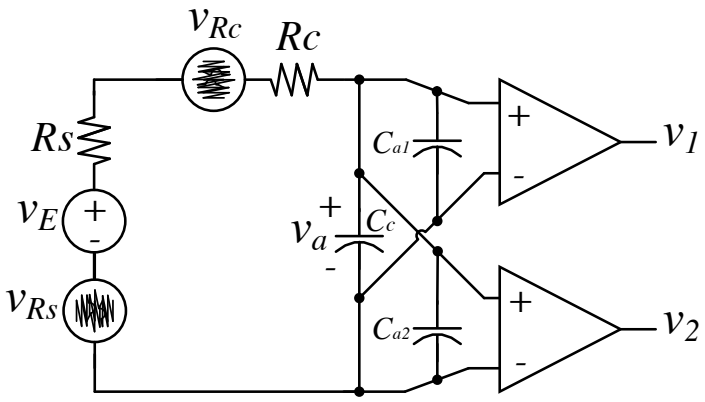

Figure 2.2: JNT system, associated noise sources, and EMI source [2]

The PSD and CPSD are calculated from the measured output noise voltages. CPSD, Equation 2.27, is calculated using a cross-correlation function and two signals' PSD. PSD, Equation 2.28, is a special case of CPSD where the two signals are the same. The full derivation of PSD and CPSD is given in Appendix A.

$$
G_{XY}(f) = \lim_{\Delta\to\infty} \mathbf{E}\left(\frac{X^*_\Delta(f)Y_\Delta(f)}{\Delta}\right) \tag{2.27}
$$

$$
G_{XX}(f) = \lim_{\Delta\to\infty} \mathbf{E}\left(\frac{X^*_\Delta(f)X_\Delta(f)}{\Delta}\right), \tag{2.28}
$$

where

$$
x_\Delta = \begin{cases} x(t), & -\frac{\Delta}{2} < t < \frac{\Delta}{2} \\ 0, & \text{otherwise} \end{cases},
$$

and the other signal has a similar definition. The PSD of chnl1 and chnl2 are defined

in Equations 2.29 and 2.30.

$$G_1(f) = \lim_{\Delta\to\infty} \mathbf{E}\left(\frac{V^*_{1,\Delta}(f)V_{1,\Delta}(f)}{\Delta}\right) \tag{2.29}$$

$$G_2(f) = \lim_{\Delta\to\infty} \mathbf{E}\left(\frac{V^*_{2,\Delta}(f)V_{2,\Delta}(f)}{\Delta}\right) \tag{2.30}$$

Using these equations and applying our signals $V_1(f)$ and $V_2(f)$, the CPSD for JNT system (with EMI) is:

$$\begin{aligned} G_{12}(f) &= \lim_{\Delta\to\infty} \mathbf{E}\left(\frac{V^*_{1,\Delta}(f)V_{2,\Delta}(f)}{\Delta}\right) \\ &= \lim_{\Delta\to\infty} \mathbf{E}\left(\frac{\left(\begin{array}{c}(\{[V_{Rs,\Delta}(f)+V_{Rc,\Delta}(f)+V_{E,\Delta}(f)]H_s(f)+V_{a1,\Delta}(f)\}H_1(f))^* \\ \{[V_{Rs,\Delta}(f)+V_{Rc,\Delta}(f)+V_{E,\Delta}(f)]H_s(f)+V_{a2,\Delta}(f)\}H_2(f)\end{array}\right)}{\Delta}\right). \end{aligned} \tag{2.31}$$

All mutually independent noise voltages, the following CPSDs are zero: $G_{Rs,Rc}(f)$, $G_{Rs,E}(f)$, $G_{Rs,a2}(f)$,$G_{Rc,Rs}(f)$, $G_{Rc,E}(f)$, $G_{Rc,a2}(f)$, $G_{E,Rs}(f)$, $G_{E,Rc}(f)$, $G_{E,a2}(f)$, $G_{a1,Rc}(f)$, and $G_{a1,a2}(f)$. This is because $\mathbf{E}\left[V_{Rs}(f)V_{Rc}(f)\right] = 0$. And the CPSD simplifies to

$$\begin{aligned} G_{12}(f) &= [G_{Rs}(f)+G_{Rc}(f)+G_E(f)]H_1^*(f)H_2(f)|H_s(f)|^2 \\ &= [G_{Rs}(f)+G_{Rc}(f)+G_E(f)]H_{12}(f), \end{aligned} \tag{2.32}$$

where $H_{12}(f) = H_1^*(f)H_2(f)|H_s(f)|^2$, is the cross power frequency response of the (sensor + cable + chnl1 + chnl2) to the noise voltage of the sensor, $G_{Rs}(f)$ is the PSD of the sensor noise voltage, $G_{Rc}(f)$ is the PSD of the cable noise voltage, and $G_E(f)$ is the PSD of the periodic EMI voltage. The PSD of the RTD (sensor, R_s), the cable resistance (R_c), and the EMI (E) are given in Equations 2.33- 2.35.

$$G_{Rs,Rs}(f) = G_{Rs}(f) = \lim_{\Delta\to\infty} \mathbf{E}\left(V^*_{Rs,\Delta}(f)V_{Rs,\Delta}(f)\right) \tag{2.33}$$

$$G_{Rc,Rc}(f) = G_{Rc}(f) = \lim_{\Delta\to\infty} \mathbf{E}\left(V^*_{Rc,\Delta}(f)V_{Rc,\Delta}(f)\right) \tag{2.34}$$

$$G_{E,E}(f) = G_{E}(f) = \lim_{\Delta\to\infty} \mathbf{E}\left(V^*_{E,\Delta}(f)V_{E,\Delta}(f)\right), \tag{2.35}$$

as t $\to \infty$: averaged over and over again.

Rearranging Equation 2.32 to solve for the PSD of the sensor or noise voltage of the sensor, without EMI:

$$\begin{aligned} G_{Rs}(f) &= \frac{G_{12}(f)}{H_{12}(f)} - G_{Rc}(f) \\ &= 2kT_sR_s \quad from \quad equation \quad 1.2. \\ 2kT_sR_s &= \frac{G_{12}(f)}{H_{12}(f)} - G_{Rc}(f) \end{aligned} \tag{2.36}$$

Solving for temperature:

$$T_s = \left[\frac{G_{12}(f)}{H_{12}(f)} - G_{Rc}(f)\right] \times \left[\frac{1}{2kR_s}\right]. \tag{2.37}$$

Note that the sensor PSD E$\left\{\frac{G_{12}(f)}{H_{12}(f)}\right\}$- $G_{Rc}(f)$ can be estimated at all frequencies as it is the same across the entire bandwidth of the measurement. While this seems straightforward, the additional EMI complicates the above calculations. A full derivation of these equations is given in Appendix A.

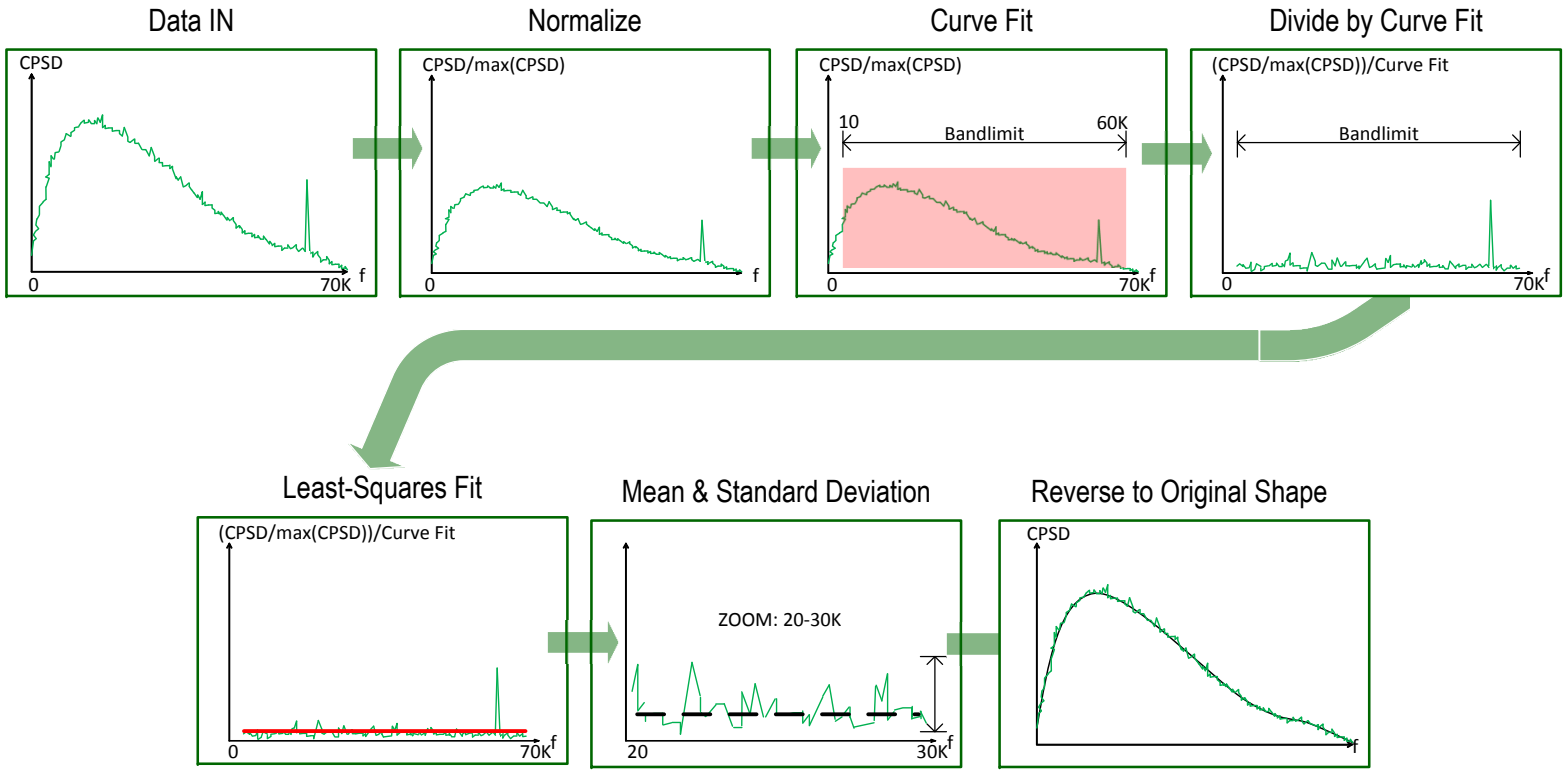

Figure 2.3: Flow chart of despike algorithm

CPSD between chnl1 and chnl2 ($G_{12}(f)$) is greatly influenced by unwanted EMI noise. To remove this noise, a "despiking" algorithm is used on the frequency domain channel voltage data (Figure 2.3). The despiking algorithm is actually a form of outlier detection. First the data are normalized by dividing the data by its maximum value. Then the data are fit using a least-squares fit. Next, the mean and standard deviation of the inliers are calculated. After that, bandpass filtering is performed to identify high energy spikes and eliminate the leakage caused by these spikes. Finally the data is reversed back to its original shape. The performance of the despiking algorithm depends on the recursivenss of the software. This means the longer the software runs, the more spikes are removed.

Coherence between the two output channels is very important; Equation 2.38 is the definition of coherence [2]. Early in the signal processing, when the first block of data is acquired, the coherence is very good. However, as more data are averaged, the coherence decreases. If coherence between the two output channels is very good (or equal to one), the EMI removal technique will be very effective. For a good coherence, the phase of the two Fourier-transformed signals need to be very similar; in other words, the phasors need to point in the same direction.

$$C_{xy}(f) = \frac{|G_{xy}(f)|^2}{G_x(f)G_y(f)} \tag{2.38}$$

$$C_{V_1V_2}(f) = \frac{|G_{12}(f)|^2}{G_1(f)G_2(f)} \tag{2.39}$$

Chapter 3

New Signal Processing Technique: Subtraction Method

An alternate method to the EMI rejection method discussed in Chapter 2 is an EMI subtraction method. This method uses an output signal from an antenna. The original four signals are the two output voltages from chnl1 and chnl2, the measured output of the PT, and the DC resistance measurement. The antenna runs the entire length of the cable and RTD sensor to detect EMI. Figure 3.1 is a block diagram of the system used in the subtraction method.

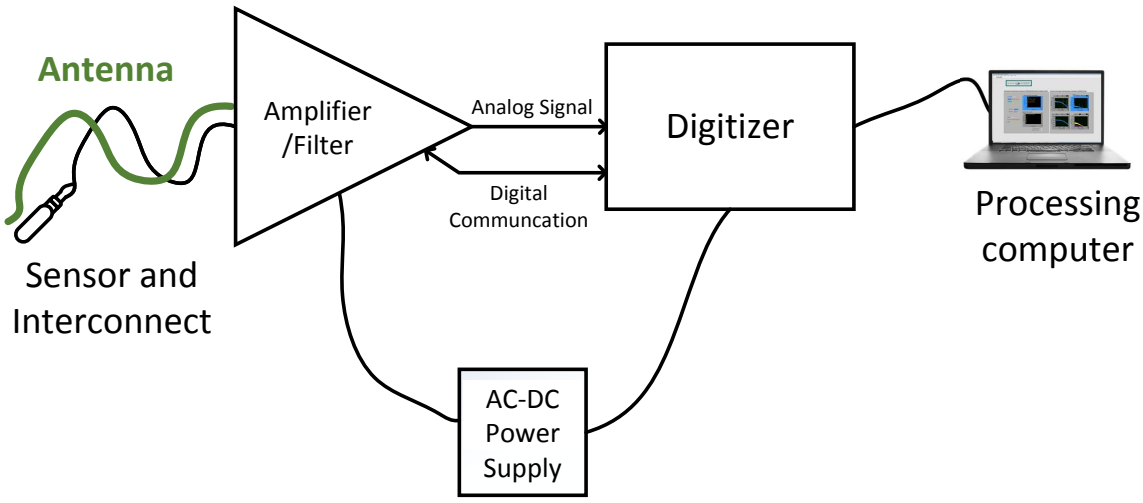

Figure 3.1: System diagram with antenna for EMI subtraction method

This system is identical to the original system with the additional channel. The antenna channel electronics are as identical to the two noise voltage channels as physically possible, allowing for comparable measurements. The circuit shown in Figure 2.2 displays how the effects of EMI are modeled electronically. Equations 2.22–2.35 explain the voltage and PSD and CPSD results from the EMI. As a known EMI signal is calculable through those equations, the signal is subtracted.

3.1 Subtracting EMI from the Output Channel Noise Voltages

As stated in Chapter 1, the JNT measurement consists of output voltages from two amplifier/filter channels each consisting of the sum of a correlated noise voltage and an uncorrelated amplifier/filter noise voltage. As the PSD/CPSD are combined and time averaged, the power of the uncorrelated noise approaches zero. Figure 1.4 displays the cross correlation concept. This same technique is used in the subtraction method. However, the subtraction method does not solely rely on cross-correlation and averaging over time to remove the EMI noise. The signal acquired using the fifth high-speed channel is then used to subtract it from each amplifier/filter channel output voltage.

The signal processing steps required to remove EMI with the subtraction method are displayed in Figure 3.2. The sample data from the amplifier/filter channels and the antenna form a block made of 16 sub-blocks. Letting V_A represent the antenna signal output voltage, Equation 3.1 represents the antenna voltage. The CPSD between the antenna and amplifier/filter channel voltage outputs is solved with Equations 3.2 and 3.3, and the PSD of V_A is found with Equation 3.4. The full derivation of these equations are in Appendix B [2].

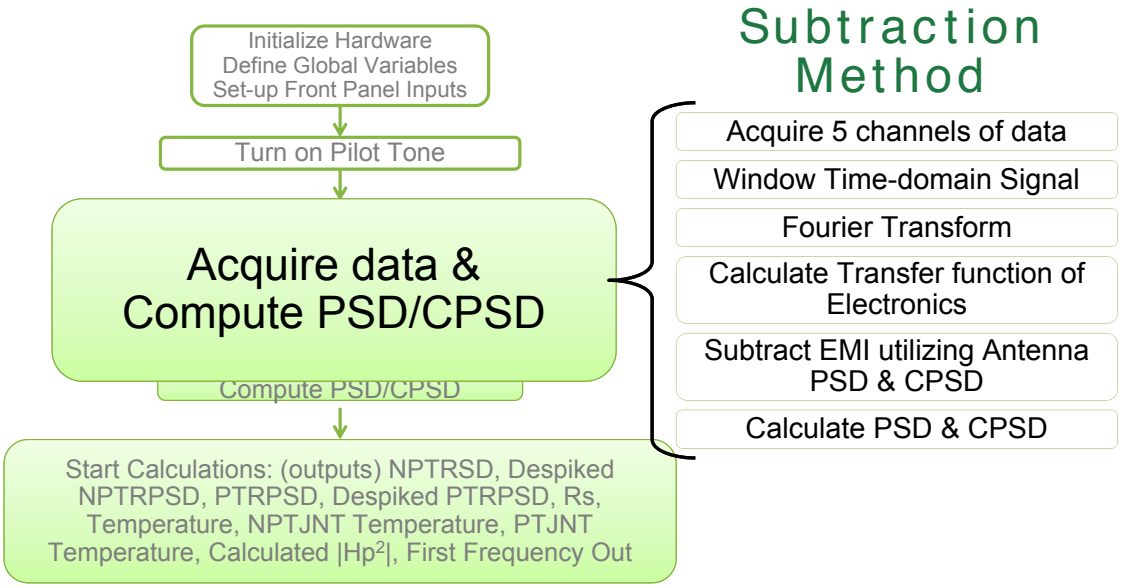

Figure 3.2: Descriptive diagram of the "Acquire data and compute PSD/CPSD" block from Figure 1.6 for subtraction method

$$\begin{aligned} v_A(t) &= [x_E(t) * h_{EA}(t) + v_{a3}(t)] * h_{a3}(t) \\ FT: V_A(f) &= [X_E(f)H_{EA}(f) + V_{a3}(f)]H_{a3}(f), \end{aligned} \tag{3.1}$$

where $H_{EA}(f)$ is the frequency response of the EMI-to-antenna voltage, $V_{a3}(f)$ is the antenna's associated amplifier channel electronics noise voltage, and $H_{a3}(f)$ is the frequency response of the antenna channel electronics. Also, $x_E(t)$ is a general excitation signal composed of conduction and induction EMI where $v_E(t) = x_E(t)h_{xs}(t)$ and $h_{xs}(t)$ is the impulse response of the EMI-to-sensor voltage [2].

$$
\begin{aligned}
G_{A1,E}(f) &= \lim_{\Delta\to\infty} \mathbf{E}\left(\frac{V^*_{A,\Delta}(f)V_{1E,\Delta}(f)}{\Delta}\right) \\
&= \lim_{\Delta\to\infty} \mathbf{E}\left(\frac{[X_{E,\Delta}(f)H_{EA}(f)+V_{a3,\Delta}(f)]^*H^*_{a3}(f)V_{E,\Delta}(f)H_s(f)H_1(f)}{\Delta}\right) \\
&= G_E(f)H^*_{EA}(f)H^*_{a3}(f)H_{Es}(f)H_s(f)H_1(f)
\end{aligned}
\tag{3.2}
$$

$$
\begin{aligned}
G_{A2,E}(f) &= \lim_{\Delta\to\infty} \mathbf{E}\left(\frac{V^*_{A,\Delta}(f)V_{2E,\Delta}(f)}{\Delta}\right) \\
&= \lim_{\Delta\to\infty} \mathbf{E}\left(\frac{[X_{E,\Delta}(f)H_{EA}(f)+V_{a3,\Delta}(f)]^*H^*_{a3}(f)V_{E,\Delta}(f)H_s(f)H_2(f)}{\Delta}\right) \\
&= G_E(f)H^*_{EA}(f)H^*_{a3}(f)H_{Es}(f)H_s(f)H_2(f)
\end{aligned}
\tag{3.3}
$$

$$
\begin{aligned}
G_A(f) &= \lim_{\Delta\to\infty} \mathbf{E}\left(\frac{|V_{A,\Delta}(f)|^2}{\Delta}\right) \\
&= \lim_{\Delta\to\infty} \mathbf{E}\left(\frac{|[X_E(f)H_{EA}(f)+V_{a3}(f)]H^*_{a3}(f)|^2}{\Delta}\right) \\
&= G_E(f)|H_{EA}(f)H_{a3}(f)|^2 + G_{a3}(f)|H_{a3}(f)|^2
\end{aligned}
\tag{3.4}
$$

Equation 3.5 shows the output voltages from the amplifier/filter channels with EMI. Equation 3.6 shows the CPSD between the antenna to the amplifier/filter output chnl1 and the antenna to the amplifier/filter output chnl2.

$$V_{1E}(f) = \frac{G_{A,1E}(f)}{G_A(f)} V_A(f)$$
$$V_{2E}(f) = \frac{G_{A,2E}(f)}{G_A(f)} V_A(f) \tag{3.5}$$

$$\begin{aligned} G_{A1}(f) &= \lim_{\Delta\to\infty} \mathbf{E}\left(\frac{V_{A,\Delta}(f)^* V_{1,\Delta}(f)}{\Delta}\right) \\ &= [G_{ARs}(f) + G_{ARc}(f) + G_{AE}(f)]H_s(f) + G_{Aa1}(f)H_1(f) \end{aligned}$$
$$\begin{aligned} G_{A2}(f) &= \lim_{\Delta\to\infty} \mathbf{E}\left(\frac{V_{A,\Delta}(f)^* V_{1,\Delta}(f)}{\Delta}\right) \\ &= [G_{ARs}(f) + G_{ARc}(f) + G_{AE}(f)]H_s(f) + G_{Aa2}(f)H_2(f) \end{aligned} \tag{3.6}$$

Removing terms with zeros because of independence, Equation 3.7 updates the CPSD between the antenna and the amplifier/filter outputs. This proves Equation 3.5 to be true.

$$\begin{aligned} G_{A1}(f) &= G_{AE}(f)H_s(f)H_1(f) \\ G_{A2}(f) &= G_{AE}(f)H_s(f)H_2(f) \end{aligned} \tag{3.7}$$

The EMI detected by the antenna and the EMI noise corrupting the channel output voltages are coherent. Equation 3.8 demonstrates how the output voltage from the amplifier/filter channel without EMI is calculated where $H_{A1}(f)$ is the frequency response from the output voltage of the antenna electronics to the amplifier/filter chnl1 output voltage. Similarly, $H_{A1}(f)$ is the frequency response from the output voltage of the antenna electronics to the amplifier/filter chnl2 output voltage.

$$V_{1-E}(f) = V_{1E}(f) - H_{A1}(f) \times V_A(f) = \{[V_{Rs}(f) + V_{Rc}(f)]H_s(f) + V_{a1}(f)\}H_1(f)$$
$$V_{2-E}(f) = V_{1E}(f) - H_{A2}(f) \times V_A(f) = \{[V_{Rs}(f) + V_{Rc}(f)]H_s(f) + V_{a2}(f)\}H_1(f) \quad (3.8)$$

The attractiveness of this method versus the rejection method is that subtracting the antenna signal is a linear mathematical computation. The rejection method is not linear and therefore more difficult to analyze. The detection of EMI is simplified and more accurate. To compute the antenna to amplifier/filter channel frequency response, use Equation 3.9. $G_{A1}(f)$ is the CPSD between the antenna and chnl1 voltage outputs.

$$H_{A1}(f) = \frac{G_{A1}(f)}{G_A(f)}$$
$$H_{A2}(f) = \frac{G_{A2}(f)}{G_A(f)} \quad (3.9)$$

Once the EMI is subtracted from the output voltages from chnl1 and chnl2, the PSD and CPSD is computed.

3.2 Computing the Power Spectral Density and Cross Power Spectral Density

Performing the calculations in the correct order is critical for the signal processing to be successful. Figure 3.3 demonstrates the necessary order of operations for the subtraction method. Note the order for computing the CPSDs: $G_{1-E+p}(f)$, $G_{2-E+p}(f)$, and $G_{12-E+p}(f)$ are computed; then the PT is subtracted from $V_{1-E}(f)$ and $V_{2-E}(f)$ and finally $G_{12-E-p}(f)$ is computed. This order is very important because the EMI noise and PT can cause a large impact on the final temperature

calculations if incorrectly handled. The CPSD between chnl1 and chnl2 output voltages with EMI subtracted is calculated in Equation 3.10. Likewise, the CPSD between chnl1 and chnl2 output voltages with EMI subtracted and the PT subtracted can be seen in section 3.3 [2].

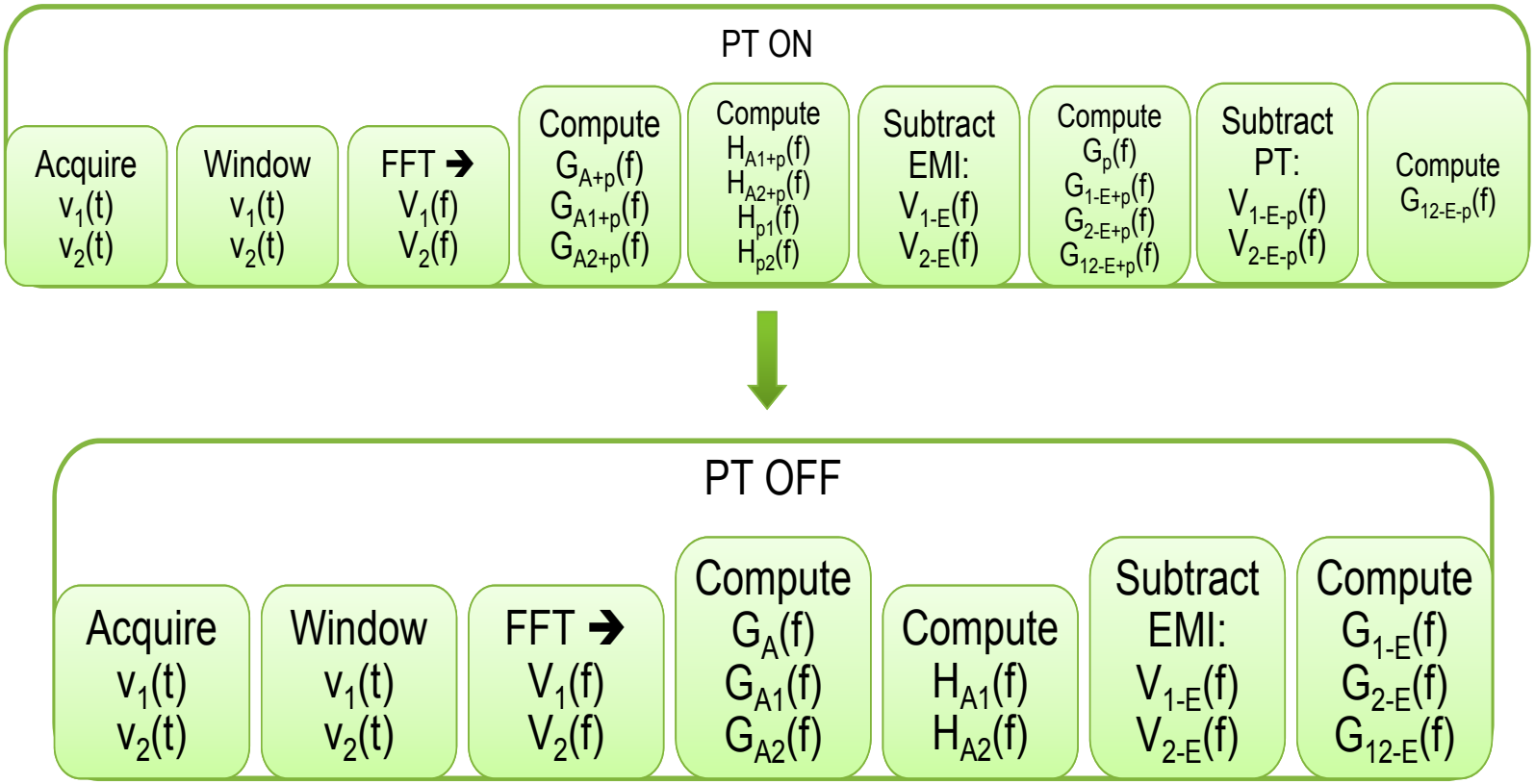

Figure 3.3: Flow chart of despike algorithm

$$
\begin{aligned}
G_{12-E}(f) &= \lim_{\Delta\to\infty} \mathbf{E}\left(\frac{V^*_{1-E,\Delta}(f)V_{2-E,\Delta}(f)}{\Delta}\right) \\
&= \lim_{\Delta\to\infty} \mathbf{E}\left(\frac{\left(\begin{array}{c}(\{[V_{Rs,\Delta}(f)+V_{Rc,\Delta}(f)]H_s(f)+V_{a1-E}(f)\}H_1(f))^* \\ (\{[V_{Rs,\Delta}(f)+V_{Rc,\Delta}(f)]H_s(f)+V_{a2-E}(f)\}H_2(f))\end{array}\right)}{\Delta}\right)
\end{aligned}
\tag{3.10}
$$

Eliminating zero terms, as before where $\mathbf{E}\left[G_{RsRc}\right] = 0$:

$$
\begin{aligned}
G_{12-E}(f) &= [G_{Rs}(f)+G_{Rc}(f)]|H_s(f)|^2H_1(f)^*H_2(f) \\
&= [G_{Rs}(f)+G_{Rc}(f)]H_{12}(f)
\end{aligned}
\tag{3.11}
$$

The CPSD between the two channels with EMI properly removed is important for the calculations leading to the final JNT temperature calculation. Before the temperature can be calculated though, the PT must be removed from the signals. The next chapter discusses the generation of the PT and how the PT is removed.

3.3 Pilot Tone Generation

As mentioned in previous chapters, a PT is required for accurate modeling of the electronics. Since the JNT measurement is applied to a system that will be running for extended periods of time, the CPSD $H_{12}(f)$ must be known at all times. Applying a PT allows for monitoring $H_{12}(f)$. The PT, has an amplitude spectrum that encompasses the entire bandwidth of the temperature measurement. An Agilent 33220a arbitrary waveform generator supplies the PT signal that is then converted from single-ended to a differential current source. The converter circuit is a balanced series R_pC_p network in which $R_p \gg R_s$ and $C_p \gg (C_c + C_{a1} + C_{a2})$.

It is important to properly select the component values for the single-ended to differential converter. Figure 3.4 displays the PT circuit. The corner frequencies need to be outside the frequency range of interest for the JNT temperature. The capacitance C_p needs to block DC currents but also set the low-corner frequency, Equation 3.12 (from PT generator $f_{start} = 1$, $f_{stop} = 131072$ which is band of interest). The frequency band for JNT temperature determination needs be well above f_{lo} (Equation 3.12) and well below f_{hi} (Equation 3.13) so that over the full bandwidth used in JNT temperature measurement the frequency response from the PT voltage to the current injected into the sensor is approximately constant (refer to Figure 3.5) [2]. The full derivation of these equations is in Appendix C [2].

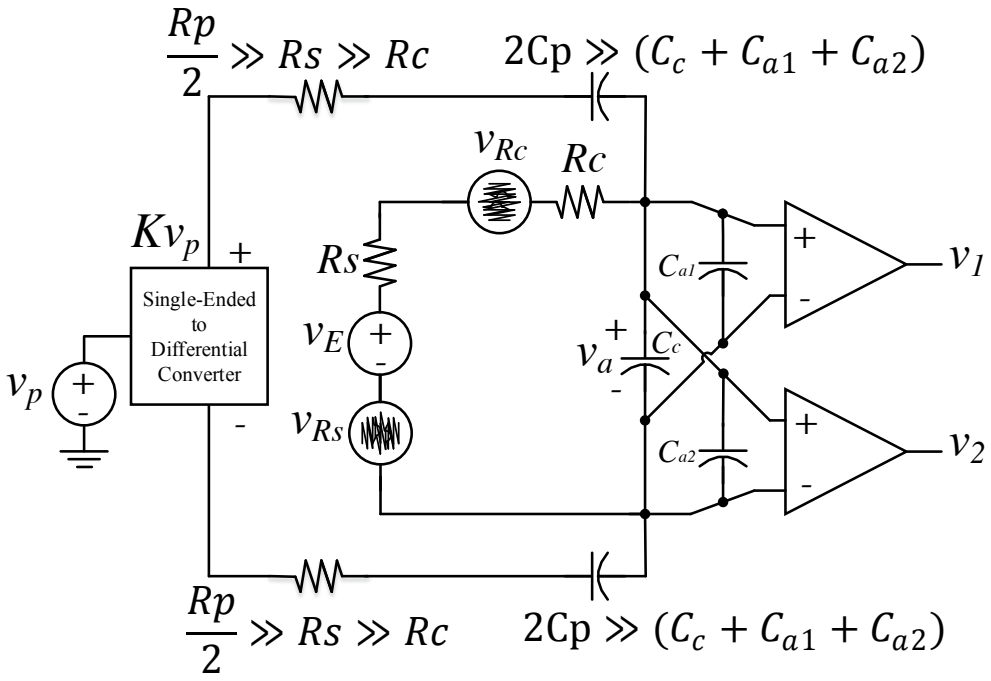

Figure 3.4: Simple electrical representation of JNT system, associated noise sources, EMI source, and simple Pilot Tone electronics representation [2]

$$f_{lo} = \frac{1}{(2\pi R_p + R_s + R_c)C_p} \cong \frac{1}{2\pi R_p C_p} \tag{3.12}$$

$$f_{hi} = \frac{1}{2\pi(R_s + R_c)(C_c + C_{a1} + C_{a2})} \tag{3.13}$$

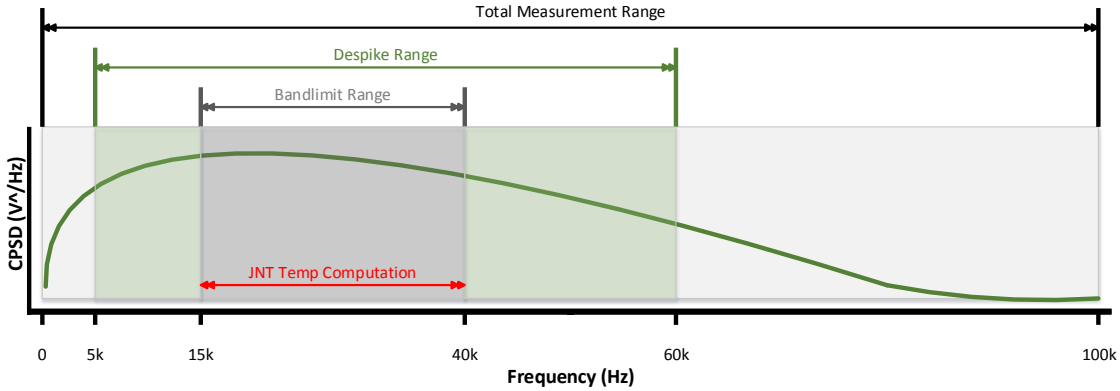

Figure 3.5: Frequency range of JNT measurement

$$\begin{aligned} G_{12-E+p}(f) &= \lim_{\Delta\to\infty} \mathbf{E}\left(\frac{V^*_{1-E,\Delta}(f)V_{2-E,\Delta}(f)}{\Delta}\right) \\ &= \{[G_{Rs}(f) + G_{Rc}(f)] + G_P(f)|Hp(f)|^2(R_s + R_c)^2\}H_1^*(f)H_2(f)|H_s(f)|^2 \\ &= 2k(T_sR_s + T_cR_c)\frac{G^*_{P1-E}(f)G_{P2-E}(f)}{G_P^2(f)|H_p(f)|^2(R_s + R_c)^2} + \frac{G^*_{P1-E}(f)G_{P2-E}(f)}{G_P(f)} \end{aligned} \tag{3.14}$$

where $G_p(f)$ is the PSD of the PT signal at the output of the generator, and $G_{p1}(f)$ is the CPSD of the PT signal and output of Chnl1. Equations 3.15 and 3.16 are used to compute the frequency response from PT voltage to amplifier/filter channel output voltage. The frequency response of the PT voltage to amplifier/filter channel outputs is important because the PT signal must also be subtracted from the voltage, Equation 3.17.

$$\begin{aligned} H_p(f) &= \frac{I_p(f)}{V_p(f)} \\ &= \frac{K}{Z_p(f) + Z_{sc}(f)} \\ &= \frac{K}{(R_p + \frac{1}{\jmath 2\pi f C_p})(\frac{R_s+R_c}{2\pi\jmath Cf(R_s+R_c)+1})} \cong \frac{K}{Z_p(f)} \end{aligned} \tag{3.15}$$

$$
\begin{aligned}
H_{p1}(f) &= \frac{G_{P1}(f)}{G_P(f)} \\
H_{p2}(f) &= \frac{G_{P2}(f)}{G_P(f)},
\end{aligned}
\tag{3.16}
$$

where $H_p(f)$ characterizes the PT attenuator. The PT is independent of all the other signals: $V_1(f)$, $V_2(f)$, and EMI $V_A(f)$. The same removal technique for removing EMI is used to remove PT from the signals. $V_{1-E-p}(f)$ and $V_{2-E-p}(f)$ represent the output voltages from amplifier/filter chnl1 and chnl2 with EMI removed and then PT removed. Equations 3.18 and 3.19 are the CPSD between chnl1 and chnl2 with EMI removed and then PT removed.

$$
\begin{aligned}
V_{1-E-p}(f) &= \{[V_{Rs}(f) + V_{Rc}(f)]H_s(f) + V_{a1}(f)\}H_1(f) \\
&= V_{1-E}(f) - H_{p1}(f) \times V_p(f) \\
V_{2-E-p}(f) &= \{[V_{Rs}(f) + V_{Rc}(f)]H_s(f) + V_{a2}(f)\}H_2(f) \\
&= V_{1-E}(f) - H_{p2}(f) \times V_p(f)
\end{aligned}
\tag{3.17}
$$

$$
G_{12-E-p}(f) = \lim_{\Delta\to\infty} \frac{V^*_{1-E-p,\Delta}(f)V_{2-E-p,\Delta}(f)}{\Delta} \tag{3.18}
$$

$$
G_{12-E-p}(f) = \lim_{\Delta\to\infty} \mathbf{E}\left(\frac{\begin{pmatrix} (\{[V_{Rs,\Delta}(f) + V_{Rc,\Delta}(f)]H_s(f) + V_{a1-E-p}(f)\}H_1(f)))^* \\ (\{[V_{Rs,\Delta}(f) + V_{Rc,\Delta}(f)]H_s(f) + V_{a2-E-p}(f)\}H_2(f) \end{pmatrix}}{\Delta} \right) \tag{3.19}
$$

The value of $|H_p(f)|^2$ is very critical for the temperature calculation because it is the characterization of the PT attenuator. Computing this value requires a calibrated RTD and averaged PSDs and CPSDs. Using Equation 3.14 and solving for $|H_p(f)|^2$, Equation 3.20 is developed. The numerator is the PSD of the noise current in the sensor and cable without the PT being on and the denominator is the amplifier

and filter noise CPSD referred to as the PT location. Since $\frac{G^*_{P1-E}(f)G_{P2-E}(f)}{G^2_P(f)}$ is the cross power frequency response from the PT to the output of the two amplifier/filter channels, then $\frac{G^*_{12+p-E}(f)G^2_P(f)}{G^*_{P1-E}(f)G_{P2-E}(f)}$ is the output CPSD from the two amplifier/filter channels with the PT on. Therefore Equation 3.20 simplifies to Equation 3.21.

$$
\begin{aligned}
|H_p(f)|^2 &= \frac{\frac{2k(T_sR_s+T_cR_c)G^*_{P1-E}(f)G_{P2-E}(f)}{G^2_P(f)(Rs+R_c)^2}}{G_{12-E}(f) - \frac{G^*_{P1-E}(f)G_{P2-E}(f)}{G_P(f)}} \\
&= \frac{\frac{2k(T_sR_s+T_cR_c)}{(R_s+R_c)^2}}{\frac{G_{12+p-E}(f)G^2_P(f)}{G^*_{P1-E}(f)G_{P2-E}(f)} - G_P} \\
&= \frac{Sensor\ noise\ current\ PSD}{Amp/filter\ noise\ CPSD\ referred\ to\ the\ PT\ location}
\end{aligned}
\tag{3.20}
$$

$$
|H_p(f)|^2 = \frac{\frac{2k(T_sR_s+T_cR_c)}{(R_s+R_c)^2}}{\frac{G^*_{12-E-p}(f)G^2_P(f)}{G^*_{P1-E}(f)G_{P2-E}(f)}} \tag{3.21}
$$

The derivations of these equations are discussed further in the Appedix C, including the derivation of $|H_p(f)|^2$ with PT off, on, and on but removed.

Chapter 4

JNT System Test Results

Physical testing of the system is performed in a variety of noise environments to explore the effect of EMI on the JNT measurement system. First, the measurements are performed in the cleanest environment possible: a laboratory with minimal EMI. After a baseline of data is established, the environments under test are modified for controlled introduction of noise. Measurement results obtained from testing the JNT system in a variety of noise environments is summarized in this chapter. Specifics relating system measurement performance with the noise environment are discussed.

4.1 EMI Noise Environments and Associated Test Results

While it would be ideal to test systems in a noise free environment, complete removal of EMI is not possible. Therefore, several practical EMI environments are considered having various types and levels of EMI. The first environment is very similar to typical facilities where JNT measurements are of interest. This is a fairly EMI clean laboratory environment with light ballasts, benchtop equipment, and 60 Hz power noise as the primary EMI contributors. Figure 4.1 is an image of the physical hardware system and Figure 4.2 is a view of the inside of the JNT front end box. All of the

testing performed and the results discussed in this chapter make use of the system displayed in these two figures.

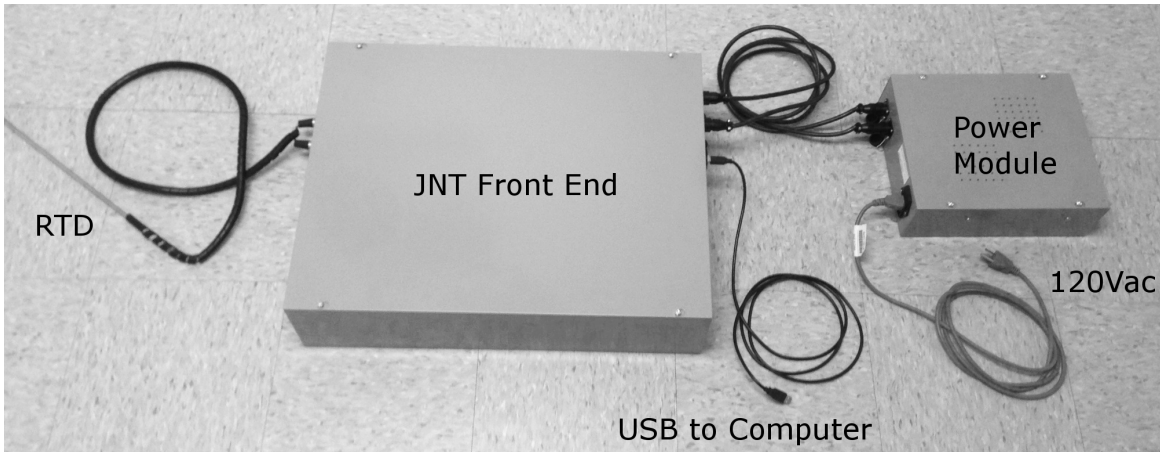

Figure 4.1: Physical JNT system hardware

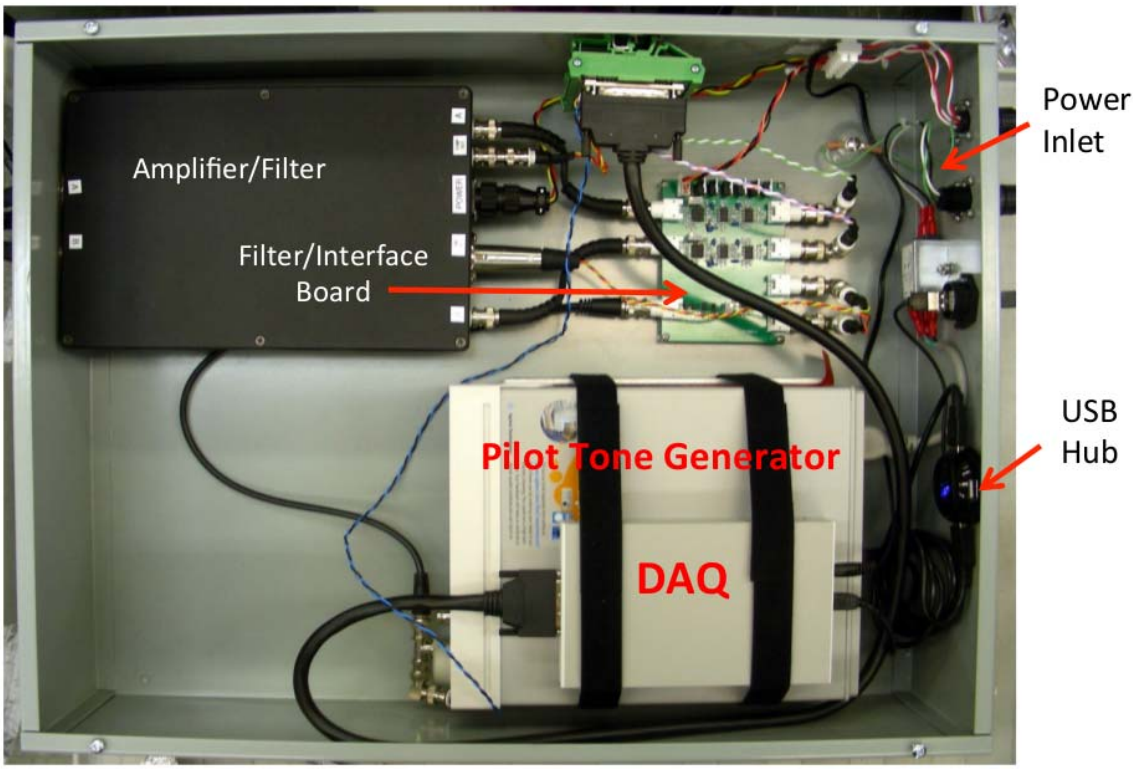

Figure 4.2: JNT front end box hardware

The test EMI environments are listed in Table 4.1. The ambient environment (Environment 1) includes the following sources of EMI: a 60-Hz source, a fluorescent light ballast, the internal JNT signal generator, and an undefined high frequency noise source. Environment 2, Environment 3, and Environment 4 are all generated using an Agilent 33521A signal generator driving a large inductor through a bipolar operational amplifier. See Figure 4.3 for the system diagram. The Sandia environment (Environment 2) is generated using a 2 kHz square wave with an amplitude of 250 mV_{pp}. Another controlled EMI environment (Environment 3) involves broadband EMI generated from a 100 Hz noise waveform with an amplitude of 250 mV_{pp}. The last controlled EMI environment (Environment 4) has a single sine wave at 20 kHz with an amplitude of 250 mV_{pp}

Table 4.1: List of Test Environment EMI Noise Sources

Environment 1	Ambient EMI at 21 °C
Environment 2	Sandia EMI at 0 °C
Environment 3	Broadband EMI at 0 °C
Environment 4	Single sine (20 kHz) EMI at 0 °C

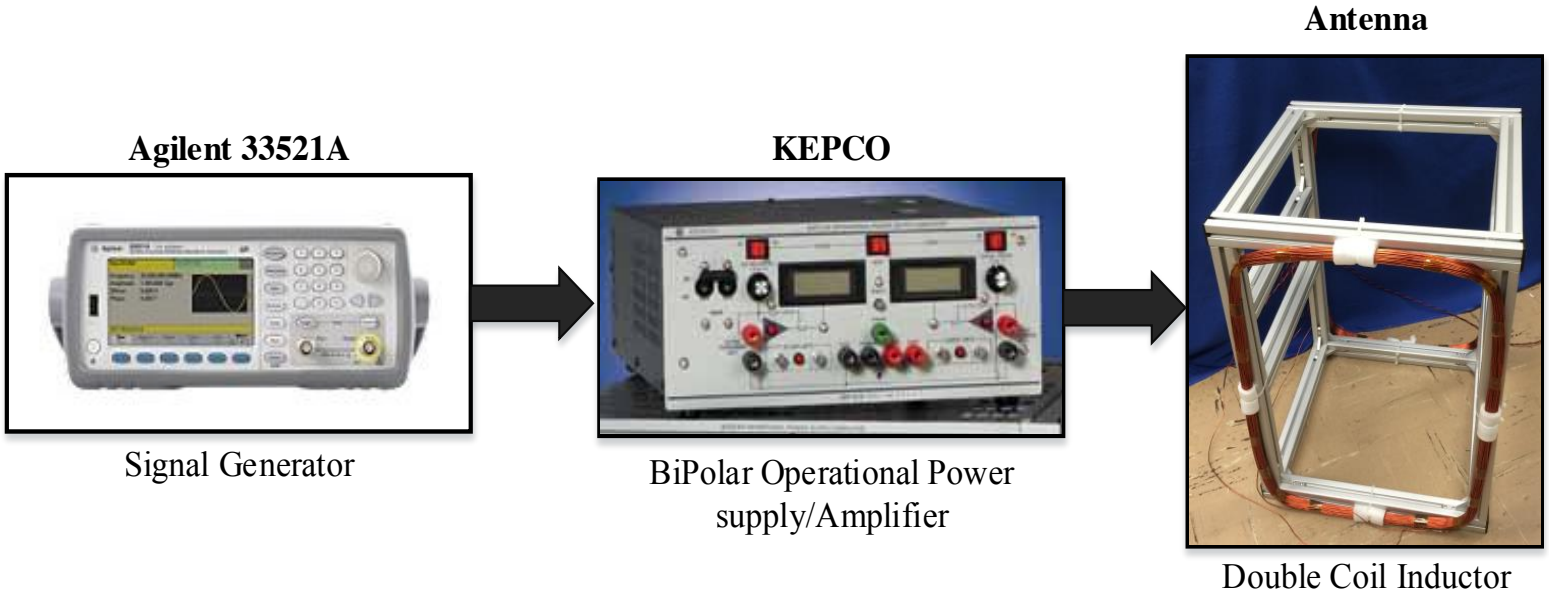

Figure 4.3: EMI environment generation system

Each of the environments are tested multiple times over the same period of time. Figure 4.4 shows the measurements results obtained using Environment 1, having the following EMI noise sources: 60 Hz noise, a 27 kHz noise source from the light ballast, a 44 kHz noise source from the internal signal generator, and a 63 kHz noise from an unknown source. $G_{12}(f)$ and $G_{12-E}(f)$ are the CPSD between the output JNT channels chnl1 and chnl2. This output directly impacts the temperature calculation and without proper EMI removal will cause an invalid temperature to be reported. $G_{12}(f)$ is the CPSD between chnl1 and chnl2 before EMI is remove and $G_{12-E}(f)$ is the CPSD after EMI is removed. The shape of the $G_{12}(f)$ and $G_{12-E}(f)$ waveforms reflects the transfer function of the JNT electronics. The JNT temperature is calculated within the 15–40 kHz range. The results displays in Figure 4.4 are at room temperature.

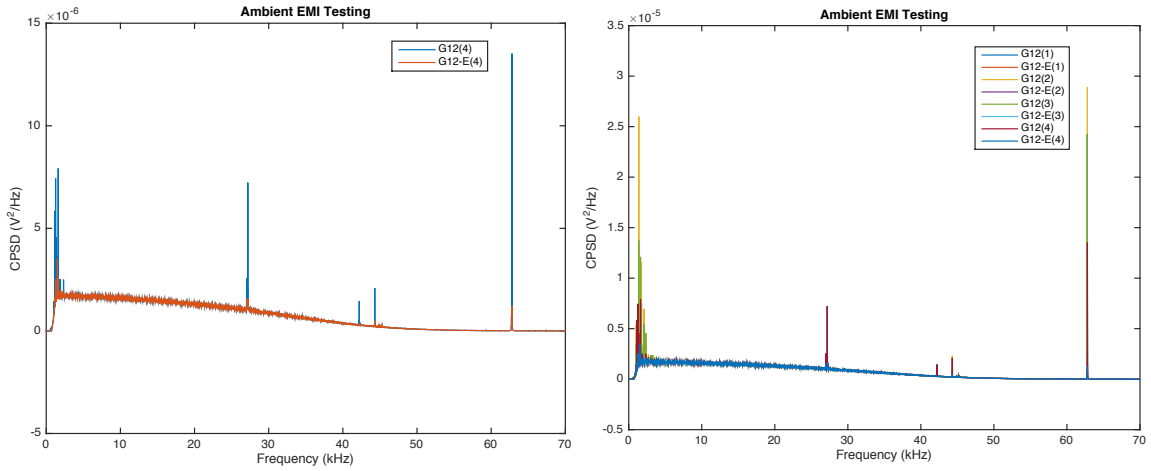

(a) Single test run **(b)** Multiple test runs

Figure 4.4: Environment 1: $G_{12}(f)$ output from 3-hour test measurement

Environment 2, see Figures 4.5 and 4.6, are the measurement results from the Sandia environment. There is a 60 Hz EMI source, a 44 kHz EMI source from the internal signal generator, a 63 kHz EMI from an unknown source, and several EMI spikes associated with a 2 kHz square wave. Figure 4.5 shows the $G_{12}(f)$ computation before and after EMI has been removed from a single test run. The EMI subtraction

method from Chapter 3 was used to remove EMI. The blue waveform represents the CPSD prior to EMI subtraction. The CPSD following noise subtraction is shown in red. The results shown in Figure 4.5b demonstrates the efficacy of the noise subtraction method, as evidenced by the removal of the spectral noise lined in Figure 4.5a. Figure 4.6 displays the results from 4 test runs with the RTD in ice. Testing performed in ice is considered a baseline test because it is a controlled temperature without adding additional EMI.

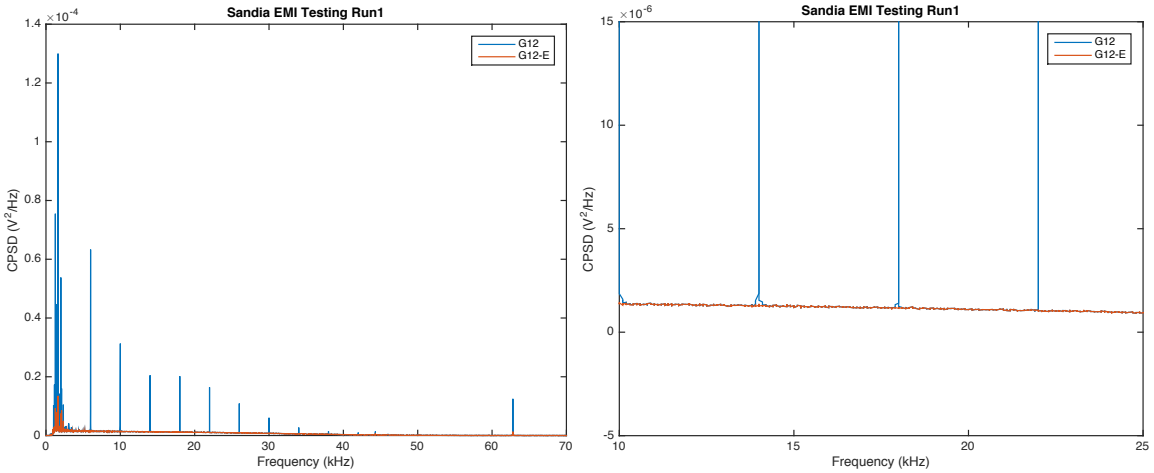

(a) Bandwidth = 0 – 70 kHz **(b)** Zoom: Bandwidth = 10 – 25 kHz

Figure 4.5: Environment 2: $G_{12}(f)$ output from a single test over a 3-hour test measurement

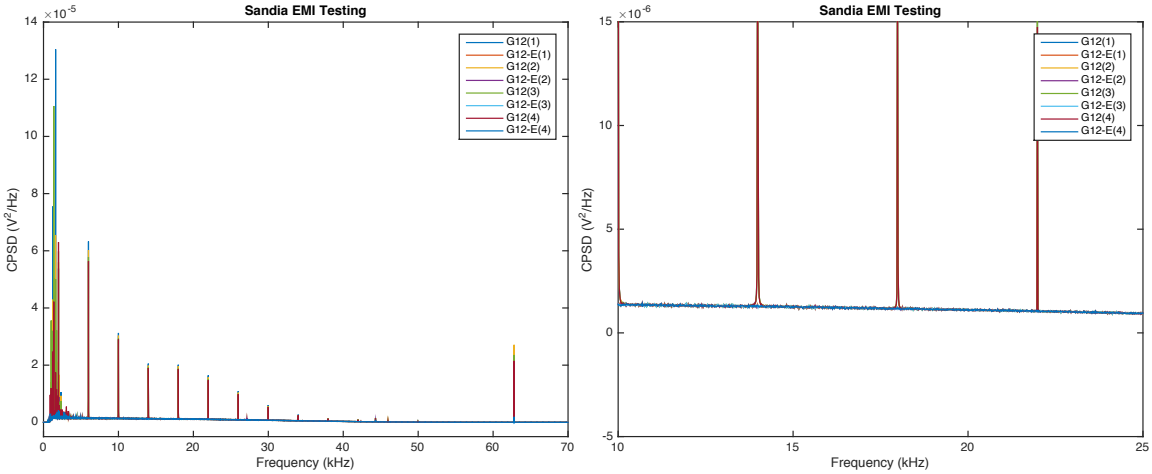

(a) Bandwidth = 0 – 70 kHz **(b)** Zoom: Bandwidth = 10 kHz – 25 kHz

Figure 4.6: Environment 2: $G_{12}(f)$ output from multiple tests over a 3-hour test measurement

Figures 4.7 and 4.8 are the measurement results from the broadband environment (Environment 3). The EMI sources are 60 Hz, added broadband EMI across the entire bandlimit, a 44 kHz EMI source from the internal signal generator, and a 63 kHz EMI from an unknown source. Figure 4.7 displays the $G_{12}(f)$ results from a single test run where the blue waveform is the CPSD prior to EMI subtractoin and the red waveform is the CPSD post EMI subtraction. Figure 4.8 display the results from multiple test runs with the RTD in ice.

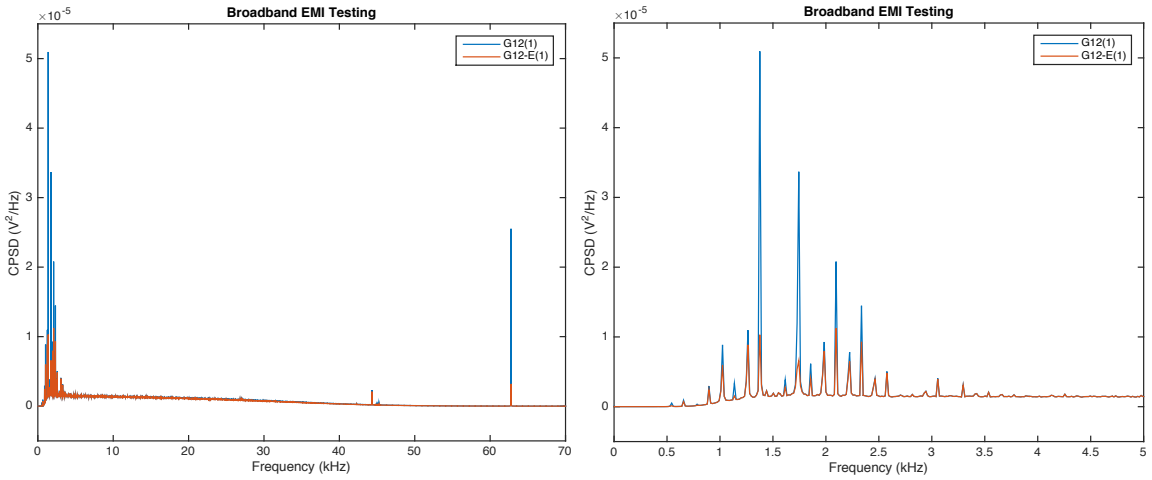

(a) Bandwidth = 0 – 70 kHz **(b)** Zoom: Bandwidth = 10 kHz – 25 kHz

Figure 4.7: Environment 3: $G_{12}(f)$ output from a single test over a 3-hour test measurement

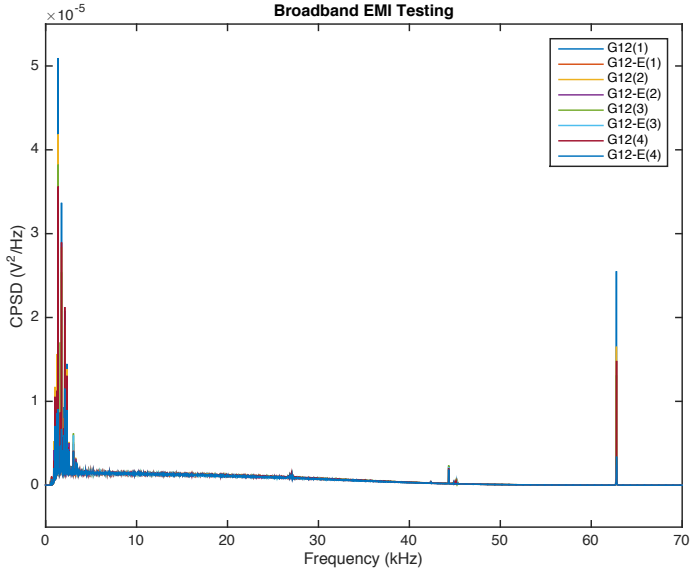

Figure 4.8: Environment 3: $G_{12}(f)$ output from multiple tests over a 3-hour test measurement

Figures 4.9 and 4.10 are the measurement results from the single sine environment (Environment 4). The EMI sources are 60 Hz, 20 kHz generated source from the EMI generation system (Figure 4.3), a 44 kHz EMI source from the internal signal

generator, and a 63 kHz EMI from an unknown source. Figure 4.9 displays the $G_{12}(f)$ results from a single test run and Figure 4.10 display the results from multiple test runs with the RTD in ice.

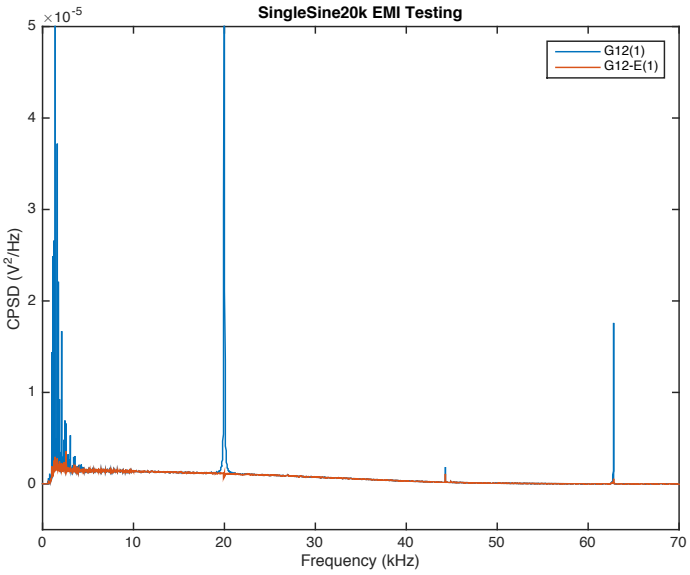

Figure 4.9: Environment 4: $G_{12}(f)$ output from single tests over a 3-hour test measurement

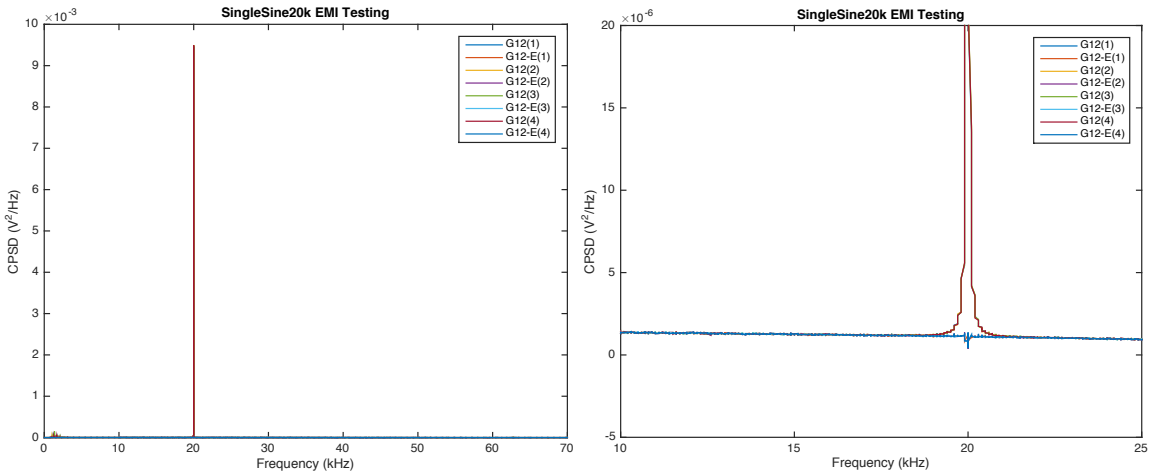

(a) Bandwidth = 0 – 70 kHz **(b)** Zoom: Bandwidth = 10 kHz – 25 kHz

Figure 4.10: Environment 4: $G_{12}(f)$ output from multiple tests over a 3-hour test measurement

Next, the system is tested at elevated temperatures in a Thermolyne F21100 tube furnace, Figure 4.11. The furnace chamber is heated using heating elements embedded in a refractory material. The furnace heating is controlled using a burp controller, which creates significant EMI bursts during operation. Table 4.2 lists the temperatures under test.

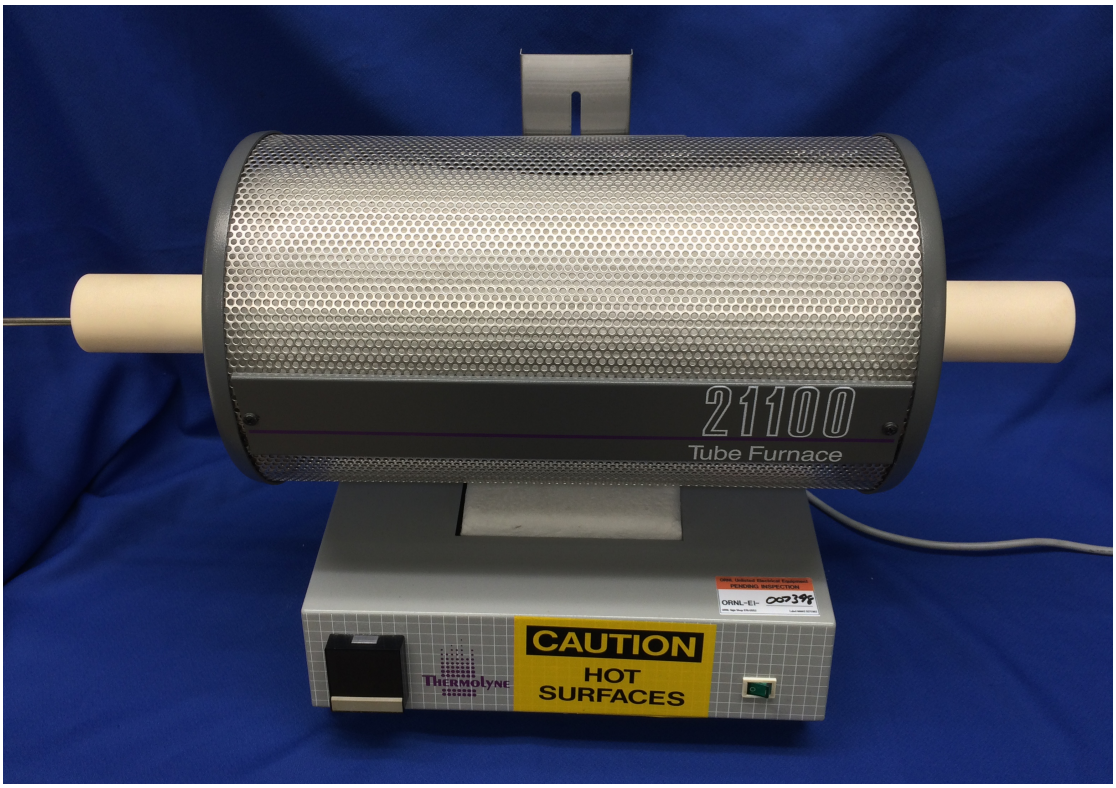

Figure 4.11: Thermolyne F21100 tube furnace

Table 4.2: List of Test Temperatures

Temperature 1	Ice (0 °C = 273.15 K)
Temperature 2	Room Temperature (21.11 °C ≈ 343.15 K)
Temperature 3	100 °C = 373.15 K
Temperature 4	150 °C = 423.15 K
Temperature 5	200 °C = 473.15 K
Temperature 6	250 °C = 523.15 K

The EMI environment for the Temperature 1 (ice) is similar to ambient (Environment 1), see Figure 4.12. This is due to the fact that the testing was performed in the same laboratory under the same EMI conditions. This is also true for Temperature 2 (room temperature), see Figure 4.13.

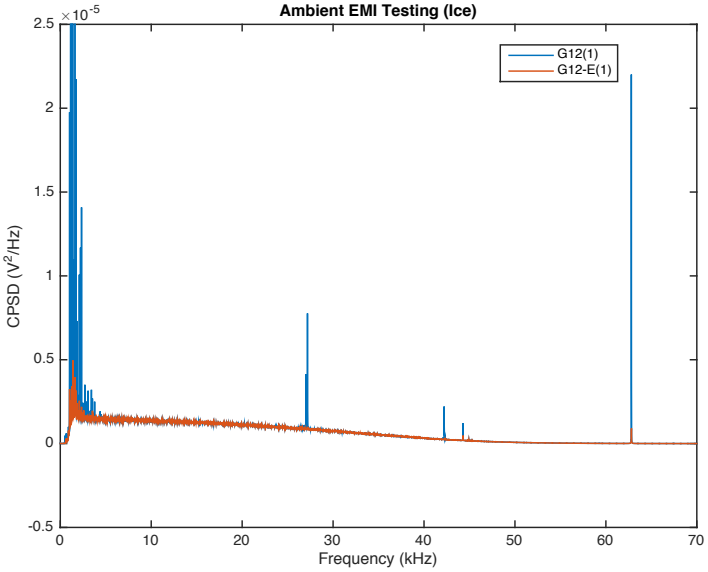

Figure 4.12: $G_{12}(f)$ Output from 3-Hour Test Measurement: Temperature 1 = 0°C

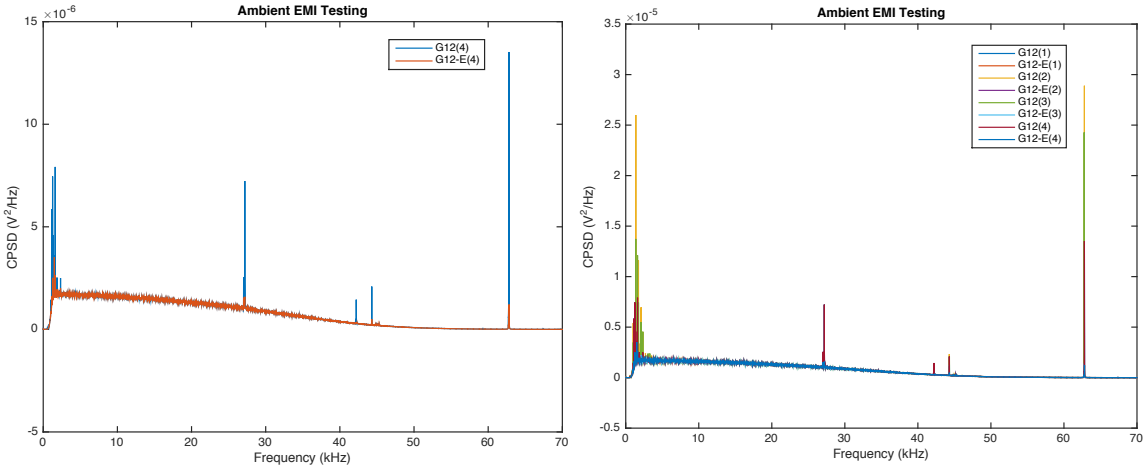

(a) Bandwidth = 0 - 70kHz (Single test) **(b)** Bandwidth = 0 - 70kHz (4x test)

Figure 4.13: $G_{12}(f)$ Output from 3-Hour Test Measurement: Temperature 2 = 21.11 °C

The shape and EMI spike locations are the same for Temperatures 3–6 because the EMI sources are the same. The sources of EMI in these cases are: ambient from the laboratory environment (Environment 1) and EMI from the burp controlled tube furnace. The EMI associated with these runs is dependent on the associated temperature, as the furnace operates for longer time periods and produces increased noise for the higher temperature scenarios. Refer to Figure 4.14-4.20 for the output CPSD between Chnl1 and Chnl2 for these temperature cases. Tables of the temperature values associated with the 4 tests performed for each temperature case are also given below. The temperatures listed are defined as follows: T_{sense} is the DC temperature, NPT JNT Temp is the non-pilot tone Johnson noise temperature, and PT JNT Temp is the Johnson noise temperature with the pilot tone on. Note the values in the tables are slightly higher than Temperature case values. For example, in Table 4.3 the values are not exactly 100°C as expected. This is due to the fact that a large copper slug is placed inside the furnace to allow for a more regulated temperature test. This slug heats up and has a slightly elevated internal temperature from the furnace temperature set point.

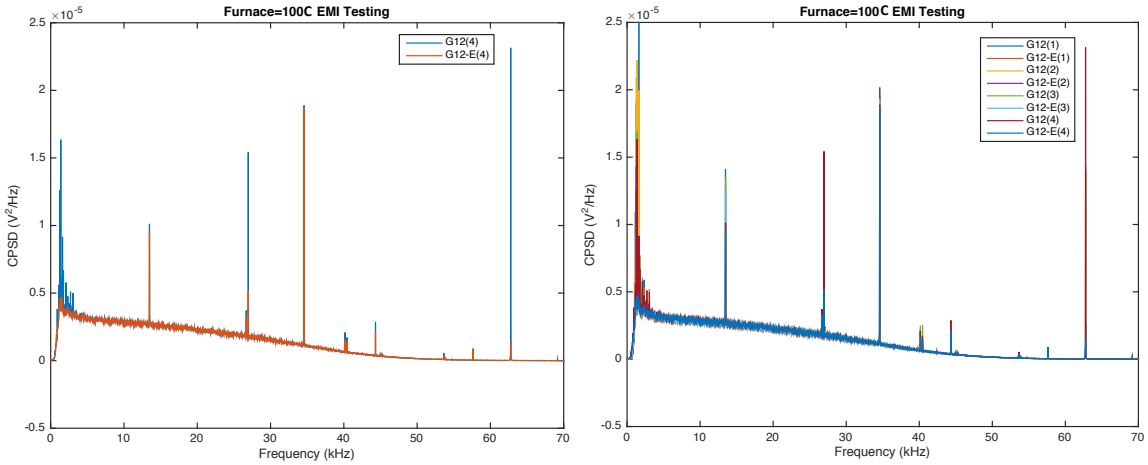

(a) Bandwidth = 0 – 70 kHz (Single test) **(b)** Bandwidth = 0 – 70 kHz (4x test)

Figure 4.14: $G_{12}(f)$ output from 3-hour test measurement:
Temperature 3 = 100 °C

Table 4.3: Temperature Output Values from Temperature 3 Case

	Test 1	Test 2	Test 3	Test 4
$\mathbf{T}_s$	114.33 °C	114.27 °C	114.27 °C	114.38 °C
NPT JNT Temp	112.70 °C	113.74 °C	114.00 °C	118.05 °C
PT JNT Temp	115.30 °C	115.30 °C	118.60 °C	120.05 °C

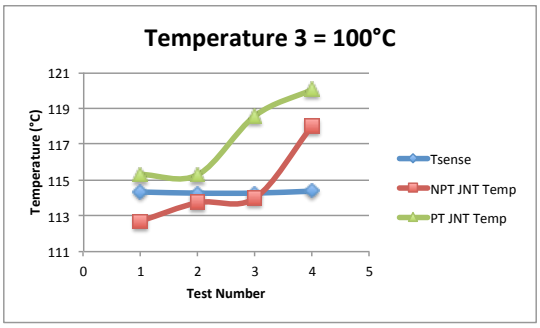

Figure 4.15: Temperature Values from Temperature 3 Case

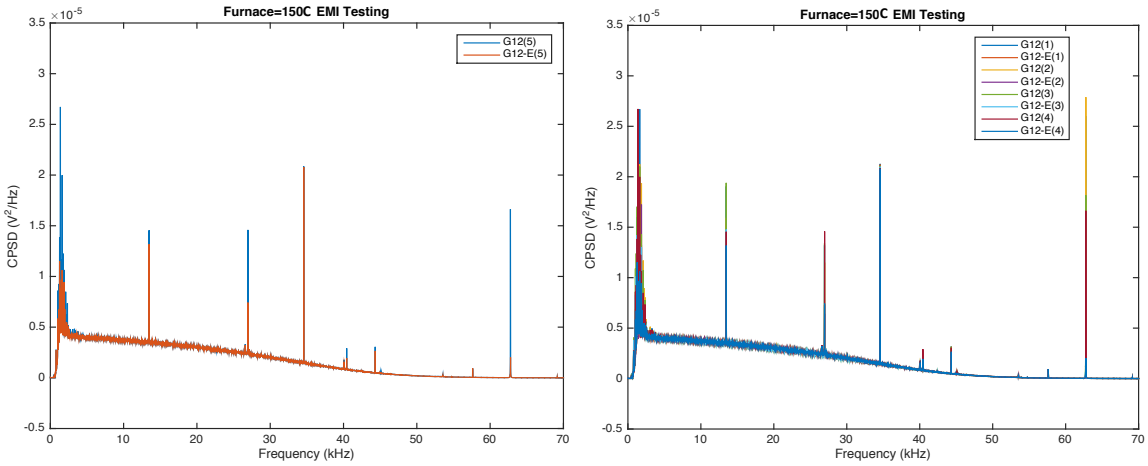

(a) Bandwidth = 0 – 70 kHz (Single test) **(b)** Bandwidth = 0 – 70 kHz (4x test)

Figure 4.16: $G_{12}(f)$ output from 3-hour test measurement:
Temperature 4 = 150 °C

Table 4.4: Temperature Output Values from Temperature 4 Case

	Test 1	Test 2	Test 3	Test 4
$\mathbf{T}_s$	168.22 °C	168.31 °C	168.16 °C	168.19 °C
NPT JNT Temp	168.41 °C	168.57 °C	167.2 °C	167.83 °C
PT JNT Temp	169.56 °C	169.88 °C	168.37 °C	169.34 °C

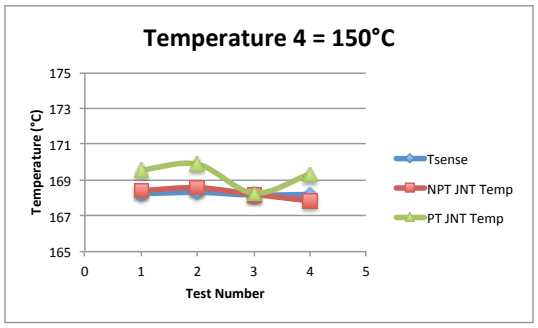

Figure 4.17: Temperature Values from Temperature 4 Case

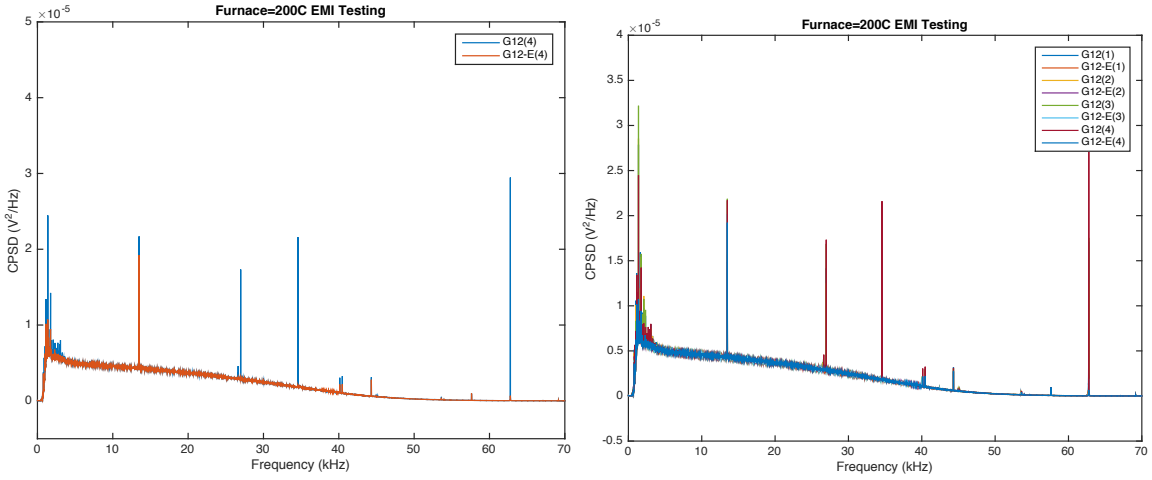

(a) Bandwidth = 0 – 70 kHz **(b)** Bandwidth = 0 – 70 kHz (4x test)

Figure 4.18: $G_{12}(f)$ output from 3-hour test measurement:
Temperature 5 = 200 °C

Table 4.5: Temperature Output Values from Temperature 5 Case

	Test 1	Test 2	Test 3	Test 4
$\mathbf{T}_s$	222.24 °C	222.27 °C	222.27 °C	222.36 °C
NPT JNT Temp	221.36 °C	222.77 °C	222.87 °C	222.10 °C
PT JNT Temp	223.53 °C	223.58 °C	223.4 °C	223.67 °C

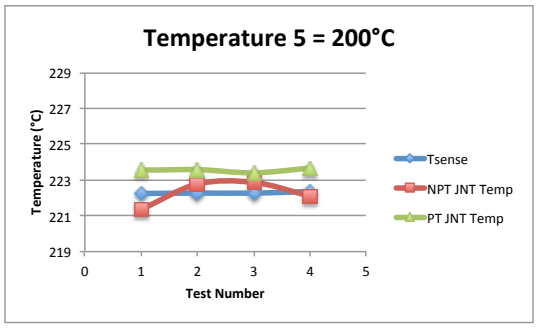

Figure 4.19: Temperature Values from Temperature 5 Case

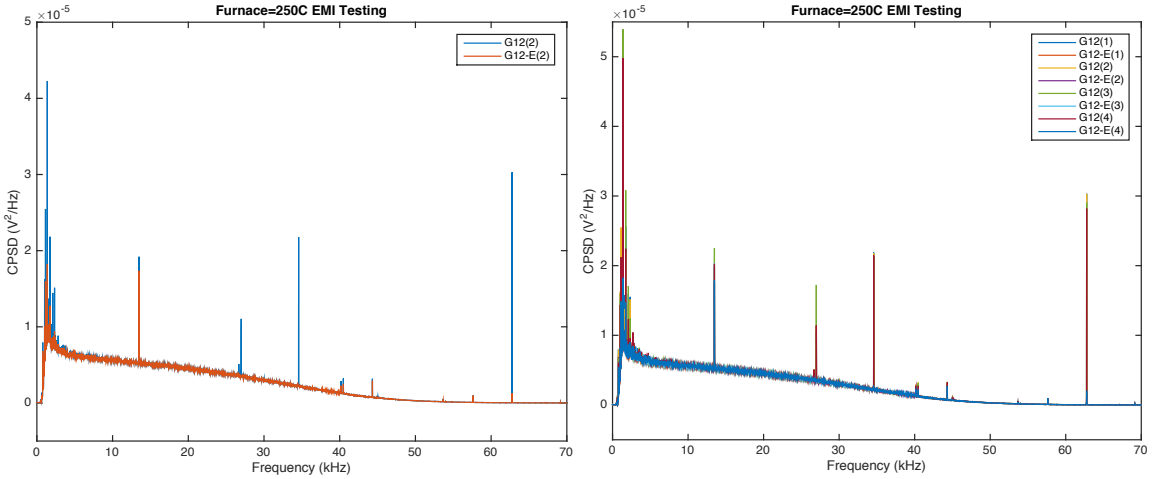

(a) Bandwidth = 0 – 70 kHz (Single test)

(b) Bandwidth = 0 – 70 kHz (4x test)

Figure 4.20: $G_{12}(f)$ output from 3 hour test measurement:
Temperature 6 = 250 °C

Table 4.6: Temperature Output Values from Temperature 6 Case

	Test 1	Test 2	Test 3	Test 4
$\mathbf{T}_s$	275.87 °C	275.90 °C	276.04 °C	275.95 °C
NPT JNT Temp	275.80 °C	276.12 °C	275.69 °C	275.09 °C
PT JNT Temp	277.88 °C	277.45 °C	277.83 °C	276.57 °C

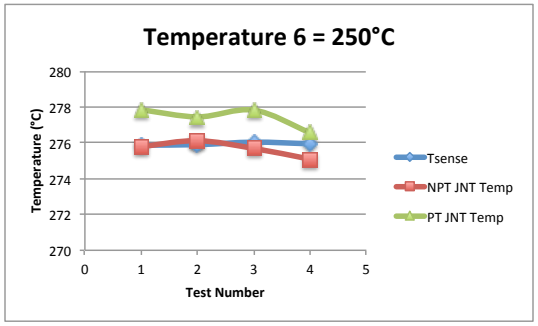

Figure 4.21: Temperature Values from Temperature 6 Case

The CPSD results in Figures 4.14, 4.16, 4.18, and 4.20 demonstrate The EMI subtraction is effective at elevated temperatures. The tables and Figures 4.15, 4.17, 4.19, and 4.21 show that the nonpilot tone JNT temperatures follow very closely with the DC temperature computed with the Callendar-VanDusen equation. The pilot tone JNT temperature is also plotted for monitoring but the calibration uses the nonpilot tone JNT temperature so that is the JNT temperature of interest. From this, it can be concluded that the EMI subtraction method is a valid and improved method from the rejection method discussed in Chapter 2. Applying the signal processing to existing technology would improve temperature monitoring within nuclear reactors.

4.2 Probability Density Function of the Resistor Power Spectral Density

The probability density function (PDF) of the resistor PSD (RPSD) is plotted (Figure 4.22) for the ambient at room temperature (295.1809 K = 22.03 °C = 71.7 F) case.

The z-axis is the PDF of each of the RPSD values, or in other words, it is the probability of each RPSD value. The y-axis is the block number ranging from block 12, 22, 52, etc. up to 20002 blocks. This figure displays the convergence of the RPSD. Spikes due to EMI that appear on the RPSD cause the tail observed in the early block numbers. As the block number increases and more EMI is removed, the RPSD approaches the expected value and the tail gets shorter. The PDF converges to approximately 8.3×10^{-16} having a gaussian shape with the area under the curve equalling one. The RPSD from block number 502 is displayed in Figure 4.23. Figure 4.24 displays the RPSD measured across a long test measurement. The z-axis is the RPSD (V^2/Hz), the x-axis is the frequency in kilohertz, and the y-axis is the block number. As the statistics converge with each block, the data converges and the "fuzz" disappears. It does not take long for the data to converge to a fairly clean RPSD signal. The spike at 27kHz is due to EMI from the environment. As the EMI is removed, the spike shrinks.

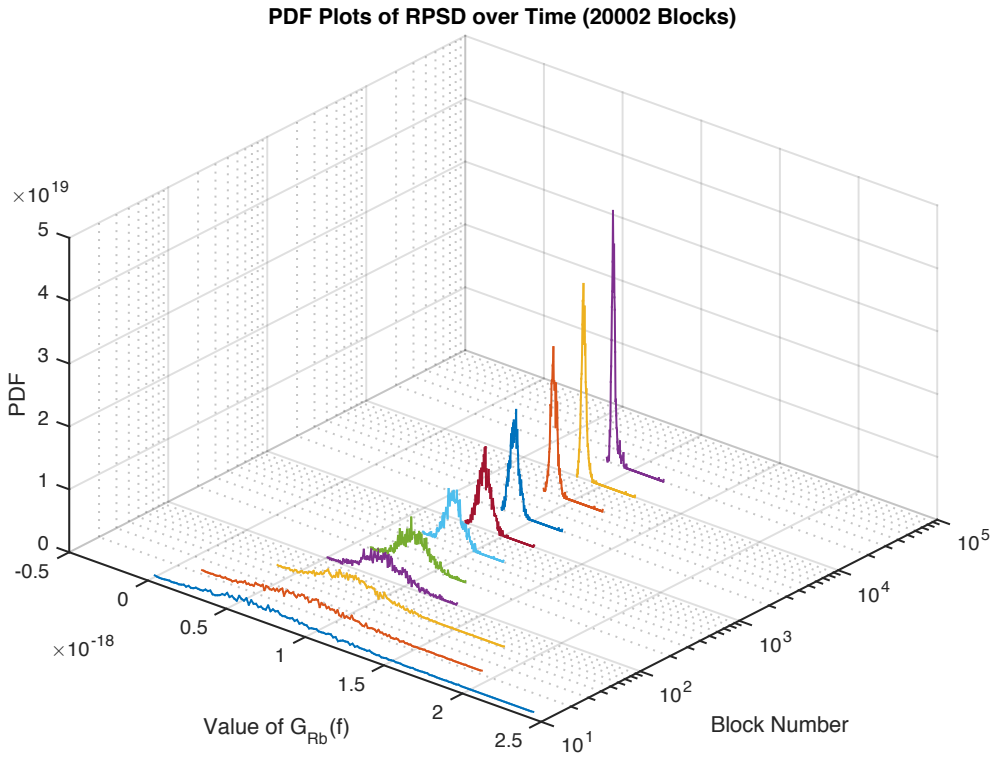

Figure 4.22: Probability density function plot of resistor power spectral density vs. block number

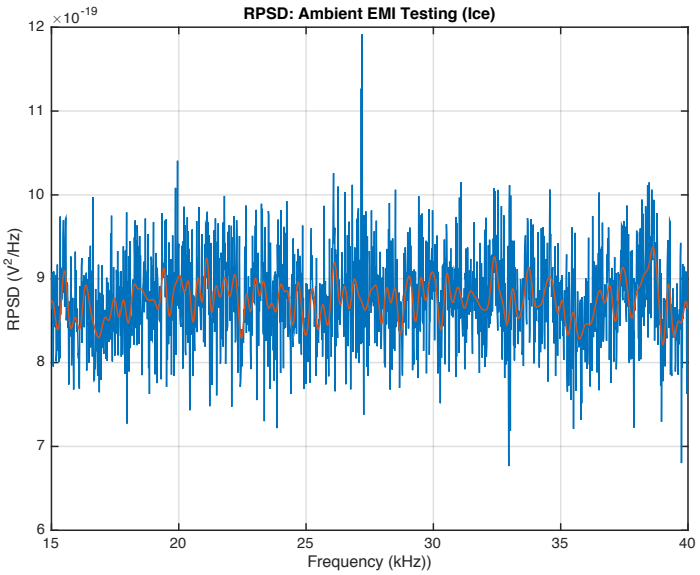

Figure 4.23: RPSD of from a single block of data

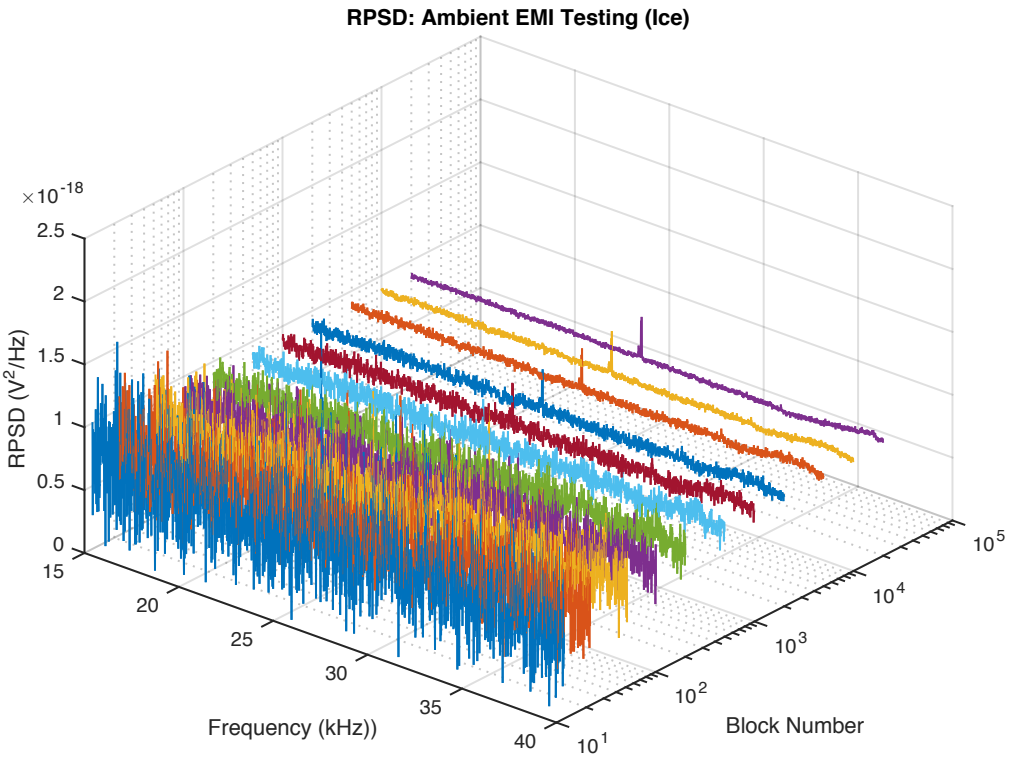

Figure 4.24: RPSD of from each block of data over a long test measurement

From this data analysis, it is obvious that the EMI is being removed and the statistical data is converging accurately. This also proves that the chi-squared distribution assumption is correct. It is important to prove this since all of the computations were based on this assumption.

Chapter 5

Modeling EMI for Simulation of Removal Techniques

Modeling and simulations of several EMI scenarios are investigated to fully understand the effects the EMI on signal processing and computations. These scenarios are designed to increasingly complicate the EMI effects. Simulations are set up to emulate the software signal processing of the JNT system, including calculate the PSD, the CPSD, and the probability density function for a single block of data up to multiple blocks of data. After the EMI models are simulated and the software simulation is validated, JNT chnl1 and chnl2 voltage data blocks from the JNT test measurements are simulated.

5.1 Modeling EMI

Correctly modeling a single block of channel voltage ($v_1(t)$ and $v_2(t)$) will have a great impact on the simulation software. The first simulation uses an ideal situation where the block of data consists of random variables without any EMI injected. Table 5.1 lists all the simulations under investigation. It is important to start with the simplest possible situation to confirm the simulation algorithm is valid. Because the signal

of interest in JNT is a random signal, very closely resembling white noise, using a random noise generator is ideal for the first simulation scenario.

Table 5.1: List of Simulations

Sim 0	White noise = block of data created from a random variable generator
Sim 1	Sim 0 + single sine wave at 20 kHz
Sim 2	Sim 0 + single sine wave at 20 kHz + single sine wave at 30 kHz
Sim 3	Sim 0 + multiple sine wave at 20 kHz + single sine wave at 30 kHz
Sim 4	Sim 0 + very small sine wave at 20 kHz
Sim 5	Sim 0 + numerous sine waves across the frequency band
Sim 6	Simulations of data from JNT system measurement

Figures 5.1–5.7 provide an overview the results of the simulations performed using MATLAB. Figure 5.1 displays the results from a simulation without any EMI added into the system. This gives a baseline for the results of the next few simulations. This waveform would be flat as the random system is symbolic of white noise, but due to the transfer function of the simulated electronics there is a Gaussian-type shape applied to the flat baseline of the white noise. Figure 5.2 displays the case where a singular example of EMI is added to the system. Both transient EMI and periodic EMI are added the the baseline. The transient EMI is random and removed first in the time domain. The periodic EMI is a time-domain sine wave with a frequency of 20 kHz. From the legend of the figures, the black waveform is the CPSD ($G_{12}(f)$) output prior to EMI removal, and the green waveform is the CPSD ($G_{12-E}(f)$) output after the EMI is subtracted. From this figure it is becomes obvious that the subtraction method is capable of removing an EMI source a single frequency location.

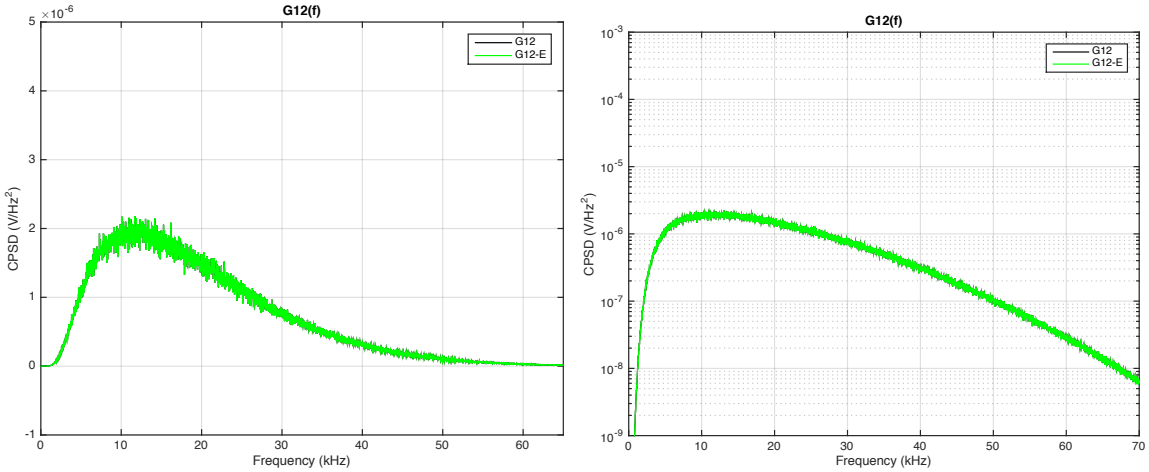

(a) Linear Scale **(b)** Log Scale

Figure 5.1: Sim 0 : White noise1 = block of data created from a random variable generator (0 °C)

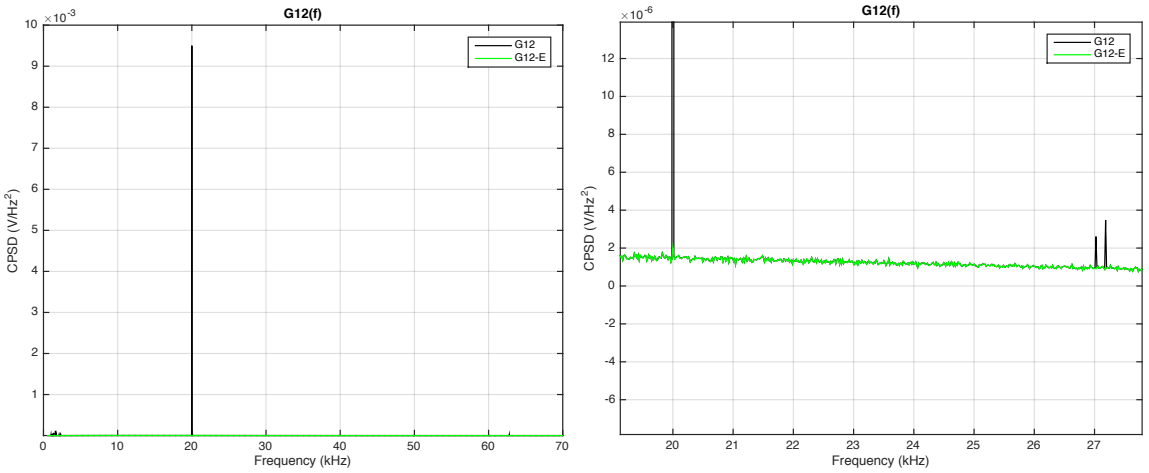

(a) Bandwidth = 0 – 70kHz **(b)** Bandwidth = 10 – 30kHz

Figure 5.2: Sim 1 : Sim 0 + single sine wave at 20 kHz (0 °C)

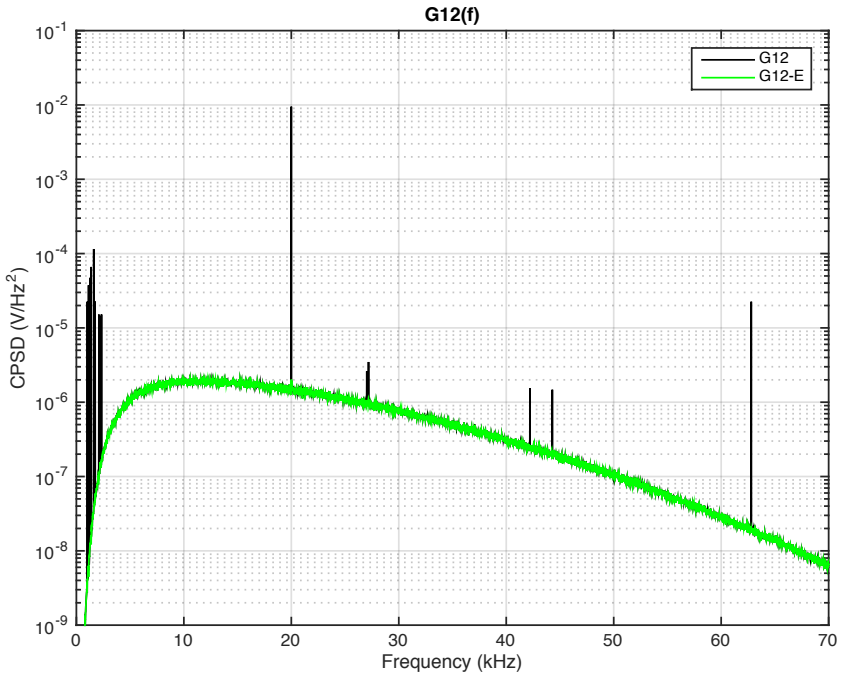

Figure 5.3: Sim 1 : Sim 0 + single sine wave at 20 kHz (0 °C) Log Scale

Figure 5.4 displays the output CPSD from the simulation of Sim 2, which is the baseline with a single time-domain sine wave with frequency at 20 kHz and a sine wave with frequency at 30 kHz. All of the simulations from Sim 1 to Sim 6 have transient EMI that is random. The EMI spikes at 20 kHz and 30 kHz are subtracted. Note that Figure 5.4a is a linear plot of the CPSDs ($G_{12}(f)$ and $G_{12-E}(f)$) and Figure 5.4b is a logarithmic plot of the same data set. The waveforms are displayed in two different formats so that the EMI subtraction is easier to demonstrate. Figure 5.5 displays the output CPSDs ($G_{12}(f)$ and $G_{12-E}(f)$) from the simulation of Sim 3, where there are multiple time-domain sine waves with a frequency of 20 kHz and a single time-domain sine wave with a frequency of 30 kHz added to the baseline white noise. Note that the spike at 20 kHz is larger in this simulation that in the previous simulation. This is because the two sine waves at 20 kHz are added together. Again, the subtraction method removes the EMI at both 20 kHz and 30 kHz.

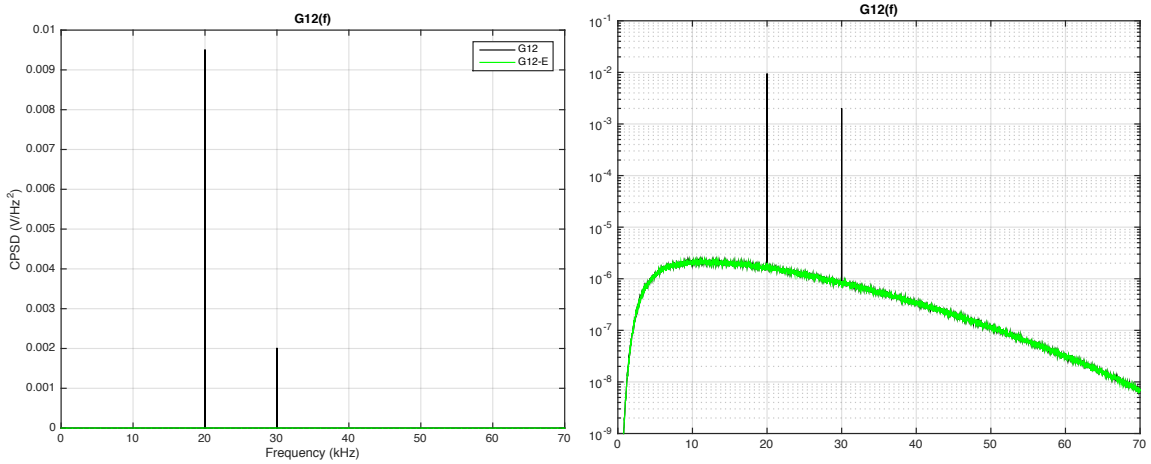

(a) Linear Scale **(b)** Log Scale

Figure 5.4: Sim 2 : Sim 0 + single sine wave at 20 kHz + single sine wave at 30 kHz (0 °C)

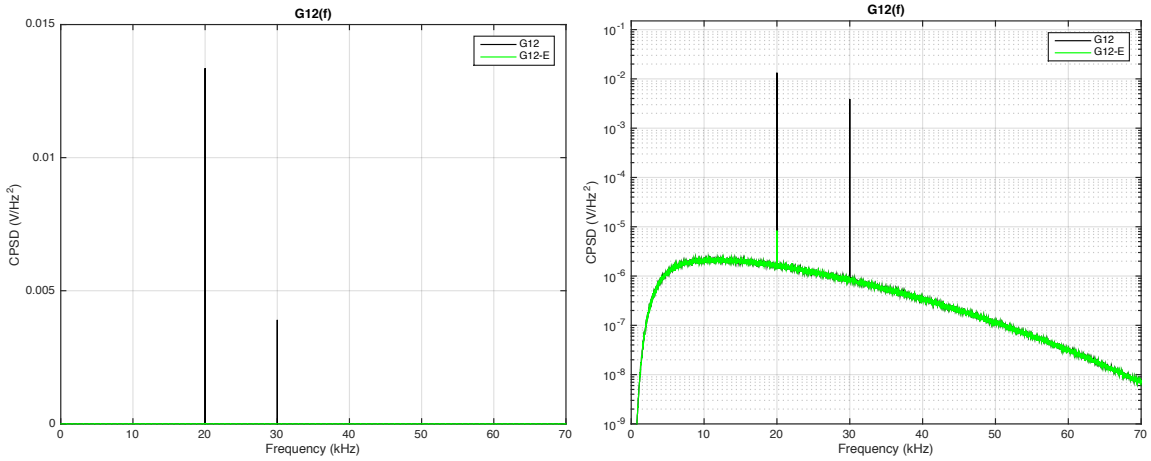

(a) Linear Scale **(b)** Log Scale

Figure 5.5: Sim 3 : Sim 0 + multiple sine wave at 20 kHz + single sine wave at 30 kHz (0 °C)

Figure 5.6 displays the simulation results from Sim 4. This simulation tests the limits of the EMI subtraction technique. The time-domain EMI is a very small sine wave at 40 kHz. This test is to see how small the sine wave can be before the EMI removal technique fails to detect and subtract periodic EMI. Sine waves with

smaller amplitudes are also tested and subtracted. However, eventually the smaller the sine wave, the harder to differentiate between the EMI and the white noise. Figure 5.7 displays the results of another limits test. This case, however, tests how much added EMI causes the subtraction to fail. This case includes a large amount of EMI, both periodic and transient. Note the negative spikes are mathematical errors in the calculation of $G_{12-E}(f)$ due to the subtraction. They can be ignored because the expected value of $G_{12-E}(f)$ is used for temperature calculations.

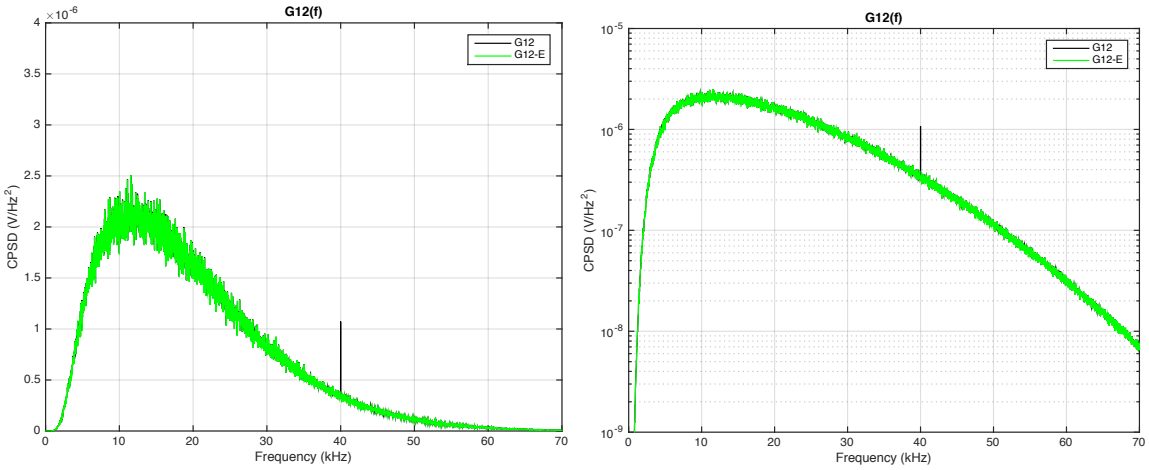

(a) Linear Scale **(b)** Log Scale

Figure 5.6: Sim 4 : Sim 0 + very small sine wave at 40 kHz (0 °C)

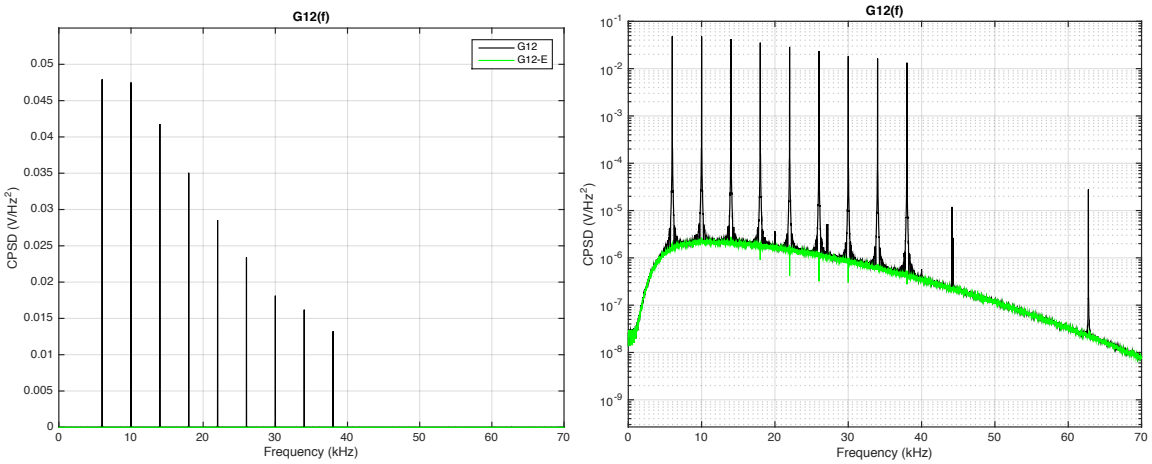

(a) Linear Scale **(b)** Log Scale

Figure 5.7: Sim 5 : Sim 0 + numerous sine waves across the frequency band (0 °C)

These simulations are important because they test the accuracy of the MATLAB model of the physical system and software. The model needs to be accurate to provide validation of the EMI subtraction technique. The MATLAB simulations are also important for quick optimization of the subtraction technique. Real-time Labview testing takes several hours for convergence, whereas the simulations take less time to converge and remove the EMI. After completing the preliminary simulations (Sim0–5), Sim 6 is simulated. Sim 6 consists of three EMI environments that are representative of the EMI environments used to test the physical system. To accurately simulate these environments the EMI spikes in a block of CPSD data set from the test measurements are detected and input into the MATLAB model simulations. The data set must first be converted from CPSD to voltage amplitude (MATLAB variable = Ep.p.A) in time and frequency location (MATLAB variable = Ep.p.f) of EMI spike (Equation 5.1).

Sim 6 is actually multiple simulations of three different EMI environments, listed in Table 5.2. The environments listed are consistent with the environments the JNT hardware system endured.

Table 5.2: List of Sim7 Simulations

1. Sim 6.A : Sim 0 + ambient EMI noise
2. Sim 6.B : Sim 0 + Sandia EMI noise = generated 2 KHz, square wave, amplitude = 250 mV_{pp}
3. Sim 6.C : Sim 0 + broadband EMI noise = blocks of noise across the entire frequency band

$$v(t) = \sqrt{\frac{G_{12}(f)H_{12}(f)}{df}} = \text{Ep.p.A(n) in MATLAB} \tag{5.1}$$

where $df = 16$ and $H_{12}(f)$ is found using Equation 5.2.

$$H_{12}(f) = \frac{G^*_{p1}(f)G_{p2}(f)}{G^2_p(f)|H_p(f)|^2(R_s + R_c)^2} \tag{5.2}$$

Figure 5.8 displays the simulated results from the baseline or Sim 0 with added "ambient EMI." The ambient EMI consists of EMI from the ballast of the florescent lights (multiple spikes around 27 kHz), noise from the Agilent 33XXX signal generator (two spikes around 44 kHz), and a large EMI spike from an unknown source around 63 kHz. The ambient EMI was observed while testing in a laboratory at Oak Ridge National Laboratory.

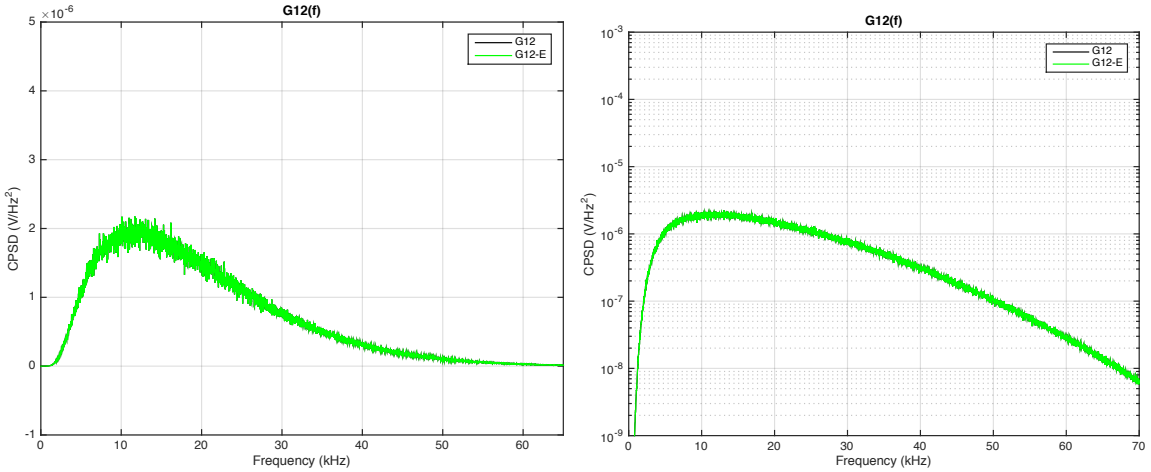

(a) Lights OFF linear scale **(b)** Lights OFF log scale

Figure 5.8: Sim 6.A : Ambient EMI noise

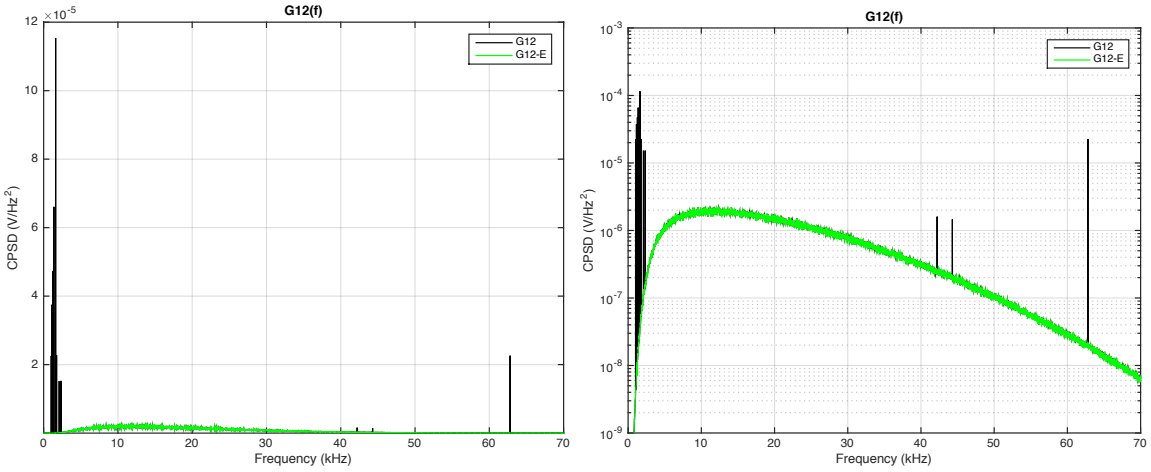

(a) Lights ON linear scale **(b)** Lights ON log scale

Figure 5.9: Sim 6.A : Ambient EMI noise

Figure 5.10 displays the output from simulations of Sim 0 with added periodic EMI noise sources similar to the EMI measured at Sandia National Laboratories. The EMI is a periodic 2 kHz square wave with amplitude of 250 mV_{pp}. The EMI is measured from the Antenna signal $G_A(f)$ from the acquired data set, converted back to the time domain using Equation 5.1 and then input into the MATLAB simulation.

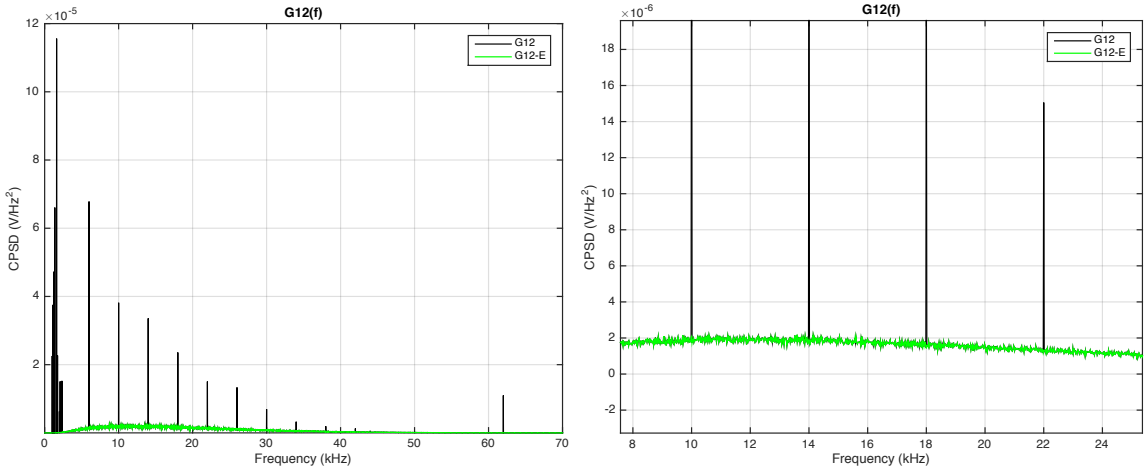

(a) Bandwidth = 0 – 70 kHz **(b)** Zoom: Bandwidth = 10 k – 25 kHz

Figure 5.10: Sim 6.B : Sandia EMI noise = generated 2 kHz, square wave, amplitude = 250 mV_{pp}

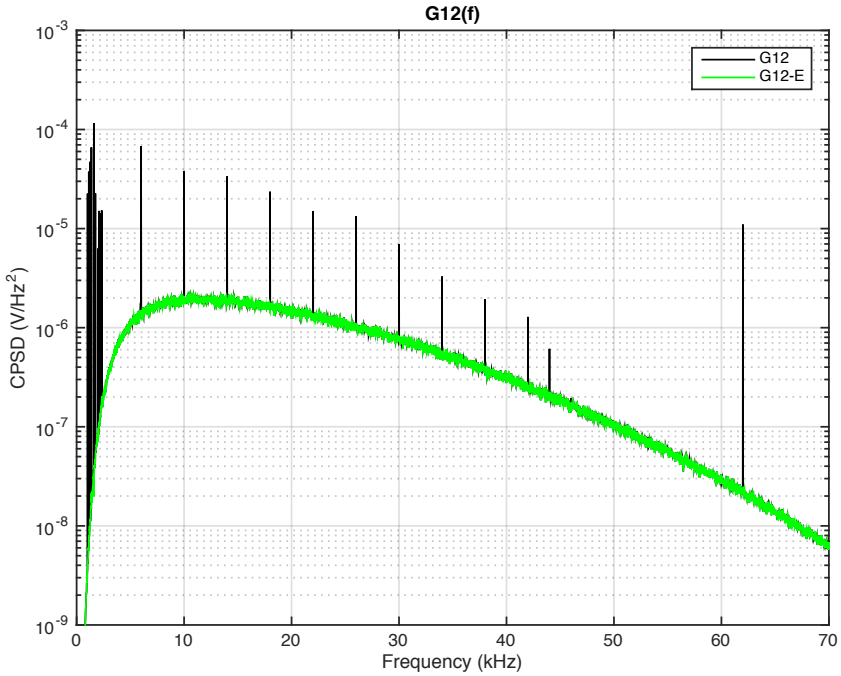

Figure 5.11: Sim 6.B : Sandia EMI noise log scale

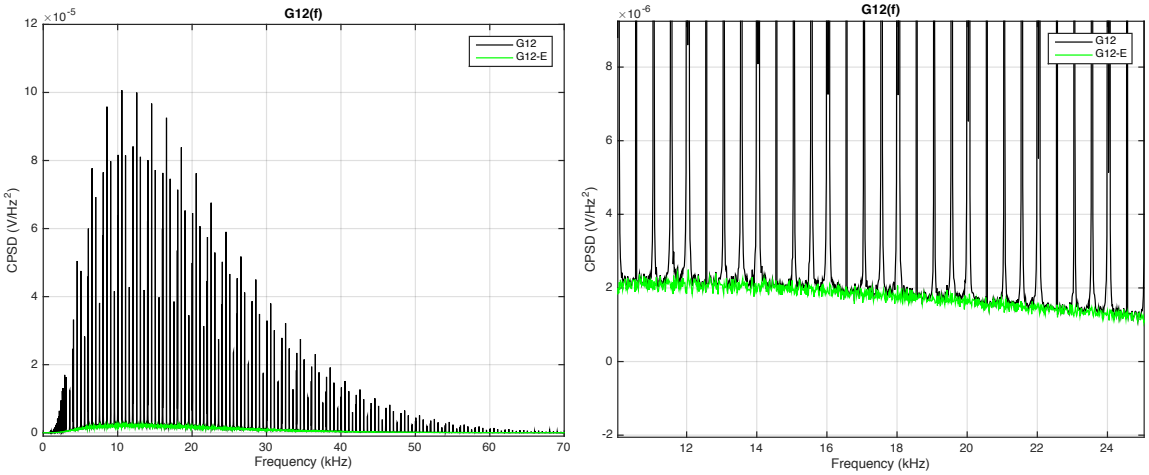

(a) Linear scale **(b)** Linear scale zoom: Broadband: 10 – 25kHz

Figure 5.12: Sim 6.C : Broadband EMI noise = blocks of noise across the entire frequency band (0 °C)

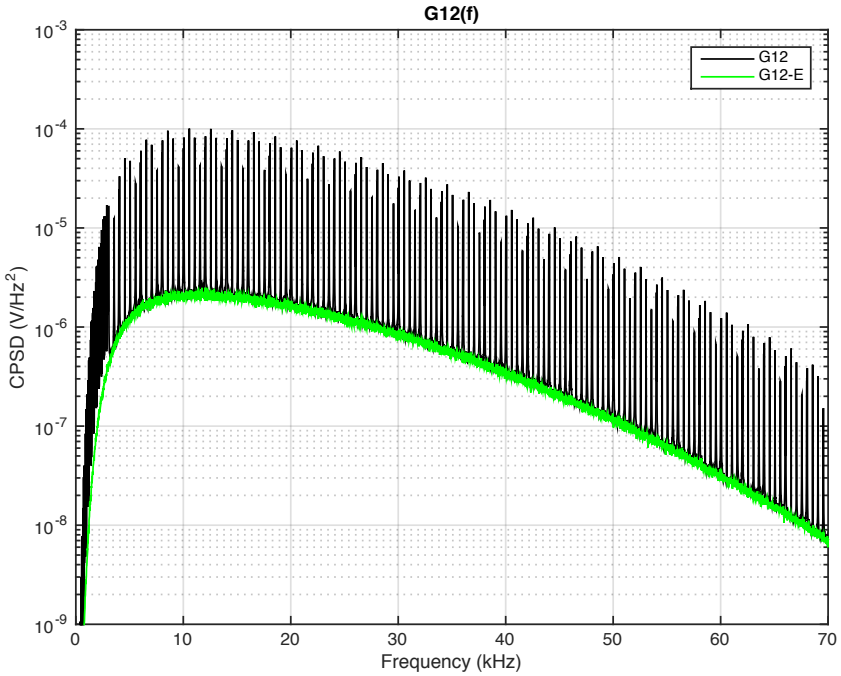

Figure 5.13: Sim 6.C : Broadband EMI noise = blocks of noise across the entire frequency band (0 °C)

The elevated temperature testing environments are also simulated for comparison with the test results. Table 5.3 lists the 4 temperature environments simulated. The only temperature environments disscussed here are 100 °C, 150 °C, 200 °C, and 250 °C. The room temperature and ice environments are discussed previously.

Table 5.3: List of Simulation Temperatures

Simulation Temperature 1	100 °C = 373.15 K
Simulation Temperature 2	150 °C = 423.15 K
Simulation Temperature 3	200 °C = 473.15 K
Simulation Temperature 4	250 °C = 523.15 K

The results from the temperature simulations (Figures 5.14–5.17) demonstrate the effectiveness of the EMI removal algorithm. The green waveform represents $G_{12-E}(f)$ and the black waveform represents $G_{12}(f)$. Note the EMI spikes shown on the black waveforms are effectively removed, as demonstrated on the green waveforms. These waveforms are very similar because the contributing noise sources are the same for all temperature cases. The difference is the magnitude of the spikes due to the added amount of EMI at each of the frequencies. Table 5.4 displays the temperature results from each of the four simulations. The JNT Temperatures simulation results are accurate and repeatable across several simulations.

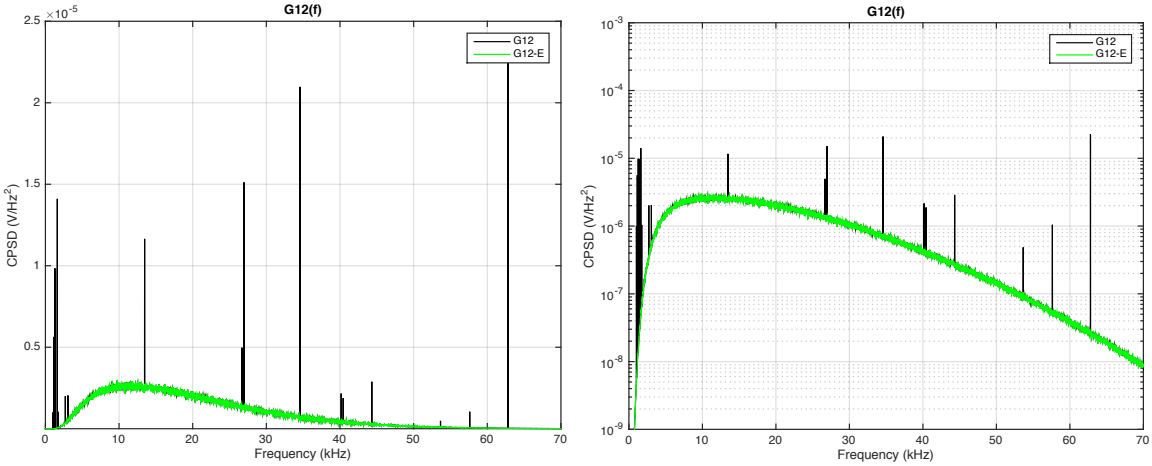

(a) Linear scale **(b)** Linear scale zoom: Broadband: 10 – 25kHz

Figure 5.14: Sim Temperature 1 : (100 °C)

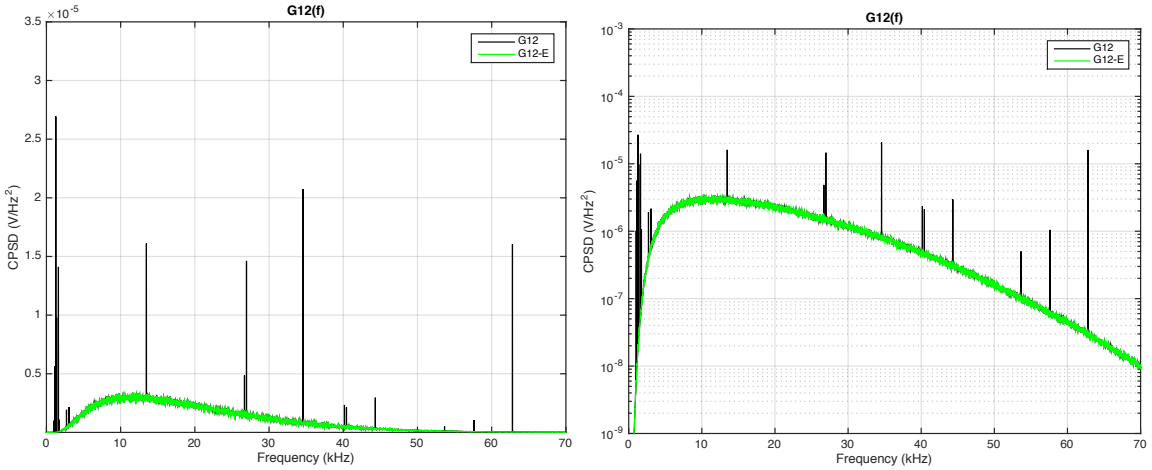

(a) Linear scale **(b)** Linear scale zoom: Broadband: 10 – 25kHz

Figure 5.15: Sim Temperature 2 : (150 °C)

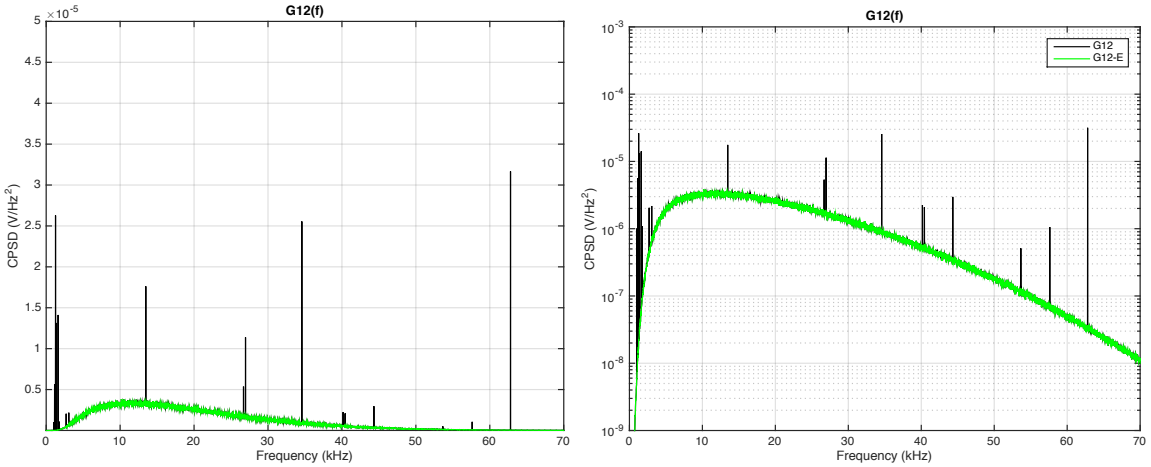

(a) Linear scale **(b)** Linear scale zoom: Broadband: 10 – 25kHz

Figure 5.16: Sim Temperature 3 : (200 °C)

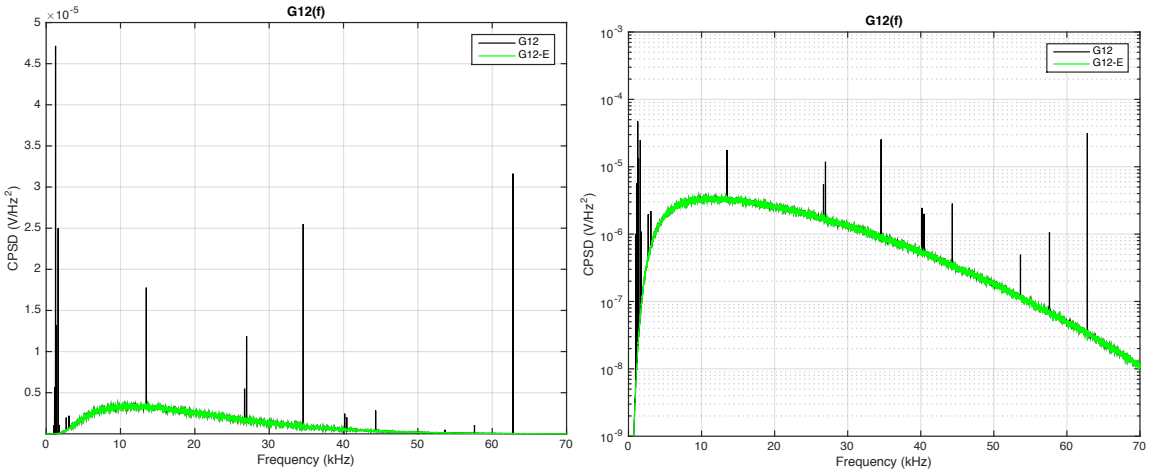

(a) Linear scale **(b)** Linear scale zoom: Broadband: 10 – 25kHz

Figure 5.17: Sim Temperature 4 : (250 °C)

Table 5.4: Output Values from Simulation of four Temperature Cases

	Sim Temperature 1	Sim Temperature 2	Sim Temperature 3	Sim Temperature 4
$\mathbf{T}_s$	373.15 °C	423.15 °C	473.15 °C	523.15 °C
JNT Temp	372.39 °C	422.54 °C	473.91 °C	522.76 °C

The following is a small section of the EMI simulation MATLAB code. The complete version of the final algorithm simulation code is provided in Appendix D. This section of code displays the set up of the transient and periodic EMI for different environment cases.

```
% Transient EMI Set-up
  Ep.t.on = 0 ; % Turn transient EMI ON = 1; OFF = 0
  Ep.t.r = 10 ;  % rate parameter of the Poisson process, per second
  Ep.t.Nav = 5 ; % avg number of pulses in a sequence
  Ep.t.Aav = 3e-5 ; % avg amplitude of the transient EMI pulses(V)
  Ep.t.tauav = 10e-6 ;  % avg amplitude of the transient EMI pulses(V)
  Ep.t.Tav = 1/20 ;  % aveg duration of a sequence of pulses (s)
```

```
% Periodic EMI Set-up
% Ep.p.f = vector of periodic E frequencies (Hz)
    Ep.p.on = 1; % Turn periodic EMI ON = 1; OFF = 0
% Sandia Simulation:
  Ep.p.f = [2000,6000,10000,14000,18000,22000,26000,30000,
            34000,38000,42000,44000,46000,50000,62000,1024,
            1136,1264,1376,1616,1744,2096,2336,2224];
  NEp = length(Ep.p.f) ;
% Ep.p.A = vector of periodic EMI amplitudes (V)
  Ep.p.A = [(0.01999/S.gain1),(0.065/S.gain2),(0.048/S.gain3),...
            (0.045/S.gain4),(0.038/S.gain5),(0.03/S.gain6),...
            (0.028/S.gain7),(0.02/S.gain8),(0.013/S.gain9),...
            (0.01/S.gain10),(0.008/S.gain11),(0.005/S.gain12),...
            (0.001/S.gain13),(0.0008/S.gain14),(0.025/S.gain15),...
            (0.038./A.gain1),(0.049/A.gain2),(0.055/A.gain3),...
            (0.065/A.gain4),(0.086/A.gain5),(0.038/A.gain6),...
            (0.031/A.gain7),(0.031/A.gain8),(0.03/A.gain11)];
%% Ambient Simulation:
% Ep.p.f = [1024,1136,1264,1376,1616,1744,2096,2336,...
```

```
347 %          42208,44288,62800]%,2224,27024,27184,];
348 % Ep.p.A = [(0.038./A.gain1),(0.049/A.gain2),(0.055/A.gain3),...
349 %           (0.065/A.gain4),(0.086/A.gain5),(0.038/A.gain6),...
350 %           (0.031/A.gain7),(0.031/A.gain8),(0.009/A.gain14),...
351 %           (0.009/A.gain15),(0.038/A.gain16)];%(0.03/A.gain11),...
352 %           (0.01/A.gain12),(0.012/A.gain13)];
353 %% Single Sine 20KHz:
354 % Ep.p.f = [1024,1136,1264,1376,1616,1744,2096,2336,2224,...
355 %           20000,27024,27184,42208,44288,62800];
356 % Ep.p.A = [(0.038./A.gain1),(0.049/A.gain2),(0.055/A.gain3),...
357 %           (0.065/A.gain4),(0.086/A.gain5),(0.038/A.gain6),...
358 %           (0.031/A.gain7),(0.031/A.gain8),(0.03/A.gain11),...
359 %           (0.78./SS.gain1),(0.01/A.gain12),(0.012/A.gain13),...
360 %           (0.009/A.gain14),(0.009/A.gain15),(0.038/A.gain16)];
361 %% Broadbrand Simulation:
362 % Ep.p.f = [[60:60:3000]';[10:2000:70000]';...
363 %           [60:500:70000]'] ;
364 % Ep.p.A = ones(NEp,1)*50e-9;
365  Ep.p.A = [Ep.p.A] ;
366  ESP = sum(Ep.p.A.^2/2) ; %   Periodic EMI signal power at the sensor
```

Chapter 6

Conclusions on Signal Processing for JNT

The goal of this research is to monitor temperature in harsh environments without corruption from EMI. Two methods are presented. Chapter 2 discusses the existing technology that used a rejection method. The rejection method rejects transient EMI through rectangular windowing in the time domain. The signal is then FTed to the frequency domain where the standard deviation of the data set is computed. Any periodic EMI that is greater than or equal to twice the standard deviation is removed and replaced with the baseline. This is a recursive algorithm where the EMI removal performance depends on time. The longer the measurement runs, the better more EMI is rejected. The second method discussed is the subtraction method in Chapter 3. The subtraction method is the new advanced algorithm and takes advantage of an antenna monitoring the EMI environment. The EMI is subtracted from the channel output voltages improving the CPSD computation between chnl1 and chnl2, therefore, improving the overall temperature calculation. The subtraction method also uses the rectangular window to remove transient EMI. This algorithm effectively removes large sources of EMI and employs recursive operations to remove

smaller EMI signals over time. The derivations of both of these methods are in the appendices.

The performance of this algorithm has been verified through testing (Chapter 4) and simulation (Chapter 5). The testing performed at Oak Ridge National Laboratory verified the capabilities of the physical system under various EMI environments and elevated temperatures. The results of these measurements demonstrated that the system is able to accurately and repeatedly compute temperature. The simulations use a model of the system and software algorithm. Simulations push the limits of the model to test validity through multiple EMI environments. The model is able to accurately subtract very large EMI and very small EMI. Also, the amount of EMI does not have an impact on the ability of the simulation model. Several of the EMI environments from the physical testing are simulated demonstrating the equivalence of the model to the physical system. Both the CPSD between chnl1 and chnl2 and the temperatures from the simulations are reported.

After performing both testing and simulation of the subtraction method, it is concluded that the algorithm is reliable and repeatable. Applying this method to existing RTDs would improve the overall temperature measurement accuracy and remove drift problems from aging sensors.

6.1 Future Research

Suggested improvements:

1. Improve antenna and associated hardware for more effective EMI detection
2. Remove signal generator from inside the front end box of JNT system because it is an unwanted source of EMI
3. Optimize data acquisition system hardware
4. Add a “self-calibration” function to the software

- Adjust the averaging process dependent on real-time resistance voltage measurement.
- If temperature is changing quickly, use a fast average and update the resistance temperature curve
- If temperature is not changing quickly, use a slow average
- Set the averaging time to justify the assumption that the random process is approximately stationary

5. Try using a time domain EMI removal technique such as Kalman filtering in lieu of of frequency domain techniques

Discussion of the suggested improvements:
The better the EMI signal represents the actual EMI, the better the subtraction method will work. To improve the model of the EMI environment, more research into the antenna hardware is needed. An off-the-shelf antenna that is capable of detecting broadband EMI in different fields would greatly improve the antenna signal. Currently the antenna only exists outside the JNT front end box and is a two wire open-ended antenna. Additional monitoring of EMI inside the box would also improve the model.

The Agilent signal generator that provides the PT signal is also a large source of EMI. Since it lives inside the JNT front end box, it has a large impact on the JNT signals. Removing this signal generator and replacing it with a different, low noise, signal generator would reduce unwanted EMI. Future work would include replacing the signal generator with a field-programmable gate array and amplifier circuit.

The system used to perform all the measurements presented here utilized two Agilent data acquisition systems that would lose communication with LabView from time to time. Since communication depended on the USB connection between the data acquisition and the computer, any time the computer would go to sleep communication would be lost. To resolve this, in the new portable system two NI data acquisition systems replaced the unreliable Agilent boxes.

Adding a "self-calibration" function to the software is critical to make this research marketable. To calibrate the system the software needs to update the resistance temperature curve. The intercept and slope from this waveform provides the information needed for the Callendar-Van Dusen temperature calculation. This function needs to adjust the averaging process depending on the rate of change of the temperature. If the temperature is changing quickly, the averaging process is fast moving and the resistance temperature curve needs updated. A minimum of three data points are required to properly update the curve. If the temperature is not changing quickly, the averaging process is slow and typical operations continue and JNT temperatures are monitored as usual.

It has been suggested that while transforming to the frequency domain simplifies the mathematics behind the calculations provided here, the transformation causes a loss in information. For this reason, research into time domain techniques for EMI removal is of interest. Time domain filtering such as the Kalman filter is one example of a possible EMI removal technique. Some initial research and simulations have proven time domain filtering is possible with this process, but application to the system has not taken place.

Bibliography

[1] M. J. Roberts, "Random process theory for engineers," January 2014, unpublished Book from EECS Course 504.

[2] ——, "Johnson noise thermometry using correlation techniques in noisy environments," 2015, unpublished document deriving PSD and CPSD.

[3] H. Brixy, "Temperature measurement in nuclear reactors by noise thermometry," *Nuclear Instruments and Methods*, vol. 97, no. 1, pp. 75–80, 1971.

[4] J. Garrison and A. Lawson, "An absolute noise thermometer for high temperatures and high pressures," *Review of Scientific Instruments*, vol. 20, no. 11, pp. 785–794, 1949.

[5] A. Einstein, *Investigations on the Theory of the Brownian Movement*. Courier Corporation, 1956.

[6] D. White, R. Galleano, A. Actis, H. Brixy, M. De Groot, J. Dubbeldam, A. Reesink, F. Edler, H. Sakurai, R. Shepard *et al.*, "The status of johnson noise thermometry," *Metrologia*, vol. 33, no. 4, p. 325, 1996.

[7] T. Blalock and R. Shepard, "Decade of progress in high-temperature johnson noise thermometry," Oak Ridge National Lab., TN (USA); Tennessee Univ., Knoxville (USA). Dept. of Electrical Engineering, Tech. Rep., 1982.

[8] J. B. Johnson, "Thermal agitation of electricity in conductors," *Nature*, vol. 119, pp. 50–51, 1927.

[9] ——, "Thermal agitation of electricity in conductors," *Physical review*, vol. 32, no. 1, p. 97, 1928.

[10] H. Nyquist, "Thermal agitation of electric charge in conductors," *Physical review*, vol. 32, no. 1, p. 110, 1928.

[11] Harvard University, "Thermal noise," http://isites.harvard.edu/fs/docs/icb.topic86897.files/October_13_Temperature/ThermalNoise.pdf, October 2013.

[12] M. Pepper and J. Brown, "Absolute high-temperature johnson noise thermometry," *Journal of Physics E: Scientific Instruments*, vol. 12, no. 1, p. 31, 1979.

[13] M. Decreton, L. Binard, C. Delrez, W. Hebel, and W. Schubert, "High temperature measurements by noise thermometry," *HIGH TEMP. HIGH PRESSURES*, vol. 12, no. 4, pp. 395–402, 1980.

[14] A. Lawson and E. A. Long, "On the possible use of brownian motion for low temperature thermometry," *Physical Review*, vol. 70, no. 3-4, p. 220, 1946.

[15] J. B. Brown and D. MacDonald, "On the possible use of brownian motion for low temperature thermometry," *Physical Review*, vol. 70, no. 11-12, p. 976, 1946.

[16] A. Lawson and E. A. Long, "Further remarks on the possible use of brownian motion in low temperature thermometry," *Physical Review*, vol. 70, no. 11-12, p. 977, 1946.

[17] P. Mörters and Y. Peres, *Brownian motion*. Cambridge University Press, 2010, vol. 30.

[18] J. Klafter, M. F. Shlesinger, and G. Zumofen, "Beyond brownian motion," *Physics today*, vol. 49, no. 2, pp. 33–39, 1996.

[19] J. Qu, S. P. Benz, A. Pollarolo, H. Rogalla, W. L. Tew, R. White, and K. Zhou, "Improved electronic measurement of the boltzmann constant by johnson noise thermometry," *Metrologia*, vol. 52, no. 5, p. S242, 2015.

[20] W. Tew, S. Benz, P. Dresselhaus, K. Coakley, H. Rogalla, D. White, and J. Labenski, "Progress in noise thermometry at 505 k and 693 k using quantized voltage noise ratio spectra," *International Journal of Thermophysics*, vol. 31, no. 8-9, pp. 1719–1738, 2010.

[21] K. Yamazawa, C. Urano, Y. Fukuyama, T. Oe, M. Maruyama, A. Domae, and N. Kaneko, "Progress of the johnson noise thermometry project at nmij/aist," *XX IMEKO World Congress, Metrology for Green Growth*, 2012.

[22] L. Callegaro, V. D'Elia, M. Pisani, and A. Pollarolo, "A johnson noise thermometer with traceability to electrical standards," *Metrologia*, vol. 46, no. 5, p. 409, 2009.

[23] C. L. Britton Jr, M. Roberts, N. D. Bull, D. E. Holcomb, and R. T. Wood, "Johnson noise thermometry for advanced small modular reactors," *ORNL/TM-2012/346, SMR/ICHMI/ORNL/TR-2012/01*, 2012.

[24] H. Brixy, R. Hecker, J. Oehmen, P. Barbonus, and R. Hans, "Development work on noise thermometry and improvement of conventional thermocouples for applications in nuclear process heat," in *Specialists? Meeting on Gas Cooled Reactor Core and High Temperature Instrumentation*, 1982, pp. 6–7.

[25] C. Borkowski and T. Blalock, "A new method of johnson noise thermometry," *Review of Scientific Instruments*, vol. 45, no. 2, pp. 151–162, 1974.

[26] M. J. Roberts, T. Blalock, and R. L. Shepard, "Application of johnson noise thermometry to space nuclear reactors," in *Space Nuclear Power Systems 1989*, vol. 1, 1992, pp. 87–93.

[27] D. E. Holcomb, R. A. Kisner, and M. J. Roberts, "Johnson noise thermometry for space reactor temperature measurement," AIP Congerence Proceedings, p. 567, 2004.

[28] D. E. Holcomb, R. A. Kisner, and C. L. Britton Jr, "Fundamental thermometry for long-term and high-temperature deployment in generation iv reactors," *Proceedings of the International Symposium on Future Instrumentation and Controls*, 2006.

[29] R. Kisner, C. Britton, U. Jagadish, J. Wilgen, M. Roberts, T. Blalock, D. Holcomb, M. Bobrek, and M. Ericson, "Johnson noise thermometry for harsh environments," in *Aerospace Conference, 2004. Proceedings. 2004 IEEE*, vol. 4. IEEE, 2004, pp. 2586–2596.

[30] M. J. Roberts, *Signals and systems: analysis using transform methods and MATLAB*. McGraw-Hill Dubuque, IA, 2004.

[31] M. V. Dusen, "Platinum-resistance thermometry at low temperatures1," *Journal of the American Chemical Society*, vol. 47, no. 2, pp. 326–332, 1925.

[32] P. Z. Peebles, J. Read, and P. Read, *Probability, random variables, and random signal principles*. McGraw-Hill Boston, Mass, USA, 2001, vol. 3.

[33] S. Primak, V. Kontorovitch, and V. Lyandres, *Stochastic methods and their applications to communications: stochastic differential equations approach*. John Wiley & Sons, 2005.

[34] P. Bromiley, "Products and convolutions of gaussian probability density functions," *Tina-Vision Memo*, vol. 3, 2003.

[35] M. D. Springer, *The Algebra of Random Variables*. John Wiley and Sons, 1979.

[36] Y. L. Luke, *The special functions and their approximations*. Academic press, 1969, vol. 53.

[37] C. Fox, "The g and h functions as symmetrical fourier kernels," *Transactions of the American Mathematical Society*, vol. 98, no. 3, pp. 395–429, 1961.

[38] H. Bateman and A. Erdelyi, "Higher transcendental functions, vol. 1," 1953.

[39] J. S. Bendat and A. G. Piersol, *Random data: analysis and measurement procedures*. John Wiley & Sons, 2011, vol. 729.

[40] I. Guttman, S. S. Wilks *et al.*, "Introductory engineering statistics," 1965.

[41] W. Wells, R. Anderson, J. W. Cell *et al.*, "The distribution of the product of two central or non-central chi-square variates," *The Annals of Mathematical Statistics*, vol. 33, no. 3, pp. 1016–1020, 1962.

Appendix

Appendix A

Derivation of PSD/CPSD for Rejection Method

A.1 Cross Power Spectral Density of JNT Channel 1 and Channel 2

The Power Spectral Density (PSD) in (V^2/Hz)

$$G_v(f) = \left[\frac{2hfR}{exp(hf/kt) - 1}\right] df \tag{A.1}$$

where R is the resistance in ohms, T is the absolute temperature in Kelvin, h is Planck's constant $(6.626x10^{-34}J/Hz)$, k is Boltzmann constant $(1.3806x10{-}23J/K)$. Since the frequency bandwidth of the measurement is low $(f << \frac{kT}{h})$, $G_v(f) \cong 2kTR$. From Chapter 4, Section 4.4 Equation 2.22:

$$\begin{aligned} v_1(t) &= \{[v_{Rs}(t) + v_{Rc}(t)] * h_s(t) + v_{a1}(t)\} * h_1(t) \\ v_2(t) &= \{[v_{Rs}(t) + v_{Rc}(t)] * h_s(t) + v_{a2}(t)\} * h_2(t) \end{aligned} \tag{A.2}$$

The transient EMI is removed with a rectangle window in the time domain. Then the signals are Fourier transformed to the frequency domain. Convolution in the time

domain transforms to multiplication in the frequency domain, using the Proof of the Convolution Theorem. Proof of the Convolution Theorem By definition,

$$f(x) * g(x) = \int_{-\infty}^{\infty} f(x)g(y-x)dx \tag{A.3}$$

The Fourier Transform of $f(x) * g(x)$ is

$$\int_{-\infty}^{\infty} \left[\int_{-\infty}^{\infty} f(x)g(y-x)dx \right] e^{-j2\pi uy} dy \tag{A.4}$$

By the Shift Property,

$$\int_{-\infty}^{\infty} g(y-x)e^{-j2\pi uy}dy = F[g(y-x)] = e^{-j2\pi ux}G(u) \tag{A.5}$$

Therefore,

$$\begin{aligned} \int_{-\infty}^{\infty} f(x) \left[\int_{-\infty}^{\infty} g(y-x)e^{-j2\pi uy}dy \right] dx &= \int_{-\infty}^{\infty} f(x)e^{-j2\pi ux}G(u)dx \\ &= \left[\int_{-\infty}^{\infty} f(x)e^{-j2\pi ux}dx \right] G(u) \\ &= F(u)G(u) \end{aligned} \tag{A.6}$$

It is concluded that, the Fourier transform $F[f * g] = F(u)G(u)$, convolution in the space/time domain is equivalent to multiplication in the frequency domain [30].

$$\begin{aligned} V_1(f) &= \{[V_{Rs}(f) + V_{Rc}(f)]H_s(f) + V_{a1}(f)\}H_1(f) \\ V_2(f) &= \{[V_{Rs}(f) + V_{Rc}(f)]H_s(f) + V_{a2}(f)\}H_2(f) \end{aligned} \tag{A.7}$$

$\rightarrow$ Note 1: $V_{Rs}(f)$, $V_{Rc}(f)$, $H_s(f)$, $V_{a1}(f)$, $V_{a2}(f)$, $H_1(f)$, and $H_2(f)$ are equivalent in the frequency domain. For example, $V_{a1}(f)$ and $V_{a2}(f)$ are the Fourier transform of the equivalent input noise voltages of amplifier channel 1 and amplifier channel 2 respectively, $H_1(f)$ and $H_2(f)$ are the frequency response of amplifier channel 1 and channel 2, and $H_s(f)$ is the frequency response of the parallel combination of the sensor resistance and cable resistance with the cable capacitance and input capacitance of the amplifier to the noise voltage of the resistor.

$\rightarrow$ Note 2: $G_{XY}(f) = \lim_{\Delta\to\infty} \mathbf{E}\left(\frac{X^*_\Delta(f)Y_\Delta(f)}{\Delta}\right)$ is the cross-power spectral density (CPSD) between signal outputs X and Y. Using the two notes above and applying them to solve for the CPSD of channel 1 and channel 2 output voltages ($V_1(f)$ and $V_2(f)$):

$$
\begin{aligned}
G_{12}(f) &= \lim_{\Delta\to\infty} \mathbf{E}\left(\frac{V_1^*(f)V_2(f)}{\Delta}\right) \\
&= \lim_{\Delta\to\infty} \mathbf{E}\left(\frac{\left(\begin{array}{c}(\{[V_{Rs,\Delta}(f)+V_{Rc,\Delta}(f)]H_s(f)+V_{a1,\Delta}(f)\}H_1(f))^* \\ \{[V_{Rs,\Delta}(f)+V_{Rc,\Delta}(f)]H_s(f)+V_{a2,\Delta}(f)\}H_2(f)\end{array}\right)}{\Delta}\right) \\
&= \lim_{\Delta\to\infty} \mathbf{E}\left(\frac{\left(\begin{array}{c}(\{[V_{Rs,\Delta}(f)H_s(f)+V_{Rc,\Delta}(f)H_s(f)]+V_{a1,\Delta}(f)\}H_1(f))^* \\ \{[V_{Rs,\Delta}(f)H_s(f)+V_{Rc,\Delta}(f)H_s(f)]+V_{a2,\Delta}(f)\}H_2(f)\end{array}\right)}{\Delta}\right) \\
&= \lim_{\Delta\to\infty} \mathbf{E}\left(\frac{\left(\begin{array}{c}[(V_{Rs,\Delta}(f)H_s(f)+V_{Rc,\Delta}(f)H_s(f)+V_{a1,\Delta}(f))^* \\ (V_{Rs,\Delta}(f)H_s(f)+V_{Rc,\Delta}(f)H_s(f)+V_{a2,\Delta}(f))]H_1^*(f)H_2(f)\end{array}\right)}{\Delta}\right) \\
&= \lim_{\Delta\to\infty} \mathbf{E}\left(\frac{\left(\begin{array}{c}[(V_{Rs,\Delta}^*(f)H_s^*(f)+V_{Rc,\Delta}^*(f)H_s^*(f)+V_{a1,\Delta}^*(f)) \\ (V_{Rs,\Delta}(f)H_s(f)+V_{Rc,\Delta}(f)H_s(f)+V_{a2,\Delta}(f))]H_1^*(f)H_2(f)\end{array}\right)}{\Delta}\right) \\
&= \lim_{\Delta\to\infty} \mathbf{E}\left(\frac{[A+B+C]H_1^*(f)H_2(f)}{\Delta}\right) \\
&= \lim_{\Delta\to\infty} \mathbf{E}\left(\frac{[D+E+F]H_1^*(f)H_2(f)}{\Delta}\right)
\end{aligned}
\tag{A.8}
$$

where

$$A = V^*_{Rs,\Delta}(f)V_{Rs,\Delta}(f)|H_s(f)|^2 + V^*_{Rs,\Delta}(f)V_{Rc,\Delta}(f)|H_s(f)|^2 + V^*_{Rs,\Delta}(f)H^*_s(f)V_{a2,\Delta}(f)$$

$$B = V^*_{Rc,\Delta}(f)V_{Rs,\Delta}(f)|H_s(f)|^2 + V^*_{Rc,\Delta}(f)V_{Rc,\Delta}(f)|H_s(f)|^2 + V^*_{Rc,\Delta}(f)H^*_s(f)V_{a2,\Delta}(f)$$

$$C = V^*_{a1,\Delta}(f)V_{Rs,\Delta}(f)H_s(f) + V^*_{a1,\Delta}(f)V_{Rc,\Delta}(f)H_s(f) + V^*_{a1,\Delta}(f)V^*_{a2,\Delta}(f)$$

$$D = (V^*_{Rs,\Delta}(f)V_{Rs,\Delta}(f) + V^*_{Rs,\Delta}(f)V_{Rc,\Delta}(f))|H_s(f)|^2 + V^*_{Rs,\Delta}(f)H^*_s(f)V_{a2,\Delta}(f)$$

$$E = (V^*_{Rc,\Delta}(f)V_{Rs,\Delta}(f) + V^*_{Rc,\Delta}(f)V_{Rc,\Delta}(f))|H_s(f)|^2 + V^*_{Rc,\Delta}(f)H^*_s(f)V_{a2,\Delta}(f)$$

and

$$F = (V^*_{a1,\Delta}(f)V_{Rs,\Delta}(f) + V^*_{a1,\Delta}(f)V_{Rc,\Delta}(f))H_s(f) + V^*_{a1,\Delta}(f)V^*_{a2,\Delta}(f)$$

$\rightarrow$ Note 3: The $\lim_{\Delta\to\infty} V^*_{Rs,\Delta}(f)V_{Rs,\Delta}(f) = G_{Rs,Rs}(f)$ as $t \to \infty$ and is averaged over and over again.

$$\begin{aligned} G_{12}(f) = {} & [(G_{Rs,Rs}(f) + G_{Rs,Rc}(f))|H_s(f)|^2 + G_{Rs,a2}(f)H^*_s(f) \\ & + (G_{Rc,Rs}(f) + G_{Rc,Rc}(f))|H_s(f)|^2 + G_{Rc,a2}(f)H^*_s(f) \\ & + (G_{a1,Rs}(f) + G_{a1,Rc}(f))H_s(f) + G_{a1,a2}(f)]H^*_1(f)H_2(f) \end{aligned} \tag{A.9}$$

where $G_{Rs,Rc}(f)$, $G_{Rs,a2}(f)$,$G_{Rc,Rs}(f)$, $G_{Rc,a2}(f)$, $G_{a1,Rc}(f)$, and $G_{a1,a2}(f) = 0$ because they are mutually independent noise voltages. Therefore,

$$\begin{aligned} G_{12}(f) &= (G_{Rs,Rs}(f) + G_{Rc,Rc}(f))|H_s(f)|^2 H^*_1(f)H_2(f) \\ &= (G_{Rs,Rs}(f) + G_{Rc,Rc}(f))H_{12}(f) \end{aligned} \tag{A.10}$$

where $G_{Rs,Rs}(f)$ and $G_{Rc,Rc}(f)$ are constants independent of frequency. Rearranging to solve for the CPSD of the sensor or the noise voltage of the sensor ($G_{Rs,Rs}(f)$):

$$G_{Rs,Rs}(f) = G_{Rs}(f) = \frac{G_{12}(f)}{H_{12}(f)} - G_{Rc}(f) = 2kT_sR_s \tag{A.11}$$

Therefore,

$$2kT_sR_s = G_{Rs}(f) = \frac{G_{12}(f)}{H_{12}(f)} - G_{Rc}(f) \tag{A.12}$$

And solving for the temperature,

$$T_s = \left[\frac{G_{12}(f)}{H_{12}(f)} - G_{Rc}(f)\right] \times \frac{1}{2kR_s} \tag{A.13}$$

Appendix B

Derivation of Subtraction Method

B.1 Cross Power Spectral Density of JNT Channels with EMI

From Chapter 4, Section 4.4 Equation 2.25:

$$\begin{aligned} v_1(t) &= \{[v_{Rs}(t) + v_{Rc}(t) + v_E(t)] * h_s(t) + v_{a1}(t)\} * h_1(t) \\ v_2(t) &= \{[v_{Rs}(t) + v_{Rc}(t) + v_E(t)] * h_s(t) + v_{a2}(t)\} * h_2(t) \end{aligned} \tag{B.1}$$

The transient EMI is removed with a rectangle window in the time domain. Then the signals are Fourier transformed to the frequency domain. Convolution in the time domain transforms to multiplication in the frequency domain, using the Proof of the Convolution Theorem, explained in the previous appendix.

$$\begin{aligned} V_1(f) &= \{[V_{Rs}(f) + V_{Rc}(f) + V_E(f)]H_s(f) + V_{a1}(f)\}H_1(f) \\ V_2(f) &= \{[V_{Rs}(f) + V_{Rc}(f) + V_E(f)]H_s(f) + V_{a2}(f)\}H_2(f) \end{aligned} \tag{B.2}$$

where

$$V_E(f) = X_E(f)H_{Es}(f) = \text{is the EMI noise voltage}$$

Using the CPSD definition,

$$G_{12}(f) = \lim_{\Delta\to\infty} \mathbf{E}\left(\frac{V^*_{1,\Delta}(f)V_{2,\Delta}(f)}{\Delta}\right)$$

$$= \lim_{\Delta\to\infty} \mathbf{E}\left(\frac{\left(\begin{array}{c}(\{[V_{Rs,\Delta}(f)+V_{Rc,\Delta}(f)+V_{E,\Delta}(f)]H_s(f)+V_{a1,\Delta}(f)\}H_1(f))^* \\ \{[V_{Rs,\Delta}(f)+V_{Rc,\Delta}(f)+V_{E,\Delta}(f)]H_s(f)+V_{a2,\Delta}(f)\}H_2(f)\end{array}\right)}{\Delta}\right)$$

$$= \lim_{\Delta\to\infty} \mathbf{E}\left(\frac{\left(\begin{array}{c}(\{[V_{Rs,\Delta}(f)H_s(f)+V_{Rc,\Delta}(f)H_s(f)+V_{E,\Delta}(f)H_s(f)]+V_{a1,\Delta}(f)\}H_1(f))^* \\ \{[V_{Rs,\Delta}(f)H_s(f)+V_{Rc,\Delta}(f)H_s(f)V_{E,\Delta}(f)H_s(f)]+V_{a2,\Delta}(f)\}H_2(f)\end{array}\right)}{\Delta}\right)$$

$$= \lim_{\Delta\to\infty} \mathbf{E}\left(\frac{\left(\begin{array}{c}[(V_{Rs,\Delta}(f)H_s(f)+V_{Rc,\Delta}(f)H_s(f)+V_{E,\Delta}(f)H_s(f)+V_{a1,\Delta}(f))^* \\ (V_{Rs,\Delta}(f)H_s(f)+V_{Rc,\Delta}(f)H_s(f)+V_{E,\Delta}(f)H_s(f)+V_{a2,\Delta}(f))]H_1^*(f)H_2(f)\end{array}\right)}{\Delta}\right)$$

$$= \lim_{\Delta\to\infty} \mathbf{E}\left(\frac{\left(\begin{array}{c}[(V^*_{Rs,\Delta}(f)H^*_s(f)+V^*_{Rc,\Delta}(f)H^*_s(f)+V^*_{E,\Delta}(f)H^*_s(f)+V^*_{a1,\Delta}(f)) \\ (V_{Rs,\Delta}(f)H_s(f)+V_{Rc,\Delta}(f)H_s(f)+V_{E,\Delta}(f)H_s(f)+V_{a2,\Delta}(f))]H_1^*(f)H_2(f)\end{array}\right)}{\Delta}\right)$$

$$= \lim_{\Delta\to\infty} \mathbf{E}\left(\frac{[A+B+C+D]H_1^*(f)H_2(f)}{\Delta}\right) \tag{B.3}$$

where

$$\begin{aligned}
A =&(V^*_{Rs,\Delta}(f)V_{Rs,\Delta}(f) + V^*_{Rs,\Delta}(f)V_{Rc,\Delta}(f) + V^*_{Rs,\Delta}(f)V_{E,\Delta}(f))|H_s(f)|^2 \\
&+ V^*_{Rs,\Delta}(f)H^*_s(f)V_{a2,\Delta}(f) \\
B =&(V^*_{Rc,\Delta}(f)V_{Rs,\Delta}(f) + V^*_{Rc,\Delta}(f)V_{Rc,\Delta}(f) + V^*_{Rc,\Delta}(f)V_{E,\Delta}(f))|H_s(f)|^2 \\
&+ V^*_{Rc,\Delta}(f)H^*_s(f)V_{a2,\Delta}(f) \\
C =&(V^*_{E,\Delta}(f)V_{Rs,\Delta}(f) + V^*_{E,\Delta}(f)V_{Rc,\Delta}(f) + V^*_{E,\Delta}(f)V_{E,\Delta}(f))|H_s(f)|^2 \\
&+ V^*_{E,\Delta}(f)H^*_s(f)V_{a2,\Delta}(f)
\end{aligned}$$

and

$$\begin{aligned}
D =&(V^*_{a1,\Delta}(f)V_{Rs,\Delta}(f) + V^*_{a1,\Delta}(f)V_{Rc,\Delta}(f) + V^*_{a1,\Delta}(f)V_{E,\Delta}(f))H_s(f) \\
&+ V^*_{a1,\Delta}(f)V^*_{a2,\Delta}(f)
\end{aligned}$$

From Note 3 in previous appendix: The $\lim_{\Delta\to\infty} V^*_{Rs,\Delta}(f)V_{Rs,\Delta}(f) = G_{Rs,Rs}(f)$ as $t \to \infty$ and is averaged over and over again.

$$\begin{aligned}
G_{12}(f) = &[(G_{Rs,Rs}(f) + G_{Rs,Rc}(f) + G_{Rs,E}(f))|H_s(f)|^2 + G_{Rs,a2}(f)H^*_s(f) \\
&+ (G_{Rc,Rs}(f) + G_{Rc,Rc}(f) + G_{Rc,E}(f))|H_s(f)|^2 + G_{Rc,a2}(f)H^*_s(f) \\
&+ [(G_{E,Rs}(f) + G_{E,Rc}(f) + G_{E,E}(f))|H_s(f)|^2 + G_{E,a2}(f)H^*_s(f) \\
&+ (G_{a1,Rs}(f) + G_{a1,Rc}(f))H_s(f) + G_{a1,a2}(f)]H^*_1(f)H_2(f)
\end{aligned} \tag{B.4}$$

where $G_{Rs,Rc}(f)$, $G_{Rs,E}(f)$, $G_{Rs,a2}(f)$,$G_{Rc,Rs}(f)$, $G_{RcE}(f)$, $G_{Rc,a2}(f)$, $G_{ERs}(f)$, $G_{E,Rc}(f)$, $G_{E,a2}(f)$, $G_{a1,Rs}(f)$, $G_{a1,Rc}(f)$, and $G_{a1,a2}(f) = 0$ because they are mutually independent noise voltages. Therefore,

$$\begin{aligned}
G_{12}(f) &= (G_{Rs}(f) + G_{Rc}(f) + G_E(f))|H_s(f)|^2H^*_1(f)H_2(f) \\
&= (G_{Rs}(f) + G_{Rc}(f) + G_E(f))H_{12}(f)
\end{aligned} \tag{B.5}$$

B.2 Cross Power Spectral Density of Antenna Channel

Reviewing the antenna output voltage:

$$V_A(f) = [X_E(f)H_{EA}(f) + V_{a3}(f)]H_{a3}(f) \tag{B.6}$$

The contribution of sensor EMI voltage to the JNT channel output voltages:

$$\begin{aligned} V_{1E}(f) &= V_E(f)H_s(f)H_1(f) \\ V_{2E}(f) &= V_E(f)H_s(f)H_2(f) \\ V_{E,\Delta}(f) &= X_{E,\Delta}(f)H_{Es}(f) \end{aligned} \tag{B.7}$$

Solving for the CPSD of the antenna to Channel 1 with EMI($V_{1E}(f)$):

$$
\begin{aligned}
G_{A,1E}(f) &= \lim_{\Delta\to\infty} \mathbf{E}\left(\frac{V^*_{A,\Delta}(f)V_{1E,\Delta}(f)}{\Delta}\right) \\
&= \lim_{\Delta\to\infty} \mathbf{E}\left(\frac{[X_{E,\Delta}(f)H_{EA}(f)+V_{a3,\Delta}(f)]^*H^*_{a3}(f)V_{E,\Delta}(f)H_s(f)H_1(f)}{\Delta}\right) \\
&= \lim_{\Delta\to\infty} \mathbf{E}\left(\frac{[X_{E,\Delta}(f)H_{EA}(f)+V_{a3,\Delta}(f)]^*H^*_{a3}(f)X_{E,\Delta}(f)H_{Es}(f)H_s(f)H_1(f)}{\Delta}\right) \\
&= \lim_{\Delta\to\infty} \mathbf{E}\left(\frac{\left(\begin{array}{r}([X_{E,\Delta}(f)H_{EA}(f)]^*H^*_{a3}(f)X_{E,\Delta}(f)H_{Es}(f)H_s(f)H_1(f)) \\ +([V_{a3,\Delta}(f)]^*H^*_{a3}(f)X_{E,\Delta}(f)H_{Es}(f)H_s(f)H_1(f))\end{array}\right)}{\Delta}\right) \\
&= \lim_{\Delta\to\infty} \mathbf{E}\left(\frac{\left(\begin{array}{r}(X^*_{E,\Delta}(f)H^*_{EA}(f)H^*_{a3}(f)X_{E,\Delta}(f)H_{Es}(f)H_s(f)H_1(f)) \\ +(V_{a3,\Delta}(f)^*H^*_{a3}(f)X_{E,\Delta}(f)H_{Es}(f)H_s(f)H_1(f))\end{array}\right)}{\Delta}\right)
\end{aligned}
\tag{B.8}
$$

Using Note 3:

$$
\begin{aligned}
G_{A,1E}(f) &= G_E(f)H^*_{EA}(f)H^*_{a3}(f)H_{Es}(f)H_s(f)H_1(f) + G_{a3,E}(f)H^*_{a3}(f)H_{Es}(f)H_s(f)H_1(f) \\
&= G_E(f)H^*_{EA}(f)H^*_{a3}(f)H_{Es}(f)H_s(f)H_1(f)
\end{aligned}
\tag{B.9}
$$

where $G_{a3,E}(f) = 0$ because it is uncorrelated (mutually independent) noise. Similarly, for $G_{A,2E}(f)$:

$$
G_{A,2E}(f) = G_E(f)H^*_{EA}(f)H^*_{a3}(f)H_{Es}(f)H_s(f)H_2(f) \tag{B.10}
$$

Solving for the PSD of the antenna voltage, $V_A(f)$:

$$
\begin{aligned}
G_A(f) &= \lim_{\Delta\to\infty} \mathbf{E}\left(\frac{V^*_{A,\Delta}(f)V_{A,\Delta}(f)}{\Delta}\right) \\
&= \lim_{\Delta\to\infty} \mathbf{E}\left(\frac{|V_{A,\Delta}(f)|^2}{\Delta}\right) \\
&= \lim_{\Delta\to\infty} \mathbf{E}\left(\frac{|[X_{E,\Delta}(f)H_{EA}(f)+V_{a3,\Delta}(f)]H_{a3}(f)|^2}{\Delta}\right) \\
&= \lim_{\Delta\to\infty} \mathbf{E}\left(\frac{|X_{E,\Delta}(f)H_{EA}(f)H_{a3}(f)+V_{a3,\Delta}(f)H_{a3}(f)|^2}{\Delta}\right) \\
&= \lim_{\Delta\to\infty} \mathbf{E}\left(\frac{\left(\begin{array}{c}|(X_{E,\Delta}(f)H_{EA}(f)H_{a3}(f)+V_{a3,\Delta}(f)H_{a3}(f))| \\ |(X_{E,\Delta}(f)H_{EA}(f)H_{a3}(f)+V_{a3,\Delta}(f)H_{a3}(f))|\end{array}\right)}{\Delta}\right) \\
&= G_E(f)|H_{EA}(f)H_{a3}(f)|^2 + G_{a3}(f)|H_{a3}(f)|^2
\end{aligned}
\tag{B.11}
$$

To remove the EMI:

$$\begin{aligned}\frac{G_{A,1E}(f)}{G_A(f)} &= \frac{G_E(f)|H_{Es}(f)H^*_{EA}(f)H_s(f)H_1(f)H^*_{a3}(f)}{G_E(f)|H_{EA}(f)H_{a3}(f)|^2 + G_{a3}(f)|H_{a3}(f)|^2} \\ &= \frac{H_{Es}(f)H_s(f)H_1(f)}{H_{EA}(f)H_{a3}(f) + \frac{G_{a3}(f)|H_{a3}(f)|^2}{G_E(f)H^*_{EA}(f)H^*_{a3}(f)}} \\ &= \frac{H_{Es}(f)H_s(f)H_1(f)}{H_{EA}(f)H_{a3}(f)} \\ &= \frac{V_{1E}(f)}{V_A(f)}\end{aligned} \tag{B.12}$$

Therefore, solving for $V_{1E}(f)$:

$$V_{1E}(f) = \frac{G_{A,1E}(f)}{G_A(f)}V_A(f) \tag{B.13}$$

Similarly, for $V_{2E}(f)$:

$$\begin{aligned}\frac{G_{A,2E}(f)}{G_A(f)} &= \frac{G_E(f)|H_{Es}(f)H^*_{EA}(f)H_s(f)H_2(f)H^*_{a3}(f)}{G_E(f)|H_{EA}(f)H_{a3}(f)|^2 + G_{a3}(f)|H_{a3}(f)|^2} \\ &= \frac{H_{Es}(f)H_s(f)H_2(f)}{H_{EA}(f)H_{a3}(f)} \\ &= \frac{V_{2E}(f)}{V_A(f)}\end{aligned} \tag{B.14}$$

Therefore, solving for $V_{2E}(f)$:

$$V_{2E}(f) = \frac{G_{A,2E}(f)}{G_A(f)}V_A(f) \tag{B.15}$$

Solving for the CPSD of the antenna to Channel 1 ($V_1(f)$):

$$
\begin{aligned}
G_{A,1}(f) &= \lim_{\Delta\to\infty} \mathbf{E}\left(\frac{V^*_{A,\Delta}(f)V_{1,\Delta}(f)}{\Delta}\right) \\
&= \lim_{\Delta\to\infty} \mathbf{E}\left(\frac{(V^*_{A,\Delta}(f)\{[V_{Rs,\Delta}(f)+V_{Rc,\Delta}(f)+V_{E,\Delta}(f)]H_s(f)+V_{a1,\Delta}(f)\}H_1(f))}{\Delta}\right) \\
&= \lim_{\Delta\to\infty} \mathbf{E}\left(\frac{\begin{pmatrix} V^*_{A,\Delta}(f)V_{Rs,\Delta}(f)H_s(f)H_1(f)+V^*_{A,\Delta}(f)V_{Rc,\Delta}(f)H_s(f)H_1(f) \\ V^*_{A,\Delta}(f)V_{E,\Delta}(f)H_s(f)H_1(f)+V_{a1,\Delta}(f)H_1(f)\end{pmatrix}}{\Delta}\right) \\
&= \{[G_{A,Rs}(f)+G_{A,Rc}(f)+G_{A,E}(f)]H_s(f)+G_{A,1}(f)\}H_1(f)
\end{aligned}
\tag{B.16}
$$

where $G_{A,Rs}(f), G_{A,Rc}(f), G_{A,1}(f) = 0$ because it is uncorrelated (mutually independent) noise.

$$G_{A,1}(f) = G_{A,E}(f)H_s(f)H_1(f) \tag{B.17}$$

It can be concluded that $G_{A,1}(f) = G_{A,1E}(f)$ and can be substituted in Equation B.13 and B.15:

$$
\begin{aligned}
V_{1E}(f) &= \frac{G_{A,1}(f)}{G_A(f)}V_A(f) \\
V_{2E}(f) &= \frac{G_{A,2}(f)}{G_A(f)}V_A(f)
\end{aligned}
\tag{B.18}
$$

B.3 Derivation of Subtracting EMI from Channel Voltages

Since both $V_1(f)$ and $V_{1E}(f)$ are known, $V_{1E}(f)$ can be subtracted from $V_1(f)$:

$$
\begin{aligned}
&V_1(f) = \{[V_{Rs}(f) + V_{Rc}(f) + V_E(f)]H_s(f) + V_{a1}(f)\}H_1(f) \\
&\Downarrow \\
&V_1(f) = \{[V_{Rs}(f) + V_{Rc}(f)]H_s(f) + V_{a1}(f)\}H_1(f) + V_E(f)H_s(f)H_1(f) \\
&\Downarrow \\
&V_1(f) = \{[V_{Rs}(f) + V_{Rc}(f)]H_s(f) + V_{a1}(f)\}H_1(f) + V_{1E}(f) \\
&\Downarrow \\
&V_1(f) - V_{1E}(f) = \{[V_{Rs}(f) + V_{Rc}(f)]H_s(f) + V_{a1}(f)\}H_1(f) \\
&\Downarrow \\
&V_1(f) - \frac{G_{A1}(f)}{G_A(f)}V_A(f) = \{[V_{Rs}(f) + V_{Rc}(f)]H_s(f) + V_{a1}(f)\}H_1(f) \\
&\Downarrow \\
&V_{1-E}(f) = \{[V_{Rs}(f) + V_{Rc}(f) + V_E(f) - V_E(f)]H_s(f) + V_{a1}(f)\}H_1(f)
\end{aligned}
\tag{B.19}
$$

Similarly, $V_{2E}(f)$ can be subtracted from $V_2(f)$:

$$
\begin{aligned}
&V_2(f) = \{[V_{Rs}(f) + V_{Rc}(f) + V_E(f)]H_s(f) + V_{a2}(f)\}H_2(f) \\
&\Downarrow \\
&V_{2-E}(f) = \{[V_{Rs}(f) + V_{Rc}(f) + V_E(f) - V_E(f)]H_s(f) + V_{a2}(f)\}H_2(f)
\end{aligned}
\tag{B.20}
$$

Therefore, the new CPSD between Channel 1 and Channel 2 with EMI subtracted becomes:

$$
\begin{aligned}
G_{12-E}(f) &= \lim_{\Delta\to\infty} \mathbf{E}\left(\frac{V^*_{1-E,\Delta}(f)V_{2-E,\Delta}(f)}{\Delta}\right) \\
&= \lim_{\Delta\to\infty} \mathbf{E}\left(\frac{\left(\begin{array}{c}(\{[V_{Rs,\Delta}(f)+V_{Rc,\Delta}(f)+V_E(f)-V_E(f)]H_s(f)+V_{a1,\Delta}(f)\}H_1(f))^* \\ \{[V_{Rs,\Delta}(f)+V_{Rc,\Delta}(f)+V_E(f)-V_E(f)]H_s(f)+V_{a2,\Delta}(f)\}H_2(f)\end{array}\right)}{\Delta}\right) \\
&= \lim_{\Delta\to\infty} \mathbf{E}\left(\frac{\left(\begin{array}{c}(\{[V_{Rs,\Delta}(f)+V_{Rc,\Delta}(f)+V_{E,\Delta}(f)-V_E(f)]H_s(f)+V_{a1,\Delta}(f)\} \\ \{[V_{Rs,\Delta}(f)+V_{Rc,\Delta}(f)+V_{E,\Delta}(f)-V_E(f)]H_s(f)+V_{a2,\Delta}(f)\}H_1(f))^*H_2(f)\end{array}\right)}{\Delta}\right) \\
&= \lim_{\Delta\to\infty} \mathbf{E}\left(\frac{[A\times B]H_1^*(f)H_2(f)}{\Delta}\right) \\
&= \lim_{\Delta\to\infty} \mathbf{E}\left(\frac{[C\times D]H_1^*(f)H_2(f)}{\Delta}\right) \\
&= \lim_{\Delta\to\infty} \mathbf{E}\left(\frac{[E+F+G+I]H_1^*(f)H_2(f)}{\Delta}\right)
\end{aligned}
\tag{B.21}
$$

where

$$A = (V_{Rs,\Delta}(f)H_s(f) + V_{Rc,\Delta}(f)H_s(f) + V_{E,\Delta}(f)H_s(f) - V_{E,\Delta}(f)H_s(f) + V_{a1,\Delta}(f))^*$$

$$B = V_{Rs,\Delta}(f)H_s(f) + V_{Rc,\Delta}(f)H_s(f) + V_{E,\Delta}(f)H_s(f) - V_{E,\Delta}(f)H_s(f) + V_{a2,\Delta}(f)$$

$$C = V^*_{Rs,\Delta}(f)H^*_s(f) + V^*_{Rc,\Delta}(f)H^*_s(f) + V^*_{E,\Delta}(f)H^*_s(f) - V^*_{E,\Delta}(f)H_s(f) + V^*_{a1,\Delta}(f)$$

$$D = V_{Rs,\Delta}(f)H_s(f) + V_{Rc,\Delta}(f)H_s(f) + V_{E,\Delta}(f)H_s(f) - V_{E,\Delta}(f)H_s(f) + V_{a2,\Delta}(f)$$

$$E = (V^*_{Rs,\Delta}(f)V_{Rs,\Delta}(f) + V^*_{Rs,\Delta}(f)V_{Rc,\Delta}(f) + V^*_{Rs,\Delta}(f)V_{E,\Delta}(f) - V^*_{Rs,\Delta}(f)V_E(f))|H_s(f)|^2 + V^*_{Rs,\Delta}(f)H^*_s(f)V_{a2,\Delta}(f)$$

$$F = (V^*_{Rc,\Delta}(f)V_{Rs,\Delta}(f) + V^*_{Rc,\Delta}(f)V_{Rc,\Delta}(f) + V^*_{Rc,\Delta}(f)V_{E,\Delta}(f) - V^*_{Rc,\Delta}(f)V_E(f))|H_s(f)|^2 + V^*_{Rc,\Delta}(f)H^*_s(f)V_{a2,\Delta}(f)$$

$$G = (V^*_{E,\Delta}(f)V_{Rs,\Delta}(f) + V^*_{E,\Delta}(f)V_{Rc,\Delta}(f) + V^*_{E,\Delta}(f)V_{E,\Delta}(f) - V^*_{E,\Delta}(f)V_{E,\Delta}(f))|H_s(f)|^2 + V^*_{E,\Delta}(f)H^*_s(f)V_{a2,\Delta}(f)$$

and

$$I = (V^*_{a1,\Delta}(f)V_{Rs,\Delta}(f) + V^*_{a1,\Delta}(f)V_{Rc,\Delta}(f) + V^*_{a1,\Delta}(f)V_{E,\Delta}(f) - V^*_{a1,\Delta}(f)V_{E,\Delta}(f))H_s(f) + V^*_{a1,\Delta}(f)V^*_{a2,\Delta}(f)$$

Using Note 3 from previous appendix:

$$\begin{aligned} G_{12-E}(f) = [&(G_{Rs,Rs}(f) + G_{Rs,Rc}(f) + G_{Rs,E}(f) - G_{Rs,E}(f))|H_s(f)|^2 + G_{Rs,a2}(f)H^*_s(f) \\ &+ (G_{Rc,Rs}(f) + G_{Rc,Rc}(f) + G_{Rc,E}(f) - G_{Rc,E}(f))|H_s(f)|^2 + G_{Rc,a2}(f)H^*_s(f) \\ &+ (G_{E,Rs}(f) + G_{E,Rc}(f) + G_{E,E}(f) - G_{E,E}(f))|H_s(f)|^2 + G_{E,a2}(f)H^*_s(f) \\ &+ (G_{a1,Rs}(f) + G_{a1,Rc}(f))H_s(f) + G_{a1,a2}(f)]H^*_1(f)H_2(f) \end{aligned} \tag{B.22}$$

where $G_{Rs,Rc}(f)$, $G_{Rs,E}(f)$, $G_{Rs,a2}(f)$,$G_{Rc,Rs}(f)$, $G_{Rc,E}(f)$, $G_{Rc,a2}(f)$, $G_{E,Rs}(f)$, $G_{E,Rc}(f)$, $G_{E,a2}(f)$, $G_{a1,Rs}(f)$, $G_{a1,Rc}(f)$, and $G_{a1,a2}(f) = 0$ because they are mutually independent noise voltages. Therefore,

$$\begin{aligned} G_{12-E}(f) &= (G_{Rs}(f) + G_{Rc}(f))|H_s(f)|^2 H_1^*(f) H_2(f) \\ &= (G_{Rs}(f) + G_{Rc}(f)) H_{12}(f) \\ &= G_{12}(f) \end{aligned} \tag{B.23}$$

Using $G_{12-E}(f)$ to solve for resistor PSD ($G_{Rs}(f)$):

$$G_{Rs,Rs}(f) = G_{Rs}(f) = \frac{G_{12-E}(f)}{H_{12}(f)} - G_{Rc}(f) = 2kT_sR_s \tag{B.24}$$

Therefore,

$$2kT_sR_s = G_{Rs}(f) = \frac{G_{12-E}(f)}{H_{12}(f)} - G_{Rc}(f) \tag{B.25}$$

And solving for the temperature,

$$T_s = \left[\frac{G_{12-E}(f)}{H_{12}(f)} - G_{Rc}(f)\right] \times \frac{1}{2kR_s} \tag{B.26}$$

Appendix C

Derivation of Pilot Tone Removal

C.1 Solving for the Pilot Tone Attenuator

$$f_{Lo} = \frac{1}{2\pi(R_p + R_s + R_c)C_p} \cong \frac{1}{2\pi R_p C_p}$$

$$f_{Hi} = \frac{1}{2\pi(R_s + R_c)(C_c + C_{a1} + C_{a2})} \tag{C.1}$$

where R_p is the series resistance and C_p blocks the DC current and sets the low-corner frequency. They form a balanced series network at the output of a single ended-to-differential ended network.

→ Note 1: $\frac{R_p}{2} \gg R_s \gg R_c$ and $2C_p \gg (C_c + C_{a1} + C_{a2})$

Solving for the pilot tone attenuator frequency response as a transconductance:

$$H_p(f) = \frac{I_p(f)}{V_p(f)}$$

$$= \frac{\text{current injected into the sensor at amplifier-filter input terminals}}{\text{pilot tone voltage}} \tag{C.2}$$

$$= \frac{K}{Z_p(f) + Z_s(f)}$$

where,

$$H_s(f) = \frac{1}{j2\pi f(C_c + C_{a1} + C_{a2})(R_s + R_c)} \tag{C.3}$$

$$Z_p(f) = R_p \frac{1}{j2\pi f C_p} \tag{C.4}$$

$$Z_s(f) = (R_s + R_c)//\frac{1}{j2\pi f(C_c + C_{a1} + C_{a2})}$$

$$= \frac{R_s + R_c}{j2\pi f(C_c + C_{a1} + C_{a2})(R_s + R_c) + 1} \tag{C.5}$$

$$= (R_s + R_c)H_s(f)$$

At any frequency, $|Z_p(f)| \geq R_p$ and $|Z_s(f)| \leq R_s + R_p$. Also, $R_p \gg R_s \gg R_c$. Therefore, $|Z_p(f)| \gg |Z_s(f)|$ and:

$$H_p(f) \cong \frac{K}{Z_p(f)}$$

$$|H_p(f)|^2 \cong \left|\frac{K}{Z_p(f)}\right|^2 \tag{C.6}$$

→ Note 2: $|H_p(f)|^2$ characterizes the pilot tone attenuator
This value is very important and needs to be monitored during the entire temperature measurement and must be known before temperature can be computed.

In the software $|H_p(f)|^2$ is computed three ways with pilot tone one, with pilot tone off, and with pilot tone on but taken out. All three calculations are displayed below:

$$|H_p(f)|^2 = \frac{\text{Sensor noise current PSD}}{\text{Amplifier/filter noise CPSD referred to the pilot tone location}}$$

With Pilot Tone ON:

$$|H_p(f)|^2 = \frac{\frac{2k(T_sR_s+T_cR_c)G^*_{P1-E}(f)G_{P2-E}(f)}{G^2_P(f)(R_s+R_c)^2}}{G_{12p-E}(f) - \frac{G^*_{P1-E}(f)G_{P2-E}(f)}{G_P(f)}} \tag{C.7}$$

$$= \frac{\frac{2k(T_sR_s+T_cR_c)}{(R_s+R_c)^2}}{\frac{G_{12p-E}(f)G^2_P(f)}{G^*_{P1-E}(f)G_{P2-E}(f)} - G_P(f)}$$

With Pilot Tone OFF:

$$|H_p(f)|^2 = \frac{\frac{2k(T_sR_s+T_cR_c)}{(R_s+R_c)^2}}{\frac{G_{12-E}(f)G^2_P(f)}{G^*_{P1-E}(f)G_{P2-E}(f)}} \tag{C.8}$$

$$= \frac{2k(T_sR_s+T_cR_c)}{(R_s+R_c)^2} \times \frac{G^*_{P1-E}(f)G_{P2-E}(f)}{G_{12-E}(f)G^2_P(f)}$$

With Pilot Tone ON but subtracted:

$$|H_p(f)|^2 = \frac{\frac{2k(T_sR_s+T_cR_c)}{(R_s+R_c)^2}}{\frac{G_{12p-E-P}(f)G^2_P(f)}{G^*_{P1-E}(f)G_{P2-E}(f)}} \tag{C.9}$$

$$= \frac{2k(T_sR_s+T_cR_c)}{(R_s+R_c)^2} \times \frac{G^*_{P1-E}(f)G_{P2-E}(f)}{G_{12p-E-P}(f)G^2_P(f)}$$

C.2 Derivation of CPSD/PSD for Pilot Tone Removal

The voltage developed at the amplifier-filter input terminals by the pilot tone:

$$V_{Pa}(f) = V_P(f)H_p(f)Z_s(f) \tag{C.10}$$

The amplifier-filter output voltages with pilot tone on and EMI removed:

$$\begin{aligned} V_{P1-E}(f) &= (\{[V_{Rs}(f) + V_{Rc}(f)]H_s(f) + V_{Pa}(f)\} + V_{a1}(f))H_1(f) \\ &= (\{[V_{Rs}(f) + V_{Rc}(f)]H_s(f) + V_P(f)H_p(f)Z_s(f)\} + V_{a1}(f))H_1(f) \end{aligned} \tag{C.11}$$

Similarly,

$$V_{P2-E}(f) = (\{[V_{Rs}(f) + V_{Rc}(f)]H_s(f) + V_P(f)H_p(f)Z_s(f)\} + V_{a2}(f))H_1(f) \tag{C.12}$$

Solving for the CPSD between the pilot tone and output voltage from amplifier-filter channel 1:

$$\begin{aligned} G_{P1-E}(f) &= \lim_{\Delta\to\infty} \frac{V^*_{P,\Delta}(f)V_{1-E,\Delta}(f)}{\Delta} \\ &= \lim_{\Delta\to\infty} \frac{\begin{pmatrix} V^*_{P,\Delta}(f)(\{[V_{Rs}(f) + V_{Rc}(f)]H_s(f) + V_P(f)H_p(f)Z_s(f)\} \\ + V_{a1}(f))H_1(f) \end{pmatrix}}{\Delta} \\ &= \lim_{\Delta\to\infty} \frac{\begin{pmatrix} ([V^*_{P,\Delta}(f)V_{Rs}(f) + V^*_{P,\Delta}(f)V_{Rc}(f)]H_s(f) \\ + V^*_{p,\Delta}(f)V_P(f)H_p(f)Z_s(f) + V^*_{P,\Delta}(f)V_{a1}(f))H_1(f) \end{pmatrix}}{\Delta} \end{aligned} \tag{C.13}$$

Using Note 3 from Appendix A:

$$\begin{aligned} G_{P1-E}(f) &= (\{[G_{P,Rs}(f) + G_{P,Rc}(f)]H_s(f) + G_P(f)H_p(f)Z_s(f)\} + G_{P,a1}(f))H_1(f) \\ &= G_P(f)H_p(f)Z_s(f)H_1(f) \\ &= G_P(f)H_p(f)[(R_s + R_c)H_s(f)]H_1(f) \end{aligned} \tag{C.14}$$

Similarly,

$$\begin{aligned} G_{P2-E}(f) &= (\{[G_{P,Rs}(f) + G_{P,Rc}(f)]H_s(f) + G_P(f)H_p(f)Z_s(f)\} + G_{P,a2}(f))H_2(f) \\ &= G_P(f)H_p(f)[(R_s + R_c)H_s(f)]H_2(f) \end{aligned} \tag{C.15}$$

$$G_{12+p-E-p}(f) = \tag{C.16}$$

Solving for $H_1(f)$ and $H_2(f)$:

$$H_1(f) = \frac{G_{P1-E}(f)}{G_p(f)H_p(f)[(R_s + R_c)H_s(f)}$$
$$H_2(f) = \frac{G_{P2-E}(f)}{G_p(f)H_p(f)[(R_s + R_c)H_s(f)} \tag{C.17}$$

Solving for the cross power frequency response from sensor to the outputs of the amplifier-filter channels 1 and 2:

$$\begin{aligned} H_{12}(f) &= H_1^*(f)H_2(f)|H_s(f)|^2 \\ &= \left[\frac{G_{P1-E}(f)}{G_P(f)H_p(f)[(R_s + R_c)H_s(f)}\right]^* \left[\frac{G_{P2-E}(f)}{G_P(f)H_p(f)[(R_s + R_c)H_s(f)}\right] |H_s(f)|^2 \\ &= \frac{G_{P1-E}^*(f)G_{p2-E}(f)}{G_P^2(f)|H_p^2(f)|(R_s + R_c)^2} \\ &= \frac{G_{P1-E}^*(f)G_{p2-E}(f)}{G_P^2(f)} \times \frac{1}{|H_p^2(f)|(R_s + R_c)^2} \end{aligned} \tag{C.18}$$

The pilot tone (PT) is subtracted the same way the EMI is subtracted. See the following steps:

Original signal with PT:

$$\begin{aligned} V_{P1-E}(f) &= (\{[V_{Rs}(f) + V_{Rc}(f)]H_s(f) + V_P(f)H_p(f)Z_s(f)\} + V_{a1}(f))H_1(f) \\ &= \{[V_{Rs}(f) + V_{Rc}(f)]H_s(f) + V_{a1}(f)\}H_1(f) + V_P(f)H_p(f)Z_s(f)H_1(f) \\ &= \begin{array}{l}\{[V_{Rs}(f) + V_{Rc}(f)]H_s(f) + V_{a1}(f)\}H_1(f) \\ \qquad + V_P(f)H_p(f)(R_s + R_c)H_s(f)H_1(f)\end{array} \end{aligned} \tag{C.19}$$

Calculating the output voltage with pilot tone removed:

$$\begin{aligned} V_{P1-E-p}(f) &= V_{P1-E}(f) - \text{voltage due to PT} \\ &= V_{P1-E}(f) - V_P(f)H_p(f)(R_s + R_c)H_s(f)H_1(f) \\ &= \{[V_{Rs}(f) + V_{Rc}(f)]H_s(f) + V_{a1}(f)\}H_1(f) \end{aligned} \tag{C.20}$$

Solving for $V_{P1}(f)$,

$$V_{P1}(f) = \frac{G_{P1}(f)}{G_P(f)} V_P(f) \tag{C.21}$$

Similarly,

$$\begin{aligned} V_{P2-E-p}(f) &= V_{P2-E}(f) - \text{voltage due to PT} \\ &= \{[V_{Rs}(f) + V_{Rc}(f)]H_s(f) + V_{a2}(f)\}H_2(f) \end{aligned} \tag{C.22}$$

Solving for $V_{P2}(f)$,

$$V_{P2}(f) = \frac{G_{P2}(f)}{G_P(f)} V_P(f) \tag{C.23}$$

Finally,

$$T_s = \frac{1}{2kR_s}\left[\frac{G_{12+p-E-p}(f)}{H_{12}(f)} - G_{Rc}(f)\right] \tag{C.24}$$

Appendix D

MatLab Simulation Code for EMI Subtraction technique

D.1 JNTBlockSImEMI2.m


```
% Program to simulate the entire JNT signal processing to estimate
% temperature.  This program uses a single-block simulator,
% JNTBlockSimEMI2, to generate the data for a single data block.
%This simulation includes eliminating the EMI by subtracting the
% EMI effects using the signal from an "EMI antenna".
%
% INPUT PARAMETERS
%
% sp = structure containing the sensor parameters
%     sp.T = sensor temperature (K)
%     sp.R = sensor resistance (ohms)
%
% N = number of samples requested from the block simulator,
%     must be an even number
```

```
15 %
16 % df = frequency-domain resolution (Hz)
17 %
18 % Ep  = structure containing the EMI parameters
19 %     Transient EMI is governed by a Poisson process.  Each time a
20 %     Poisson process event occurs a sequence of exponentially-
21 %     decaying pulses occurs.  The number of pulses in the
22 %     sequence, their amplitudes, their time constants and the
23 %     duration of the sequenceare all random with a specified
24 %     mean and and are exponentially distributed
25 %     Ep.t.on = flag indicating add transient EMI (1) or don't (0)
26 %     Ep.t.r = rate parameter of the Poisson process, per second
27 %     Ep.t.Nav = average number of pulses in a sequence
28 %     Ep.t.Aav = average amplitude of the transient EMI pulses (V)
29 %     Ep.t.tauav = average time constant for an individual pulse, (s)
30 %     Ep.t.Tav = average duration of a sequence of pulses (s)
31 %     Ep.p.on = flag indicating add periodic EMI (1) or don't (0)
32 %     Ep.p.f = vector of periodic EMI frequencies (Hz)
33 %     Ep.p.A = vector of periodic EMI amplitudes (V)
34 %     EP.p.f and Ep.p.A must be the same length
35 %
36 % cp = structure containing the cable parameters
37 %     cp.T = cable temperature (K)
38 %     cp.R = cable resistance (ohms)
39 %     cp.C = cable capacitance (F)
40 %
41 % ptp = structure containing the pilot tone parameters
42 %     ptp.on = flag indicating add a pilot tone (1) or don't (0)
43 %     ptp.typ = flag indicating FM ('F') or random ('R') pilot tone
44 %     ptp.A = pilot tone amplitude (as generated) (V)
45 %         *for FM signals ptp.A is the (constant) amplitude
46 %         *for random signals ptp.A is the rms value
47 %     ptp.R = series resistance of pilot tone attenuator (ohms)
48 %     ptp.C = series capacitance of the pilot tone attenuator (F)
```

```
49 %     ptp.K = gain of single-ended to differential converter (V/V)
50 %
51 % ap = structure containing the amplifier-filter parameters
52 %     ap.R = equivalent noise resistance of an amplifier-filter (ohms)
53 %     ap.T = equivalent noise temperature of an amplifier-filter (K)
54 %     ap.C = input capacitance of one amplifier-filter input (F)
55 %
56 % fp = structure containing the amplifier-filter parameters
57 %     fp.z = vector of filter zero locations (Hz)
58 %     fp.p = vector of filter pole locations (Hz)
59 %     fp.k = filter gain constant (V/V)
60 %
61 % fEAp = structure containing the parameters characterizing the
62 %     of the EMI-to-antenna frequency response
63 %     fEAp.z = vector of frequency response zero locations (Hz)
64 %     fEAp.p = vector of frequency response pole locations (Hz)
65 %     fEAp.k = frequency response gain constant (V/V)
66 %
67 % win = type of window to be used in the analysis, 'rect','blackman'
68 %     or 'flattop'
69 %
70 % OUTPUTS
71 %
72 % vraw = structure containing raw data samples from all the signals
73 %     acquired by the data acquisition system
74 %     vraw.c1 = vector of N samples from amplifier-filter 1 (V)
75 %     vraw.c2 = vector of N samples from amplifier-filter 2 (V)
76 %     vraw.A  = vector of N samples from an "EMI antenna" signal (V)
77 %     vraw.p = vector of N samples from the pilot tone (V)
78 %
79 % v  = structure containing data samples from all the signals after
80 %     windowing and blanking of saturating transient EMI and after
81 %     removal of EMI and/or the pilot one
82 %     v.c1 = vector of N samples from amplifier-filter 1 after
```

```
83  %          blanking saturating EMI (V)
84  %      v.c2 = vector of N samples from amplifier-filter 2 after
85  %          blanking saturating EMI (V)
86  %      v.A  = vector of N samples from an "EMI antenna" signal after
87  %          blanking the same time blocks as used in v.c1 and v.c2 (V)
88  %      v.p = vector of N samples from the pilot tone after
89  %          blanking the same time blocks as used in v.c1 and v.c2 (V)
90  %      v.c1mE = vector of N samples from amplifier-filter 1 after
91  %          subtracting EMI from v.c1 (V)
92  %      v.c2mE = vector of N samples from amplifier-filter 2 after
93  %          subtracting EMI from v.c2 (V)
94  %      v.c1mEmp = vector of N samples from amplifier-filter 1 after
95  %          subtracting the pilot tone from v.c1mE (V)
96  %      v.c2mEmp = vector of N samples from amplifier-filter 2 after
97  %          subtracting the pilot tone from v.c2mE (V)
98  %
99  %
100 % G  = structure containing all the PSD's and CPSD's used in the
101 %      analysis.
102 %
103 %  This first group is averaged with previous PSD's and CPSD's after
104 %  over each data block acquisition
105 %
106 %      G.c1 = vector of N PSD estimates for the amplifier-filter 1
107 %              output  voltage with the pilot tone off (V^2/Hz)
108 %      G.c2 = vector of N PSD estimates for the amplifier-filter 2
109 %              output  voltage with the pilot tone off (V^2/Hz)
110 %      G.c12 = vector of N CPSD estimates for amplifier-filters 1 and
111 %              2 output voltages with the pilot tone off (V^2/Hz)
112 %      G.c12p = vector of N CPSD estimates for amplifier-filters 1 and
113 %              2 output voltages with the pilot tone on (V^2/Hz)
114 %       G.p1 = vector of N CPSD estimates for amplifier-filter 1  and
115 %              pilot tone output voltages (V^2/Hz)
116 %      G.p2 = vector of N CPSD estimates for amplifier-filter 2  and
```

```
117 %             pilot tone output voltages (V^2/Hz)
118 %     G.p = vector of N PSD estimates for the pilot tone voltage
119 %             (V^2/Hz)
120 %    G.A1 = vector of N CPSD estimates for amplifier-filter 1  and
121 %             antenna output voltages (V^2/Hz)
122 %             **with the pilot tone off
123 %     G.A2 = vector of N CPSD estimates for amplifier-filter 2  and
124 %             antenna output voltages (V^2/Hz)
125 %             **with the pilot tone off
126 %     G.A1p = vector of N CPSD estimates for amplifier-filter 1  and
127 %             antenna output voltages (V^2/Hz)
128 %             **with the pilot tone on
129 %     G.A2p = vector of N CPSD estimates for amplifier-filter 2  and
130 %             antenna output voltages (V^2/Hz)
131 %             **with the pilot tone on
132 %     G.A = vector of N PSD estimates for the antenna output voltage
133 %             (V^2/Hz)
134 %             **with the pilot tone off
135 %
136 %  This second group is freshly computed after each data block
137 %  acquisition from the averaged PSD's and CPSD's in the first
138 %  group
139 %
140 %     G.c1mE  = vector of N PSD estimates for the amplifier-filter 1
141 %             output voltage with the pilot tone off and effects of
142 %             EMI subtracted (V^2/Hz)
143 %     G.c2mE  = vector of N PSD estimates for the amplifier-filter 2
144 %             output voltage with the pilot tone off and effects of
145 %             EMI subtracted (V^2/Hz)
146 %     G.c12mE = vector of N CPSD estimates for amplifier-filters 1 and
147 %             2 output voltages with the pilot tone off and effects of
148 %             EMI subtracted (V^2/Hz)
149 %     G.c12pmE = vector of N CPSD estimates for amplifier-filters 1
150 %             and 2 output voltages with the pilot tone on and effects
```

```
151 %             of EMI subtracted (V^2/Hz)
152 %     G.c12pmEmp = vector of N CPSD estimates for amplifier-filters 1
153 %             and 2 output voltages with the pilot tone on and effects
154 %             of EMI and pilot tone subtracted (V^2/Hz)
155 %     G.R = vector of N PSD estimates for the sensor noise voltage
156 %             with the pilot tone off and effects of EMI subtracted
157 %             (V^2/Hz)
158 %     G.Rp = vector of N PSD estimates for the sensor noise voltage
159 %             with the pilot tone on and effects of EMI and pilot tone
160 %             subtracted(V^2/Hz)
161 %
162 %  H = structure containing all the frequency response estimates used
163 %  in the analysis
164 %     H.p1 = vector of N frequency response estimates from the pilot
165 %             tone voltage to the amp-filter 1 output voltage (V/V)
166 %     H.p2 = vector of N frequency response estimates from the pilot
167 %             tone voltage to the amp-filter 2 output voltage (V/V)
168 %     H.A1 = vector of N frequency response estimates from the EMI
169 %             antenna voltage to the amp-filter 1 output voltage
170 %             with the pilot tone off (V/V)
171 %     H.A2 = vector of N frequency response estimates from the EMI
172 %             antenna voltage to the amp-filter 2 output voltage
173 %             with the pilot tone off (V/V)
174 %     H.A1p = vector of N frequency response estimates from the EMI
175 %             antenna voltage to the amp-filter 1 output voltage
176 %             with the pilot tone on (V/V)
177 %     H.A2p = vector of N frequency response estimates from the EMI
178 %             antenna voltage to the amp-filter 2 output voltage
179 %             with the pilot tone on (V/V)
180 %
181 %     Appending a "t" on any of these indicates the theoretically exact
182 %     value of the same quantity
183 %
184 %     Appending a "b" on any of these indicates the same quantity
```

```
%     except bandlimited
%
function JNTSimEMI3,

% Initialize all parameters and internal variables
% Set sensor parameters
  sp.T = 294; % LabView = 294 (Green RTD)
  sp.R = 99.9996;  % LabView = 99.9996
    % sp.T=273.15 %(ICE)
    % sp.T=294.261 %(RoomTemp=70F)
    % sp.T=373.15 %(100C)
    % sp.T=423.15 %(150C)
    % sp.T=473.15 %(200C)
    % sp.T=523.15 %(250C)

% Set data acquisition parameters
  N = 2^14; % Number of data points per block
  df = 16; % Frequency resolution (Hz)
  fs = N*df; % Sampling rate (samples/s)
  Ts = 1/fs; % Time between samples (s)
  t = Ts*[0:N-1]'; % Time vector for time-domain signals (s)
  f = df*[0:N-1]'; % Freq vector for freq-domain signals (Hz)
  kB = 1.38e-23; % Boltzmann's constant (J/K)
  SVNSP = 2*kB*sp.T*sp.R*fs; % Sensor voltage noise signal power (V^2)
  disp(['Sensor Voltage Noise Signal Power = ',num2str(SVNSP),'V^2']);

% Define measurement bandwidth
 flo = 15000; % Low end of bandwidth used (Hz)
 fhi = 40000; % High end of bandwidth used (Hz)

% Set cable parameters
 cp.T = 294; % Labview = 294
 cp.R = 0.98;  % LabView = Minimun Cable
 cp.C = 1e-10; % LabView = 1E-10
```

```
219
220 % Set pilot tone parameters
221  ptp.typ = 'F';
222  ptp.A = 1;
223  ptp.K = 0.01;
224  ptp.R = 1e6;
225  ptp.C = 1e-6;
226
227 % Set amplifier-filter input parameters
228   ap.R = 50;
229   ap.T = 294;
230   ap.C = 50e-12;
231
232 % Set filter frequency response parameters
233   fp.z = [0,0,0]';
234   fp.p = [-2000,-3000,-4000,-50000,-60000,...
235         -75000,-100000]';
236   fp.k = 1e11*prod(abs(fp.p))/5000^3;
237
238 % Set EMI-to-Antenna frequency response parameters
239   fEAp.z = 0;
240   fEAp.p = -50000;
241   fEAp.k = 1;
242
243 % Initialize all PSD's and CPSD's to zero
244
245 % First group of PSD's and CPSD's averaged after each block of data
246 % acquired
247   G.c1 = 0*f; G.c2 = 0*f; G.c1t = 0*f; G.c2t = 0*f;
248   G.c12 = 0*f; G.c12p = 0*f;
249   G.p1 = 0*f; G.p2 = 0*f; G.p = 0*f;
250   G.A1 = 0*f; G.A2 = 0*f; G.A = 0*f;
251   G.A1p = 0*f; G.A2p = 0*f; G.Ap = 0*f;
252
```

```
253 Nblks = 20000; % Number of blocks to average
254
255 % Set "s" as the independent variable of the Laplace transform
256   s = tf('s');
257 % With a digital filter, simulate the analog filtering effect of
258 % cable and amplifier-filter input capacitance
259 % Compute the sensor-cable transfer function
260   Hsc = 1/(s*(sp.R+cp.R)*(cp.C + 2*ap.C) + 1);
261   [bca,aca] = tfdata(Hsc,'v');
262   [bcd,acd] = bilinear(bca,aca,fs); % Numerator and denominator
263                                     % coefficients of digital filter
264   w = 2*pi*f; % Analog radian frequency vector
265   W = w/fs; % Digital radian frequency vector
266   Hscd = freqz(bcd,acd,W); % Digital filter frequency response
267   Zscd = Hscd*(sp.R+cp.R); % Impedance of the input RC network
268
269 % With a digital filter, simulate the JNT amplifier-filter effects
270 % Set numerator and denominator coefficients of the amplifier-filter
271 % from the zeros, poles and gain
272   [ba,aa] = zp2tf(2*pi*fp.z,2*pi*fp.p,fp.k);
273 % Set numerator and denominator coefficients of the digital filter
274 % that simulates the analog filter
275   [bd,ad] = bilinear(ba,aa,fs);
276   Hd = freqz(bd,ad,W); % Digital filter frequency response
277
278    % Ambient EMI
279         [A.f1,I11] = min(abs(1024-f));
280         A.gain1 = abs(Hd(I11));
281         [A.f2,I12] = min(abs(1136-f));
282         A.gain2 = abs(Hd(I12));
283         [A.f3,I13] = min(abs(1264-f));
284         A.gain3 = abs(Hd(I13));
285         [A.f4,I14] = min(abs(1376-f));
286         A.gain4 = abs(Hd(I14));
```

```
287         [A.f5,I15] = min(abs(1616-f));
288         A.gain5 = abs(Hd(I15));
289         [A.f6,I16] = min(abs(1744-f));
290         A.gain6 = abs(Hd(I16));
291         [A.f7,I17] = min(abs(2096-f));
292         A.gain7 = abs(Hd(I17));
293         [A.f8,I18] = min(abs(2336-f));
294         A.gain8 = abs(Hd(I18));
295 %         [A.f9,I19] = min(abs(44304-f)); %No Lights
296 %         A.gain9 = abs(Hd(I19)); %No Lights
297 %         [A.f10,I110] = min(abs(62784-f)); %No Lights
298 %         A.gain10 = abs(Hd(I110)); %No Lights
299 %Lights ON
300 %         [A.f11,I111] = min(abs(2224-f));
301 %         A.gain11 = abs(Hd(I111));
302 %         [A.f12,I112] = min(abs(27024-f));
303 %         A.gain12 = abs(Hd(I112));
304 %         [A.f13,I113] = min(abs(27184-f));
305 %         A.gain13 = abs(Hd(I113));
306         [A.f14,I114] = min(abs(42208-f));
307         A.gain14 = abs(Hd(I114));
308         [A.f15,I115] = min(abs(44288-f));
309         A.gain15 = abs(Hd(I115));
310         [A.f16,I116] = min(abs(62800-f));
311         A.gain16 = abs(Hd(I116));
312     % SANDIA EMI
313         [S.f1,I1] = min(abs(2000-f));
314         S.gain1 = abs(Hd(I1));
315         [S.f2,I2] = min(abs(6000-f));
316         S.gain2 = abs(Hd(I2));
317         [S.f2,I3] = min(abs(10000-f));
318         S.gain3 = abs(Hd(I3));
319         [S.f3,I4] = min(abs(14000-f));
320         S.gain4 = abs(Hd(I4));
```

```
321         [S.f4,I5] = min(abs(18000-f));
322         S.gain5 = abs(Hd(I5));
323         [S.f5,I6] = min(abs(22000-f));
324         S.gain6 = abs(Hd(I6));
325         [S.f6,I7] = min(abs(26000-f));
326         S.gain7 = abs(Hd(I7));
327         [S.f7,I8] = min(abs(30000-f));
328         S.gain8 = abs(Hd(I8));
329         [S.f8,I9] = min(abs(34000-f));
330         S.gain9 = abs(Hd(I9));
331         [S.f9,I10] = min(abs(38000-f));
332         S.gain10 = abs(Hd(I10));
333         [S.f9,I11] = min(abs(42000-f));
334         S.gain11 = abs(Hd(I11));
335         [S.f9,I12] = min(abs(44000-f));
336         S.gain12 = abs(Hd(I12));
337         [S.f9,I13] = min(abs(46000-f));
338         S.gain13 = abs(Hd(I13));
339         [S.f9,I14] = min(abs(50000-f));
340         S.gain14 = abs(Hd(I14));
341         [S.f9,I15] = min(abs(62800-f));
342         S.gain15 = abs(Hd(I15));
343 % Single Sine wave
344     [SS.f1,I17] = min(abs(20000-f));
345     SS.gain1 = abs(Hd(I17));
346     [SS.f1,I18] = min(abs(20000-f));
347     SS.gain2 = abs(Hd(I18)); % Find the Hd value at index for f=20k
348 % Multiple Sine wave
349     [MS.f1,I19] = min(abs(30000-f));
350     MS.gain = abs(Hd(I19)); % Find the Hd value at index for f=30k
351 % Single Sine wave
352     [ssS.f1,I20] = min(abs(40000-f));
353     ssS.gain1 = abs(Hd(I20)); % Find the Hd value at index for f=40k
354
```

```
% With a digital filter, simulate the EMI-to-antenna frequency
% response. Set numerator and denominator coefficients from the
% zeros, poles and gain
  [baEA,aaEA] = zp2tf(2*pi*fEAp.z,2*pi*fEAp.p,fEAp.k);
% Set numerator and denominator coefficients of the digital filter
% that simulates EMI-to-antenna frequency response
  [bdEA,adEA] = bilinear(baEA,aaEA,fs);
  HEAd = freqz(bdEA,adEA,W); % Digital filter frequency response

% Set transient EMI parameters
  Ep.t.on = 1;
  Ep.t.r = 10;
  Ep.t.Nav = 5;
  Ep.t.Aav = 3e-5;
  Ep.t.tauav = 10e-6;
  Ep.t.Tav = 1/20;

 %   Set periodic EMI parameters
 % Ep.p.f = vector of periodic E frequencies (Hz)
    Ep.p.on = 1; % Turn periodic EMI ON = 1; OFF = 0
% Sandia Simulation:
    Ep.p.f = [2000,6000,10000,14000,18000,22000,26000,30000,
                34000,38000,42000,44000,46000,50000,62000,1024,
                1136,1264,1376,1616,1744,2096,2336,2224];
    NEp = length(Ep.p.f) ;
% Ep.p.A = vector of periodic EMI amplitudes (V)
    Ep.p.A = [(0.01999/S.gain1),(0.065/S.gain2),(0.048/S.gain3),...
           (0.045/S.gain4),(0.038/S.gain5),(0.03/S.gain6),...
           (0.028/S.gain7),(0.02/S.gain8),(0.013/S.gain9),...
           (0.01/S.gain10),(0.008/S.gain11),(0.005/S.gain12),...
           (0.001/S.gain13),(0.0008/S.gain14),(0.025/S.gain15),...
           (0.038./A.gain1),(0.049/A.gain2),(0.055/A.gain3),...
           (0.065/A.gain4),(0.086/A.gain5),(0.038/A.gain6),...
           (0.031/A.gain7),(0.031/A.gain8),(0.03/A.gain11)];
```

```
% Ambient Simulation:
%  Ep.p.f = [1024,1136,1264,1376,1616,1744,2096,2336,...
%         42208,44288,62800]%,2224,27024,27184,];
%  Ep.p.A = [(0.038./A.gain1),(0.049/A.gain2),(0.055/A.gain3),...
%            (0.065/A.gain4),(0.086/A.gain5),(0.038/A.gain6),...
%            (0.031/A.gain7),(0.031/A.gain8),(0.009/A.gain14),...
%            (0.009/A.gain15),(0.038/A.gain16)];%(0.03/A.gain11),...
%            (0.01/A.gain12),(0.012/A.gain13)];
% Single Sine 20KHz:
%  Ep.p.f = [1024,1136,1264,1376,1616,1744,2096,2336,2224,...
%                20000,27024,27184,42208,44288,62800];
%  Ep.p.A = [(0.038./A.gain1),(0.049/A.gain2),(0.055/A.gain3),...
%                  (0.065/A.gain4),(0.086/A.gain5),(0.038/A.gain6),...
%                  (0.031/A.gain7),(0.031/A.gain8),(0.03/A.gain11),...
%                  (0.78./SS.gain1),(0.01/A.gain12),(0.012/A.gain13),...
%                  (0.009/A.gain14),(0.009/A.gain15),(0.038/A.gain16)];
% Broadbrand Simulation:
%  Ep.p.f = [[60:60:3000]';[10:2000:70000]';...
%                [60:500:70000]'] ;
%  Ep.p.A = ones(NEp,1)*50e-9;
    Ep.p.A = [Ep.p.A] ;
    ESP = sum(Ep.p.A.^2/2) ; %   Periodic EMI signal power at the sensor
disp(['Periodic EMI Signal Power (at sensor)=',num2str(ESP),'V^2']);

% With a digital filter, simulate the pilot-tone to amplifier-filter
% frequency response
  Zp = ptp.R + 1/(s*ptp.C);
  Hp = ptp.K/Zp;
  [num,den] = tfdata(Hp,'v');
  [bptd,aptd] = bilinear(num,den,fs);
  Hpd = freqz(bptd,aptd,W);

% Compute the theoretical values of some frequency responses, PSD's
% and CPSD's for comparison with the numerical results
```

```
423    [H,G] = Theory(G,sp,cp,fs,Hscd,Hd,Hpd,N,kB,ap,ptp);
424
425    win = 'rect'; % Choose a window
426    TempmE = []; % Estimated sensor temperature, (K) with EMI
427                 % subtraction with the pilot tone off
428    TempmEmp = []; % Estimated sensor temperature, (K) with EMI and
429                   % pilot tone subtraction with the pilot tone on
430
431  % "nfr" = counter for the first phase of computation in which the
432  % frequency responses from pilot tone to amplifier-filter voltage
433  % outputs and from the EMI antenna to the amplifier-filter output
434  % voltages are estimated
435    nfr = 0;
436  % "yesnosum" = 16 element vector, each of which accumulates the
437  % number of times a sub-block is NOT blanked during multiple
438  % iterations of estimating the frequency responses
439    yesnosum = zeros(16,1);
440  % Initialize H.p1, H.p2, H.A1p, H.A2p, H.A1 and H.A2 to empty to
441  % indicate they have not yet been estimated
442    H.p1 = []; H.p2 = []; H.A1p = []; H.A2p = []; H.A1 = []; H.A2 = [];
443  % "nfrmin" = minimum number of loops through the preliminary
444  % frequency response estimation process
445    nfrmin = 1 ;
446  % Loop until there are at least "nfrmin" non-blanked instances of each
447  % subblock used in estimating the frequency responses.  This is to
448  % insure that the initial estimates of pilot tone frequency responses
449  % not have any "gaps" because of blanking some of the pilot tone
450  % signal during transient EMI
451    while min(yesnosum) < nfrmin,
452      % Increment and display the frequency response loop counter
453        nfr = nfr + 1;
454        disp(nfr);
455        ptp.on = 1; % Turn pilot tone on
456     % Simulate signals for one block with pilot tone
```

```
457       vraw = JNTBlockSimEMI2(sp,N,df,Ep,cp,ptp,ap,Hscd,Hd,HEAd,Hpd);
458       %   Blank any subblock with transient EMI that saturates the
459       %   amplifier-filters and window the signals
460       [v,yesno] = WindowSignals(N,win,vraw,H,Ts);
461       while sum(yesno) == 0 | sum([v.c1;v.c2;v.A;v.p]) == 0,
462         vraw = JNTBlockSimEMI2(sp,N,df,Ep,cp,ptp,ap,Hscd,Hd,HEAd,Hpd);
463         [v,yesno] = WindowSignals(N,win,vraw,H,Ts);
464       end
465     % Accumulate data on how many times subblocks are not blanked
466       yesnosum = yesnosum + yesno;
467     % Fourier transform the signals
468       V = FT(v,Ts) ;
469     % Update antenna signal PSD and CPSD's with amplifier-filters
470     % 1 and 2 with the pilot tone on
471       G = UpdateGApandGA1pandGA2p(G,V,df,nfr);
472     % Compute the frequency responses from the EMI antenna signal to
473     % the amplifier-filter 1 and amplifier-filter 2 output voltages
474     % with the pilot tone on
475     % Initialize the frequency responses to zero
476       H.A1p = 0*G.A1p ; H.A2p = 0*G.A2p;
477     % Use only the most signficant values of G.Ap, G.A1p and G.A2p in
478     % computing H.A1p and H.A2p and leave the other frequency
479     % response estimates at zero
480       G.Apmax = max(G.Ap);
481       I = find(G.Ap > G.Apmax/10000);
482       H.A1p(I) = G.A1p(I)./G.Ap(I);
483       H.A2p(I) = G.A2p(I)./G.Ap(I);
484     % Subtract EMI from amplifier-filter output voltages using the
485     % latest estimate of the EMI-antenna-to-sensor frequency response
486     %  V = SubtractEMIp(V,G,H) ;
487     % Update pilot tone PSD and CPSD's with the output voltages from
488     % amplifier-filters 1 and 2 after subtracting EMI effects
489       G = UpdateGpandGp1andGp2(G,V,df,nfr);
490    % Initialize the frequency responses to zero
```

```
491       H.p1 = 0*G.p1; H.p2 = 0*G.p2;
492     % Compute the frequency responses from the pilot tone to the
493     % amplifier-filter 1 and amplifier-filter 2 output voltages
494       % Use only the most signficant values of G.p, G.p1mE and G.p2mE in
495       % computing H.p1 and H.p2 and leave the other frequency
496       % response estimates at zero
497         G.pmax = max(G.p);
498         I = find(G.p > G.pmax/10000);
499         H.p1(I) = G.p1(I)./G.p(I);
500         H.p2(I) = G.p2(I)./G.p(I);
501         ptp.on = 0 ; % Turn the pilot tone off
502       % Simulate signals for one block with the pilot tone off
503         vraw = JNTBlockSimEMI2(sp,N,df,Ep,cp,ptp,ap,Hscd,Hd,HEAd,Hpd);
504       % Remove any transient EMI that saturates the amplifier-filters
505       % from the signals and window the signals
506         [v,yesno] = WindowSignals(N,win,vraw,H,Ts);
507         while sum(yesno) == 0 | sum([v.c1;v.c2;v.A;v.p]) == 0,
508           vraw = JNTBlockSimEMI2(sp,N,df,Ep,cp,ptp,ap,Hscd,Hd,HEAd,Hpd);
509           [v,yesno] = WindowSignals(N,win,vraw,H,Ts) ;
510         end
511       % Fourier transform the signals
512         V = FT(v,Ts);
513       % Update antenna signal PSD and CPSD's with amplifier-filters 1
514       % and 2 with the pilot tone off
515         G = UpdateGAandGA1andGA2(G,V,df,nfr);
516       % Initialize the frequency responses to zero
517         H.A1 = 0*G.A1; H.A2 = 0*G.A2;
518       % Use only the most signficant values of G.A, G.A1 and G.A2 in
519       % computing H.A1 and H.A2 and leave the other frequency
520       % response estimates at zero
521         G.Amax = max(G.A);
522         I = find(G.A > G.Amax/10000);
523         H.A1(I) = G.A1(I)./G.A(I);
524         H.A2(I) = G.A2(I)./G.A(I);
```

```
525   end
526
527   dn = 1; % Number of computations between graph refreshes
528
529 % Average all PSD's and CPSD's over "Nblks" blocks
530   for n = 1:Nblks,
531     % Increment the frequency response loop counter
532       if mod(n,10) == 0, disp(n) ; end
533       nfr = nfr + 1;
534       grflag = n < dn | mod(n,dn) == 0;
535       ptp.on = 1; % Turn pilot tone on
536     % Simulate signals for one block with the pilot tone on
537         vraw = JNTBlockSimEMI2(sp,N,df,Ep,cp,ptp,ap,Hscd,Hd,HEAd,Hpd);
538     % Blank any subblock with transient EMI that saturates the
539     % amplifier-filters and window the signals
540       [v,yesno] = WindowSignals(N,win,vraw,H,Ts);
541       while sum(yesno) == 0 | sum([v.c1;v.c2;v.A;v.p]) == 0,
542         vraw = JNTBlockSimEMI2(sp,N,df,Ep,cp,ptp,ap,Hscd,Hd,HEAd,Hpd);
543         [v,yesno] = WindowSignals(N,win,vraw,H,Ts);
544       end
545       while sum(isnan(v.c1)) > 0,
546         vraw = JNTBlockSimEMI(sp,N,df,Ep,cp,ptp,ap,Hscd,Hd,HEAd,Hpd);
547         [v,yesno] = WindowSignals(N,win,vraw,H,Ts);
548       end
549     % Fourier transform the signals
550       V = FT(v,Ts) ;
551     % Update antenna signal PSD and CPSD's with amplifier-filters 1
552     % and 2
553       G = UpdateGApandGA1pandGA2p(G,V,df,nfr);
554       if sum(G.Ap == 0) == 0,
555          H.A1p = G.A1p./G.Ap;
556          H.A2p = G.A2p./G.Ap;
557       end
558       H.A1p(1) = 0 ; H.A2p(1) = 0;
```

```
559      % Subtract EMI from amplifier-filter output voltages in frequency
560      % domain
561        V = SubtractEMIp(V,G,H);
562      % Compute amplifier-filter 1 and 2 time-domain signals without EMI
563        v.c1mE = real(ifft(V.c1mE))*fs;
564        v.c2mE = real(ifft(V.c2mE))*fs;
565      % Subtract the pilot tone from amplifier-filter output voltages
566      % in frequency domain
567        V = SubtractPilotToneF(V,H);
568      % Compute amplifier-filter 1 and 2 signals with EMI and pilot tone
569      % effects subtracted in time domain
570          v.c1mEmp = real(ifft(V.c1mEmp))*fs;
571          v.c2mEmp = real(ifft(V.c2mEmp))*fs;
572      % Update all the PSD's & CPSD's except EMI with the pilot tone on
573          G = UpdateGp(G,V,df,n);
574          G.c12pmE = G.c12p - G.A.*conj(H.A1).*H.A2;
575          G.c12pmEmp = G.c12pmE - G.p.*conj(H.p1).*H.p2;
576      % Compute the frequency responses from the pilot tone to the
577      % amplifier-filter 1 and amplifier-filter 2 output voltages
578        if sum(G.p == 0) == 0,
579           H.p1 = G.p1./G.p;
580           H.p2 = G.p2./G.p;
581        end
582
583        H.p1(1) = 0; H.p2(1) = 0;
584
585        ptp.on = 0; % Turn the pilot tone off
586      % Simulate signals for one block with the pilot tone off
587        vraw = JNTBlockSimEMI2(sp,N,df,Ep,cp,ptp,ap,Hscd,Hd,HEAd,Hpd);
588      % Blank any subblock with transient EMI that saturates the
589      % amplifier-filters window the signals
590        [v,yesno] = WindowSignals(N,win,vraw,H,Ts);
591        while sum(yesno) == 0 | sum([v.c1;v.c2;v.A;v.p]) == 0,
592          vraw = JNTBlockSimEMI2(sp,N,df,Ep,cp,ptp,ap,Hscd,Hd,HEAd,Hpd);
```

```
593           [v,yesno] = WindowSignals(N,win,vraw,H,Ts);
594         end
595         while sum(isnan(v.c1)) > 0,
596           vraw = JNTBlockSimEMI(sp,N,df,Ep,cp,ptp,ap,Hscd,Hd,HEAd,Hpd);
597           [v,yesno] = WindowSignals(N,win,vraw,H,Ts);
598         end
599       % Fourier transform the signals
600         V = FT(v,Ts);
601       % Update the antenna signal PSD and CPSD's with amplifier-filters
602       % 1 and 2
603         G = UpdateGAandGA1andGA2(G,V,df,nfr);
604         if sum(G.A == 0) == 0,
605            H.A1 = G.A1./G.A;
606            H.A2 = G.A2./G.A;
607         end
608         H.A1(1) = 0 ; H.A2(1) = 0 ;
609         I = find(isnan(H.A1)); H.A1(I) = 0;
610         I = find(isnan(H.A2)); H.A2(I) = 0;
611       % Subtract EMI from amplifier-filter output voltages in frequency
612       % domain
613         V = SubtractEMI(V,G,H);
614       % Compute amplifier-filter 1 and 2 signals without EMI in time
615       % domain
616         v.c1mE = real(ifft(V.c1mE))*fs ; v.c2mE = real(ifft(V.c2mE))*fs;
617       % Update all the PSD's and CPSD's with the pilot tone off
618         G = UpdateG(G,V,df,n);
619       % Confine the analysis from here on to flo to fhi range
620       % The suffix "b" indicates "bandlimited".
621 %       if trans, pause ; end
622         I = find(f>flo & f<fhi);
623         fb = f(I);
624         G.c12pb = G.c12p(I);
625         G.p1b = G.p1(I); G.p2b = G.p2(I); G.pb = G.p(I);
626         H.c12tb = H.c12t(I) ;
```

```
627         G.A1pb = G.A1p(I); G.A2pb = G.A2p(I);
628         G.Ab = G.A(I);
629         Hscdb = Hscd(I); Hpdb = Hpd(I);
630         H.A1pb = G.A1pb./G.Ab;
631         H.A2pb = G.A2pb./G.Ab;
632         G.c1b = G.c1(I); G.c2b = G.c2(I);
633         G.c12b = G.c12(I);
634         G.A1b = G.A1(I); G.A2b = G.A2(I);
635         G.Ab = G.A(I);
636         H.A1b = G.A1b./G.Ab; H.A2b = G.A2b./G.Ab;
637         H.p1b = H.p1(I); H.p2b = H.p2(I);
638
639         G.c1mE = G.c1 - G.A.*abs(H.A1).^2;
640         G.c2mE = G.c2 - G.A.*abs(H.A1).^2;
641         G.c12mE = G.c12 - G.A.*conj(H.A1).*H.A2;
642         G.c1mEb = G.c1mE(I); G.c2mEb = G.c2mE(I);
643         G.c12mEb = G.c12mE(I); G.c12pmEb = G.c12pmE(I);
644         G.c12pmEmpb = G.c12pmEmp(I);
645
646       % Compute the cross-power frequency response from the sensor to
647       % the amplifier-filter output voltages, with and without the pilot
648       % tone
649         H.c12b = conj(G.p1b).*G.p2b.*abs(Hscdb).^2./(abs(Hpdb).^2.*...
650                       (sp.R + cp.R).^2.*G.pb.^2);
651
652       % Compute the latest best estimate of the |Hp(f)|^2 factor that
653       % characterizes the pilot tone attenuator
654         Hpmagsq = 2*kB*(sp.T*sp.R+cp.T*cp.R)./((((G.c12pmE.*G.p)./...
655                  (conj(G.p1).*G.p2))-1).*G.p.*(sp.R+cp.R)^2);
656         Hpmagsqm = abs(mean(Hpmagsq(I)));
657         Hpdbm = abs(mean(Hpdb));
658       % Compute the sensor PSD with the pilot tone off
659         G.Rb = G.c12mEb./H.c12b - 2*kB*cp.T*cp.R;
660       % Compute the sensor PSD with the pilot tone on
```

```
661       G.Rpb = G.c12pmEmpb./H.c12b - 2*kB*cp.T*cp.R;
662     % Compute temperature estimates with and without the pilot tone
663     % and using subtraction of sensor EMI
664       TempmE = [TempmE;mean(abs(G.Rb))/(2*kB*sp.R)];
665       TempmEmp = [TempmEmp;mean(abs(G.Rpb))/(2*kB*sp.R)];
666
667     %  Plot G12 and G12-E
668         plot(f./1000,abs(G.c12),'k');
669         hold on;
670         plot(f./1000,abs(G.c12mE),'b');
671         %axis([0 65 -0.001 0.055]); %Sandia plot
672         %axis([10 25 -0.000005 0.000015]); %Sandia zoom plot
673         %axis([0 65 -1E-7 2E-6]); %broadband plot
674         %axis([0 65 -1E-7 8E-7]); %NO NOISE
675         %axis([0 65 -1E-7 5E-7]); %small sine plot
676         axis([0 65 -1e-6 0.5e-5]); %ambient plot zoom
677         %axis([0 65 -1e-6 3.5e-5]); %ambient plot
678         title('G12(f)');
679         xlabel('Frequency (kHz)');
680         %yt = get(gca,'ytick');
681         %set(gca,'yticklabel', [-1:1:5.5].*1e-5);% Ambient
682         ylabel('CPSD (V/Hz^2)');
683         legend('G12','G12-E');
684         hold off;
685   end
686
687
688
689
690 %-------------------------------------------------------------------------
691 \section{JNTBlockSImEMI2.m}
692
693 All rights reserved to Michael J. Roberts.
694 \begin{lstlisting}
```

```
695 %   Function to simulate the acquisition of one block of data in the
696 %   measurement of temperature using two amplifier-filter channels and
697 %   correlation with a pilot tone to measure the frequency response.
698 %   This simulation includes the effects of transient and periodic
699 %   EMI and returns an "EMI antenna" signal for use in subtracting
700 %   out effects of EMI.
701 %
702 %   sp = structure containing the sensor parameters
703 %       sp.T = sensor temperature (K)
704 %       sp.R = sensor resistance (ohms)
705 %
706 %   N = number of samples requested from this block simulator;
707 %       must be an even integer
708 %
709 %   df = frequency-domain resolution (Hz)
710 %
711 %   Ep  = structure containing the EMI parameters
712 %       Transient EMI is governed by a Poisson process.  Each time a
713 %       Poisson process event occurs a sequence of exponentially-
714 %       decaying pulses occurs.  The number of pulses in the
715 %       sequence, their amplitudes, their time constants and the
716 %       duration of the sequence are all random with a specified
717 %       mean and and are exponentially distributed
718 %       Ep.t.on = flag indicating add transient EMI (1) or don't (0)
719 %       Ep.t.r = rate parameter of the Poisson process, per second
720 %       Ep.t.Nav = average number of pulses in a sequence
721 %       Ep.t.Aav = average amplitude of the transient EMI pulses (V)
722 %       Ep.t.tauav = average amplitude of the transient EMI pulses (V)
723 %       Ep.t.Tav = average duration of a sequence of pulses (s)
724 %       Ep.p.on = flag indicating add periodic EMI (1) or don't (0)
725 %       Ep.p.f = vector of periodic E frequencies (Hz)
726 %       Ep.p.A = vector of periodic EMI amplitudes (V)
727 %       EP.p.f and Ep.p.A must be the same length
728 %
```

```
729 %   cp = structure containing the cable parameters
730 %       cp.T = cable temperature (K)
731 %       cp.R = cable resistance (ohms)
732 %       cp.C = cable capacitance (F)
733 %
734 %   ptp = structure containing the pilot tone parameters
735 %       ptp.on = flag indicating either add a pilot tone (1)
736 %                or don't (0)
737 %       ptp.typ = flag indicating either FM ('F') or random ('R')
738 %                 pilot tone
739 %       ptp.A = pilot tone amplitude (V) (as generated)
740 %           For FM signals ptA is the (constant) amplitude
741 %           For random signals ptA is the rms value
742 %
743 %   ap = structure containing the amplifier-filter parameters
744 %       ap.R = equivalent noise resistance of an amplifier-filter
745 %       channel (ohms)
746 %       ap.T = equivalent noise temperature of an amplifier-filter
747 %       channel (K)
748 %       ap.C = input capacitance of one amplifier-filter input (F)
749 %
750 %   Hscd = vector of frequency responses of the cable-sensor RC
751 %       circuit at discrete-time radian frequencies
752 %       W = 2*pi*df*[0:N-1]'/fs
753 %
754 %   Hd = vector of frequency responses of one amplifier-filter at
755 %       discrete-time radian frequencies W = 2*pi*df*[0:N-1]'/fs
756 %
757 %   HEAd = vector of frequency responses of the EMI-to-
758 %       antenna-mechanism at discrete-time radian frequencies
759 %       W = 2*pi*df*[0:N-1]'/fs
760 %
761 %   Hpd = vector of frequency responses of the pilot-tone-voltage-
762 %       to-sensor-current at discrete-time radian frequencies
```

```
763 %       W = 2*pi*df*[0:N-1]'/fs
764 %
765 %   v   = structure containing samples from all the signals acquired
766 %       by the data acquisition system
767 %       v.c1 = vector of N samples from channel 1 (V)
768 %       v.c2 = vector of N samples from channel 2 (V)
769 %       v.A = vector of N samples from an "EMI antenna" signal (V)
770 %       v.p = vector of N samples from the pilot tone, as generated (V)
771 %
772 %   JNTBlockSimEMI2(sp,N,df,Ep,cp,ptp,ap,Hscd,Hd,HAd,Hptd)
773 %
774
775 function v = JNTBlockSimEMI2(sp,N,df,Ep,cp,ptp,ap,Hscd,Hd,HEAd,Hpd),
776
777 % Check to see whether N is even or not.  If not, display an error
778 % message and return.
779     if mod(N,2) ~= 0,
780         disp('Block size is not an even number');
781         v.c1 = NaN; v.c2 = NaN; v.A = NaN; v.p = NaN;
782         return;
783     end
784
785     fs = N*df; % Sampling rate, in samples/s
786     Ts = 1/fs;  % Time between samples (s)
787
788     kB = 1.38e-23; % Boltzmann's constant (J/K)
789     GRs = 2*kB*sp.T*sp.R; % Sensor noise voltage PSD (V^2/Hz)
790     GRc = 2*kB*cp.T*cp.R; % Cable noise voltage PSD (V^2/Hz)
791     Ga = 2*kB*ap.T*ap.R;  % Amplifier-filter equiv input noise voltage
792                           % PSD (V^2/Hz)
793
794     rng('shuffle'); % Seed random number generator based on current time
795     vRs = sqrt(GRs*fs)*randn(N,1); % Sensor noise voltage (V)
796     vRc = sqrt(GRc*fs)*randn(N,1); % Cable noise voltage (V)
```

```
797     va1 = sqrt(Ga*fs)*randn(N,1); % Amplifier-filter 1 input noise
798                                   % voltage (V)
799     va2 = sqrt(Ga*fs)*randn(N,1); % Amplifier-filter 2 input noise
800                                   % voltage (V)
801     vRsRc = vRs + vRc; % Sensor and cable noise voltage (V)
802     t = Ts*[0:N-1]'; % Time vector for one data block (s)
803 % Add the pilot tone if requested.  Otherwise set it to zero.
804     if ptp.on,
805         switch ptp.typ
806             case 'F',
807                 fmin = 0 ; fmax = fs/2; % Range of FM pilot tone
808                                         % frequencies (Hz)
809                 dptf = (fmax-fmin)/N; % Resolution of FM pilot
810                                       % tone (Hz)
811                 ptf = fmin + dptf*[0:N-1]'; % Vector of pilot tone
812                                             % frequencies
813                 ss = ceil(rand(1,1)*N); % Pick a random starting freq
814                 ptf = [ptf(ss:end);ptf(1:ss-1)];
815                 ptpha = cumsum(2*pi*ptf*Ts); % Phase of FM pilot tone
816                                              % signal
817                 v.p = ptp.A*sin(ptpha); % Pilot tone voltage as
818                                         % generated
819                 v.p = v.p - mean(v.p); % Keep average value at zero
820             case 'R'
821                 v.p = randn(N,1).*ptp.A; % Generate a bandlimited
822                                          % white noise pilot tone
823         end
824         V.p = fft(v.p);
825     % Account for the pilot tone attenuator
826         v.pa = real(ifft(V.p.*Hpd.*Hscd.*(sp.R + cp.R)));
827     else
828         v.p = 0*t ; v.pa = 0*t; % Pilot tone is zero in this case
829     end
830     vRsRcp = vRsRc + v.pa; % Total sensor voltage without EMI (V)
```

```
831
832     vE = 0*t ; % Initialize EMI signal to zero
833     if Ep.t.on,
834     % Add transient EMI at random times.
835         Pev = Ep.t.r*Ts; % Probability of a Poisson event in one
836                          % sample time
837         Evs = rand(N,1)<Pev; % Event markers, 1 for event, 0 for no
838                              % event
839         I = find(Evs == 1); % Find time indices of Poisson events
840         % Generate a sequence of EMI pulses for each Poisson event
841         for n = 1:length(I),
842         % Number of pulses in this sequence
843             Np = round(exprnd(Ep.t.Nav));
844             A = exprnd(Ep.t.Aav*ones(Np,1)); % Pulse amplitudes
845         % Make some of the amplitudes negative
846             A = A.*(2*(rand(Np,1)>0.5)-1);
847             tau = exprnd(Ep.t.tauav*ones(Np,1)); % Pulse time constant
848             T = exprnd(Ep.t.Tav); % Pulse sequence duration
849             t0 = I(n)*Ts + T*rand(Np,1); % Pulse beginning times
850             for m = 1:Np, % Generate the pulse sequence
851                 % Generate one pulse
852                 vEt = A(m)*exp(-(t-t0(m))/tau(m)).*us(t-t0(m));
853                 II = find(isnan(vEt)); vEt(II) = 0;
854                 vE = vE + vEt; % Add the pulse to the EMI voltage
855             end
856         end
857     end
858
859     if Ep.p.on, % Add periodic EMI, if requested
860         vEp = t*0; % Initialize periodic EMI to zero.
861     % Generate a set of sinusoidal EMI voltages at random phase
862     % angles
863         for n = 1:length(Ep.p.f),
864            vEp = vEp + Ep.p.A(n)*cos(2*pi*Ep.p.f(n)*t+rand(1,1)*2*pi);
```

```
865          end
866          vE = vE + vEp; % Add periodic EMI
867      end
868
869  % Add the EMI signal to the sensor noise and pilot tone voltage (V)
870      vRsRcpE = vRsRcp + vE ;
871
872  % Simulate the analog filtering effect of cable and amplifier-filter
873  % input capacitance with a digital filter
874      f = df*[0:N-1]'; % Analog cyclic frequency vector
875      w = 2*pi*f; % Analog radian frequency vector
876      W = w/fs; % Digital radian frequency vector
877      VRsRcpE = fft(vRsRcpE); % FFT of total sensor voltage
878      vRsRcpEf = real(ifft(VRsRcpE.*Hscd)); % Input voltage for both
879                                            % amplifier-filters without
880                                            % their own voltage noise(V)
881      v1 = vRsRcpEf + va1; % Total input voltage for amp-filter 1 (V)
882      v2 = vRsRcpEf + va2; % Total input voltage for amp-filter 2 (V)
883
884  % Simulate the JNT analog filter with a digital filter
885  % Filter and amplify input signals for both channels
886      V1 = fft(v1); % FFT of input voltage for amplifier-filter 1
887      V2 = fft(v2); % FFT of input voltage for amplifier-filter 2
888      v.c1 = real(ifft(V1.*Hd)); % Amplifier/filter 1 output voltage (V)
889      v.c2 = real(ifft(V2.*Hd)); % Amplifier/filter 2 output voltage (V)
890      v.c1 = min(v.c1,10); % Simulate saturation of amplifier-filter
891      v.c1 = max(v.c1,-10); % 1 output
892      v.c2 = min(v.c2,10); % Simulate saturation of amplifier-filter
893      v.c2 = max(v.c2,-10); % 2 output
894
895  % Simulate the antenna frequency response with a digital filter
896  % Filter the EMI signal to create the antenna signal
897      VE = fft(vE); % FFT of EMI voltage
898      v.A = real(ifft(VE.*HEAd)); % Antenna voltage (V)
```

```
899
900 % Function to implement the Dirichlet function without using the
901 % MATLAB "diric" function
902 function y = us(x),
903     y = (sign(x) + 1)/2;
```

Vita

Nora Dianne Bull was born in Ft. Knox, KY, to parents Thomas and Beverly Bull. She is the younger of two daughters. She attended the University of Tennessee (UT) and graduated with a Bachelors of Science in Electrical Engineering from the College of Engineering in the Spring of 2007. Still curious to learn more about electronic design, Nora continued her education and completed a Master's Degree from the University of Tennessee, College of Engineering in the Winter of 2010. While finishing her Master's, she started an internship at Oak Ridge National Laboratory as a Post Master's Student Intern. She was hired shortly after as a full-time employee in July 2010. After working at Oak Ridge National Laboratory (ORNL) for a year, ORNL supported Nora through their education program to pursue a Ph.D. from the University of Tennessee. Nora started taking classes, while continuing as a full-time employee, and passed her qualifying exams in the Fall of 2013. Nora was then awarded an education sabbatical to complete her research at UT in August of 2014. After graduation, Nora will return to ORNL to continue as a research and development engineer with a focus in electrical systems design, including integration of electronics and signal processing design.